Flexural Strengthening of Reinforced Concrete Beams with Externally Bonded CFRP Plates with Lap Splices

Prepared by

Nathan Matthew Porter
James Michael Stallings

Submitted to

Highway Research Center
Auburn University, AL

June 2001

ACKNOWLEDGMENTS

Funding for this research was provided by the Auburn University Highway Research Center. All composite materials were donated by FiberCote Industries, Inc. of Waterbury, Connecticut. Technical advice was provided by Fibercote Industries and by J.W. White Enterprises of Montgomery. The assistance and support of these organizations is gratefully acknowledged.

DISCLAIMER

The contents of this report reflect the views of the authors who are responsible for the facts and accuracy of the data presented. The contents do not necessarily reflect the official views or policies of the sponsors. The report does not constitute a standard, specification, or regulation.

SUMMARY

In recent years, the search for cost effective methods for bridge beam rehabilitation have lead to the use of externally bonded continuous Fiber Reinforced Plastics (FRPs) plates as an alternative to the established techniques. Few studies have explored the use of butt joints reinforced by lapped splice plates as a means of splicing FRP plates. This report provides a foundation for the development of bridge rehabilitation techniques using FRP splices by studying potential problems associated with the use of splice plates.

Eight reinforced concrete beams, six initially damaged and two undamaged, were used to test the flexural performance of beams externally reinforced with epoxy bonded Carbon Fiber Reinforced Plastic (CFRP) primary and splice plates. The plates were bonded to the tension face of the beams using a two-part epoxy. An analytical model, using strain compatibility relationships, was developed and used as a basis for comparison with experimental data.

Comparison of the analytical and experimental results demonstrated the ability to predict beam yield strength and normal strain levels in CFRP. Increases in strength (over the service load range) from 18 to 32 percent and increases in stiffness from 2 to 21 percent were achieved with the application of the CFRP primary and splice plates. Failure of all but one of the beams resulted from complete splice plate debonding. It was determined that complete splice plate debonding, initiating at the ends of the splice plates, was the result of high shear stresses at the primary plate/adhesive interface. The high shear stresses were caused by differences in normal strain levels occurring in the primary and splice plate at the ends of the splice plate.

TABLE OF CONTENTS

LIST OF TABLES

LIST OF FIGURES

CHAPTER ONE

INTRODUCTION

Background

In recent years the use of Fiber Reinforced Plastics (FRPs) has become a subject of great interest in the structural community. The aging of the nation's infrastructure in a tight economic environment has necessitated the search for innovative and cost effective solutions. Several studies have focused on the use of externally bonded FRPs to reinforce existing structures in need of rehabilitation. Although FRPs are more expensive than traditional structural materials, the savings in labor and equipment costs associated with the use of FRPs make them an attractive alternative.

One important recent study occurred in Bullock County, Alabama. A deteriorating multi-girder reinforced concrete bridge suffering from significant flexural cracking was repaired by externally bonding Carbon Fiber Reinforced Plastic (CFRP) laminates to the under strengthened girders. Down time for the bridge repairs was less than one week. Repairs were completed by four laborers with minimal equipment required.

The flexural performance of the bridge was improved by the application of multiple plates of CFRP spliced together approximately at third points for all

girders. The Bullock County bridge repair project represents one of the initial attempts at reinforcing existing structures with the combination of CFRP primary and splice plates. Although splice plates were used in the repairs, flexural performance of the bridge was the focus of the Bullock County study. The research presented here stems from this earlier endeavor.

Project Objectives

The research project objectives were: (1) to design and construct eight reinforced concrete beams for lab testing, (2) to develop an analytical program for comparison of actual and theoretical flexural behavior of concrete beams externally reinforced with CFRP primary and splice plates, (3) to study the flexural performance of beams externally reinforced with CFRPs, and (4) to analyze epoxy bonded primary and splice plate behavior.

Scope of Report

The focus of this report is to evaluate the feasibility of using epoxy bonded CFRP primary and splice plates for flexural strengthening of reinforced concrete beams.

The literature review presented in Chapter Two highlights recent studies in the use of FRPs in structural rehabilitation. In addition, the literature review includes descriptions of recent field applications of FRPs for repairs of damaged and deteriorating structures.

Chapter Three emphasizes several key topics; the design and fabrication of eight reinforced beams used for laboratory testing, the composite plate

properties as well as epoxy adhesive selection is described. The method used for bonding plates to the concrete surface, instrumentation used during beam tests, and data reduction techniques are presented also.

The development of, and results generated by, a computer program which analyzes doubly reinforced concrete beams strengthened with unidirectional CFRP plate/s are discussed in Chapter Four. Data provided by the computer model initially assisted in determining critical load points during loads tests and provided a basis for comparison with experimental data.

To develop a basic understanding of plate behavior on preexisting concrete beams, Crack Tests were devised and implemented to produce initial damage in the beam specimens. Six beams were subjected to the initial crack tests, and the remaining two were left undamaged. Crack Tests were also used to validate the computer program developed in this study. Chapter Five provides a description of test procedures and results.

Chapter Six presents results of six damaged and two undamaged beams strengthened with CFRP primary and splice plates as well as the performance of the plates themselves. Initial discussions with a number of materials suppliers in the composites industry identified little or no concern about adhesive failure between the primary and splice plates at lap splice joints. The critical concern was the bond between the CFRP and concrete surface. The original testing plan for this thesis was focused on the effect of fatigue on the adhesive bond between the primary plate and concrete surface at crack locations along the beam. Attempted fatigue tests of beams one and two, demonstrated that the

adhesive bond between the primary and splice plate does pose a problem. Therefore, Ultimate Load Tests (i.e. static load tests) were designed to determine the initial cause of splice plate debonding.

To determine if splice plate debonding characteristics could be accurately predicted with simple test procedures, Tension Tests specimens using representative testing materials applied in large scale testing were devised. Chapter Seven describes the specimen design, instrumentation, test procedure, and results of five Tension Tests. Chapter Eight provides a summary of all test performed.

CHAPTER TWO

LITERATURE REVIEW

Introduction

Due to a growing need for innovative and alternative methods for the rehabilitation of existing concrete bridges, recent studies have focused on the use of Fiber Reinforced Plastics (FRPs) as strengthening materials for these structures.

Early post-strengthening techniques of reinforced concrete beams, which have been studied and used in field applications, were directed toward the use of epoxy bonded steel plates. Although the use of steel plates provided insight into the increase in flexural strength and flexural stiffness capabilities of externally applied reinforcement, steel plates had some disadvantages. Some of the most notable where: (1) difficulty in handling during installation; (2) possibility of corrosion affecting the bond surface at the steel/adhesive interface; and (3) the problem of forming clean butt joints with relatively short plates (Meier et al. (1991)). This prompted further investigation into the use of alternative materials (FRPs).

For the most part, FRPs have been used in the aircraft and space industries with few applications in civil engineering. Due to advancements in

epoxy adhesives, these materials have recently been introduced to the civil engineering structures community. It has been shown in results presented by Saadatmanesh and Ehsani (1990), that suitable epoxies are available for bonding FRPs to concrete, thus increasing the flexural performance of beams. FRPs are characterized by their low unit weight, extremely high stiffness, excellent fatigue properties, corrosion resistance, and electromagnetic neutrality. For rehabilitation purposes, their light weight makes them easier to manage during installation. However, with the desirable qualities comes greater cost. For example, the carbon fiber reinforced plastic (CFRP) plates used in this study, generally would cost about 5 to 10 times more, per unit weight, than steel. If one considers the cost of the labor involved in the application of steel plates in comparison to CFRP plates however, the price no longer seems so extreme.

A summary of results from recent articles pertaining to the use of FRPs in flexural strengthening of concrete beams is addressed in this chapter. Recently reported field applications of FRPs on wooden and concrete bridges are also included.

Flexural Strengthening of Reinforced Concrete Beams

In the 1980's, research began at the Swiss Federal Laboratories for Material Testing and Research (EMPA) to investigate the feasibility of replacing steel plates with CFRP plates for flexural strengthening of concrete beams (Meier et al. 1991, 1992). Meier and his fellow associates conducted tests on twenty-six beams with span lengths of 2 m and one beam with a span length of 7 m. The strengthening of beams was achieved by bonding a continuous

unidirectional CFRP (0.3 mm to 1.0 mm thick) plate to the extreme tension face of the beams. Two types of epoxy adhesive were used in the application of the plates, XB-3074 and Sikadur 31. The selection was based on earlier research conducted by EMPA for steel plates. To insure a strong bond between the plates and concrete surface, careful surface preparation measures were taken. The plates were sanded to remove any excess resin, and the beams were sandblasted to remove all loose fragments from the surface. The plates as well as the beams were then washed with a degreasing detergent before application. The authors stressed the importance of a strictly even bonding surface for thin plates. After the plates were coated with adhesive and positioned on the beams, pressure was applied to the laminates during the curing process with vacuum bags or lightweight clamps.

The results of the tests indicated ultimate strength increases in the 2 m span beams of approximately twice the original strength. Meier et al. stated that the beam having a 7 m span had a more realistic steel reinforcement ratio, and the increase in strength of that beam was about 22 percent. The failure mode for all beam specimens was tension failure of the CFRP plates which occurred at beam deflections 50 percent lower than those of the unstrengthened beams. Although brittle failure did occur in the plates, the authors concluded that sufficiently ductile behavior was observed before failure. The research also showed the validity of analyzing beam behavior through a strain-compatibility analysis of the cross section.

Ritchie et al. (1991) presented results from tests conducted on sixteen

under reinforced concrete beams. The beams were tested under a two point loading with span length of 2.74 m. The research was designed to test the feasibility of reinforcing concrete beams with a variety externally applied FRP plates. In addition, a theoretical analysis was developed to see whether or not reinforced beam behavior could be accurately predicted for further development of design procedures. Splice plates were considered, then deemed undesirable by the authors due to the stage of the investigation. No tests were performed on beams with splice plates.

Various types of FRP plates and fiber orientations were used by Ritchie et al. for flexural strengthening. The three types of fibers selected were glass, carbon, and aramid with orientations ranging from 0 to 90 degrees. In some cases multiple orientations were used. Mild steel plates were also used. Fourteen beams were tested with external reinforcement. Two beams without plates were tested as control specimens for comparison of results. All beams were loaded to their ultimate load.

A two part rubber toughened adhesive was selected for bonding the FRP plates to the extreme tension face of the beam specimens. The adhesive was selected for its tolerance of variations in mix proportions and ability to cure at room temperatures. Before bonding, surface preparations were conducted on the FRP and steel plates as well as concrete surface. The bonding surfaces of the FRP plates were sanded to remove the shine, and the steel plates were sandblasted to remove mill scale. For the concrete surface, an abrasive stone with water was used. The adhesive was applied to both bonding surfaces with a

metal spatula, and steel weights were used to apply pressure during curing.

During initial tests, premature concrete shear failure occurred at the depth of the tension reinforcement at ends of the partial length FRP plates. Four modifications were made in subsequent testing. The first three modifications were directed toward using end anchorages for the partial length plates, and the fourth was to continue the plates to the supports. With the modifications, the failure modes of only two of the remaining beams were shifted to the constant moment region. The authors suggested that continuing the FRP plates to the supports would be more effective for beams with lower shear to moment ratios (longer spans).

The results of the tests indicated that the load capacity and stiffness of the beams was moderately increased, and in some cases greatly increased by the application of the FRP plates. The increase in stiffness above that of the control specimens ranged from 17 to 99 percent over the service load range. The stiffness was determined using the slope of a line from the origin through a point on the measured load-deflection plot at a deflection equal to the span length divided by 480. Similar strength increases, from 19 to 99 percent, in the service load range were also seen. At ultimate, the increase in strength ranged from 28 to 97 percent despite premature brittle concrete shear failure occurring in many beams.

Results from a theoretical analysis program, developed to determine load-deflection relationships using strain compatibility, proved fairly successful in the prediction of beam behaviors with bonded FRP plates.

Chajes et al. (1994) performed tests on fourteen under-reinforced concrete beams with externally bonded composite fabrics. Comparisons were made between beams having additional internal steel reinforcement and those having additional external fabric reinforcement. The beams were tested under two point loading with span lengths of 1.12 m. Based on stress-strain relationships of the concrete, steel and composite fabrics, an analytical method for predicting the behavior of the beams was designed for comparison against experimental results. The method was based off an analysis and parametric study conducted by An et al. (1991).

Three types of composite fabrics were used in the study: (1) plain-weave aramid fabric; (2) crow-foot satin-weave E-glass fabric; and (3) plain-weave graphite fabric. All fabrics had fiber orientations of 0 and 90 degrees. In some cases multiple layers of the same fabric were used. Nine beams were tested with external reinforcement, two with additional steel reinforcement and three as control specimens. All beams were tested to failure.

The adhesive, Sikadur 32, used for bonding fabrics to the extreme tension face of the beams was selected based on ongoing research by authors dealing with composite plates. Sikadur 32 is a two-component, high-modulus, high-strength, construction epoxy with a mix ratio of 1:1 that can be cured at room temperature. The surface preparation conducted on the concrete was similar to that used by Richie et al. (1991). A vacuum bag system was employed during the curing process.

Two bonding schemes were used throughout testing. In early testing,

fabrics were bonded to the entire length of the beam specimens. Subsequently, due to the premature debonding in one test, end tabs were added. This ensured failure modes of either compression failure of the concrete or tension failure of the fabric.

The results of the study indicated average increases in flexural capacity of 53, 46, and 45 percent for the beams strengthened with aramid, E-glass, and graphite fabrics, respectively. An average increase in flexural stiffness of 40 percent was seen for all externally reinforced beam specimens. The stiffness was determined using the slope of the line from the origin through a point on the measured load deflection plot at a deflection equal to the span length divided by 480. The authors also noted that, prior to beam failure, some degree of ductility was observed in the fabric strengthened beams. Comparison of results of the additional internal steel reinforced beams with those of the external reinforced beams showed similarities in terms of strengthening.

From comparison of the experimental results and theoretical calculations, the authors concluded that with the use of the analytical method, the ultimate flexural capacity, mode of failure and surface strains of the fabrics could accurately be predicted.

Field Applications

In addition to lab studies, field applications of FRP were performed to strengthen an existing wooden bridge, a prestressed concrete bridge, and most recently a reinforced concrete bridge.

Meier et al. (1992) described results from two bridges in Switzerland

reinforced with CFRP plates. The Ibach bridge, built in 1969 in the County of Lurence, was damaged during installation of new traffic lights, when prestressing tendons in the outer web of a box girder were severed with an oxygen lance. Due to traffic considerations through the underpass, repairs had to be made at night. Two 150 x 5000 x 1.75 mm and one 150 x 5000 x 2.00 mm CFRP sheets were used in the rehabilitation of the damaged section. After load testing, it was determined that the application of the CFRP sheets yielded satisfactory rehabilitation of the bridge girder. Participants in the application of the CFRP plates were pleasantly surprised with the simplicity of the processes.

A repair project was initiated on a historic wooden bridge in Sins, constructed in 1807, due to an increase in traffic loads. Two of the most highly loaded cross-beams were strengthened by the EMPA using 1.00 mm thick CFRP sheets. The application of the sheets provided practical experience and confidence in the use of this type of material in the preservation of historic bridges.

Recently, Tedesco et al. (1996) presented findings from a study conducted on a damaged multi-girder reinforced concrete bridge in Bullock County, Alabama. The study was conducted for the Alabama Department of Transportation (ALDOT). The goal was to determine the feasibility of using CFRP plates in the rehabilitation of a simple span reinforced concrete bridge deteriorated by traffic loading. The hope was that the life of the bridge could be extended by the use of external reinforcement. To reduce the amount of labor involved in the application of the CFRP plates, a primary plate with butt joints, at

approximately the third points of the span, was bonded to the extreme tension face of the girders. The length of the primary plates made the application fairly simple. Although butt joints simplified the installation process, this made the use of lap splice plates necessary. Glass fiber reinforced laminates were also bonded to the sides of the beams for additional stiffness and shear strengthening. The time required for installation of all reinforcing plates was one week, during which time traffic was rerouted. Results from static and dynamic load tests conducted before and after the application of the reinforcement indicated favorable service load strength and stiffness results. Although the initial results provided some indication of the ability of the CFRP to strengthen the damaged bridge girders, the site investigation is continuing on the effects of environmental changes and fatigue on the plates and adhesive bond.

The tests and results presented in later chapters of this thesis stem from an interest in the research conducted on the Bullock County Bridge. The use of splice plates as well as the effect of fatigue on the adhesive bond of CFRP plates on damaged girders were of particular interest and are a focus of this thesis.

CHAPTER THREE

EXPERIMENTAL STUDY

Beam Design

Eight reinforced concrete beams with simply supported span lengths of 7.32 m, and a cross-section of 254 x 457 mm were tested under a two point loading. The beams were designed in compliance with the specifications given by the American Concrete Institute (ACI 1989). The internal flexural reinforcement of each beam consisted of two #6 and two #3 deformed bars extending the entire length as shown in Figure 3.1. In addition, a #6 and #4 bar with lengths of 4.27 m and 3.05 m, respectively, were instrumented with strain gages and centered at midspan just prior to casting the concrete. Details of the beam geometry, flexural reinforcement locations, and applied loading are illustrated in Figure 3.1.

Using the specified minimum yield strength of 414 MPa for the reinforcing bars, the section satisfies the ACI (1989) ductility requirement for the area of steel ratio ($\rho_{min} = 0.0033 < \rho = 0.0084 < 0.75\rho_b = 0.0283$). This steel ratio allowed the addition of external reinforcement without causing premature brittle failure due to crushing of the concrete.

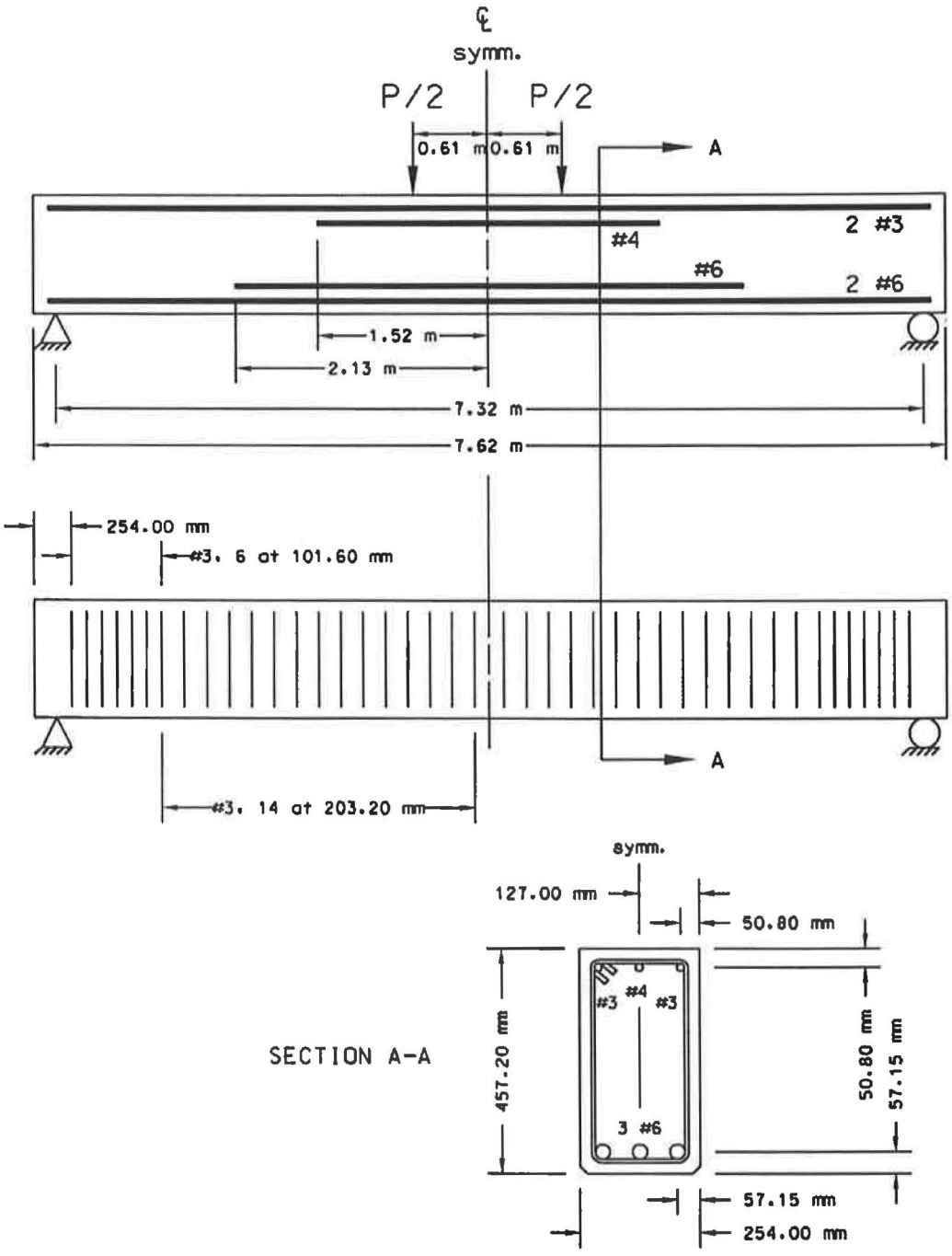

FIGURE 3.1. Beam Geometry, Flexural Reinforcement, and Applied Load

Shear reinforcement consisting of #3 closed stirrups spaced along the beam was used (see Figure 3.1). The beams were designed for twice the anticipated shear to avoid brittle shear failure with the increased load capacity of the strengthened beams. Also, the ends of each beam were designed for a roller bearing. The bearing, bolted directly to the beam, provided lateral stability during testing and allowed the beam to rotate freely through large deflections (see Figure 3.2).

The beam specimens were originally designed for fatigue tests. The reinforcement ratio was selected to create strain levels in the bottom reinforcement, at a load P=44.5 kN, approximately equal to maximum strain levels measured at maximum service loads in field tests of a simply supported reinforced concrete bridge.

Concrete Beam Fabrication

The beam specimens were manufactured by Sherman Prestressed Concrete in Pelham, Alabama and cast in steel forms. A batch plant on site produced the concrete used in the beams. The specified minimum 28-day compressive strength of mix design was 41.4 MPa with an early compressive strength of 27.6 MPa. The early strength allowed the beams to be moved within a few days after casting which in turn decreased the time of construction. In Table 3.1, a detailed description of the mix design is given.

A different batch of concrete was used for each beam, and six test cylinders (152 x 305 mm) were made for each batch. One cylinder was tested for early strength requirements, and two others were used by the beam

FIGURE 3.2. Beam Roller Bearing

TABLE 3.1. Concrete Mix Design

(a) Mix Proportions

Material	Description	Specific Gravity	Volume [m^3]	Weight [N]
Water	Potable	1.00	0.1195	1174
Cement	Citadel III	3.14	0.1087	3345
Limestone	#67	2.83	0.3248	9008
Sand	#100, Natural	2.62	0.1906	4893
Air	3%	0.00	0.0306	0

(b) Admixtures

Description	Dosage [Oz/Cwt]	[cc/N of cement]
400N (super)	14	0.9308
MBLVR (retd.)	4	0.2659
MBVR (air)	0.9	0.0598

(c) Mix Characteristics

Design Compressive Strength = 41.4 MPa
Water-Cement Ratio = 0.35
Sand-Coarse Aggregate Ratio = 0.35
Slump = 102 mm
Unit Weight = 23.7 KN/m^3

producer to verify that the minimum 28-day compressive strength of the beam was achieved. The remaining cylinders were stored with the beam to insure representative compressive strength. These cylinders were tested after all flexural load tests were conducted. The average compressive strength of the three cylinders was considered to be the actual concrete strength at the time of testing. In Table 3.2, the cylinder compressive strengths of each are given. The average compressive strength was 53.81 MPa, and no beam had a compressive strength more than 11% from the average.

Composite Plates

The composite plates used in all beam strengthening tests were 12K Unigraphite/E-77, two ply, Carbon Fiber Reinforced Plastic (CFRP) laminates manufactured by FiberCote Industries, Incorporated. The plates were manufactured with a peel ply fabric which was removed prior to use. Unigraphite fibers are oriented in one direction. In this study the fibers were oriented longitudinally, with 12,000 fibers per square inch (12K). The average cross-sectional dimensions of the plates were 1.25 x 152.40 mm. Ultimate tensile strength and modulus of elasticity were determined for standard tension test specimens of width 12.70 mm by FiberCote and found to be 1517 MPa and 128 GPa, respectively. The material's stress-strain relationship was linear-elastic to failure.

Three names or descriptors were given to the various plates used in beam testing: (1) primary plates which were bonded directly to the tension face of the beam; (2) splice plates which were bonded directly to the primary plates and

Table 3.2. Cylinder Compressive Strengths

Beam/Batch	1 Day Strength [MPa]	Testing Strength [MPa]
1	31.94	51.86
2	33.89	53.93
3	37.43	54.79
4	31.94	49.38
5	44.87[a]	59.50
6	38.65	53.61
7	36.82	52.63
8	44.51[a]	54.79

[a]Cylinder Strength at 3 Days.

used to bridge the gap, or butt joint, of two primary plates; and (3) dummy plates which were bonded directly to the primary plate, not at the butt joint. An illustration of the types of plates used during flexural strengthening tests are shown in Figure 3.3. The length of the plates used varied from test to test. Locations, lengths, and the reasons behind plate selection are discussed in detail in the following sections and in Chapter Five.

Adhesive Selection

Based on previous research and on the recommendation of one of the leading structural adhesive manufactures (Hysol®), EA9460 two component epoxy was selected. EA9460 was chosen for it's high peel strength, excellent shear strength properties, and its ability to bond dissimilar substrates.

The EA9460 is a two part epoxy with a mix ratio of 1:1 by volume or weight which has a long work life of 40-50 minutes and can be cured at room temperature. Tensile lap shear test on 25.40 mm wide by 25.40 mm overlap specimens at 12.70 mm per second on bonded plastic substrates were conducted by the manufacture. The results indicated a lap shear strength of 13.79 MPa with fiber tear failure controlling.

Splice Plates

Splice plate lengths where designed according to lap shear strength provided. Two lengths were used in the beam tests performed. The splice plate lengths used were 609.60 mm and 914.40 mm, centered over the butt joint of two primary plates, which provided lap areas of 46452 mm^2 and 69677 mm^2,

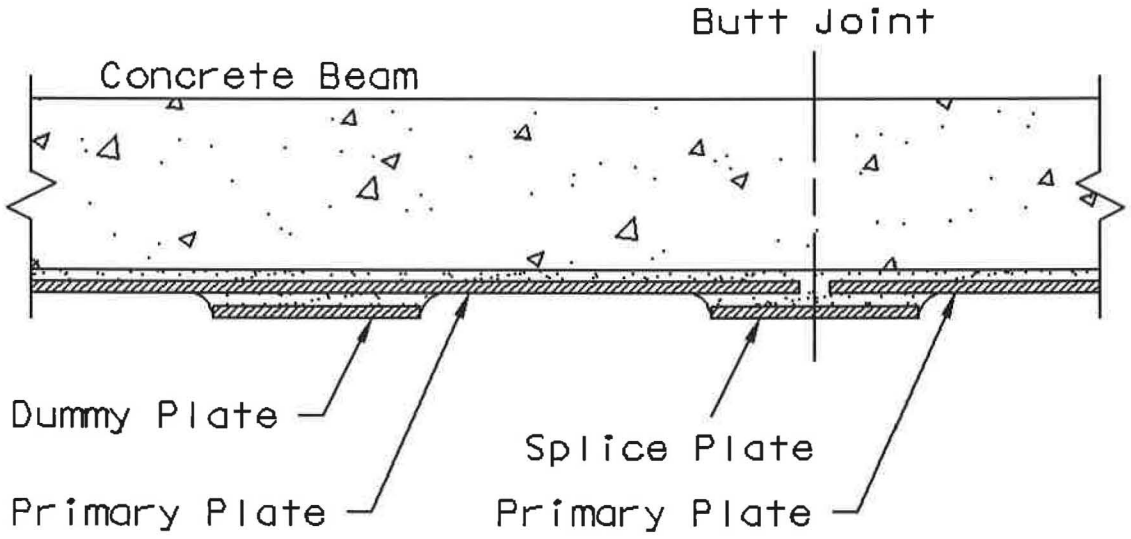

FIGURE 3.3. Plates Used During Flexural Strengthening Tests of Concrete Beams

respectively. The shear capacity of the adhesive, for the two splice plate lengths selected, exceeded twice the average shear stress required to reach the ultimate tensile strength of the plate.

Bonding of CFRP Plates to Beams

All plates used in beam strengthening (i.e. primary plates, splice plates, and in some cases dummy plates) were bonded simultaneously. Bonding all plates at one time insured a good continuous bond between the plates and the concrete surface. The technique applied and described herein was based on a vacuum bag system utilizing standard vacuum bag materials and hardware.

Prior to bonding the CFRP plates to the extreme tension face of the beams, the concrete surface was prepared by sand blasting to remove all loose fragments or particles resulting from fabrication. The surface was then washed with a cleaning detergent and a coarse brush. After the appropriate plate lengths where selected the bonding surfaces of the beam and CFRP plates were washed down with a degreasing agent, Methyl Ethel Ketone (MEK). Once the beam and plates were ready for bonding, the two part adhesive was mixed by weight with a electric hand held mixing tool and applied to the CFRP plates with a 3.2 mm grooved trowel. The application of the adhesive, with the trowel, was done perpendicular to length of the plates which in turn created groves for trapped air to escape during the vacuum process. By applying the adhesive in this fashion, the amount of air pockets created between the two bonding surfaces was reduced.

After all plates were pressed into position with a hand held roller, the vacuum system was placed around the beam (see Figure 3.4). The system consisted of two layers of a bag release film, one layer of an air weave which allowed the vacuum to propagate along the beam surface, four vacuum valves spaced equidistant along the beam, and hoses attached to the vacuum valves and then to a vacuum tank. Adhesive tape sealed the outer layer of the bag release film at the top and ends of the beam. All beams where sealed at the top to prevent vacuum leakage through flexural cracks formed during crack tests. A 5 HP portable vacuum pump was attached to the vacuum tank. The use of the vacuum tank allowed for immediate and substantial air volume decrease in the system as soon as the valves were open. A vacuum gage attached to the tank and vacuum bag provided pressure readings during the curing time of the adhesive. The average vacuum pressure obtained by the system for each specimen was approximately 94 KPa.

After the CFRP plates were put under vacuum, the adhesive was allowed to cure for 8 hours. The vacuum was then removed, and the adhesive was allowed to cure for a minimum of 72 hours before tests were conducted.

Instrumentation and Data Acquisition

The instrumentation used for all tests consisted of electrical resistance strain gages, for measuring steel reinforcement, CFRP, and concrete surface strains at various locations in and on the beam. Linear Variable Differential Transformers (LVDTs) were also employed for measuring vertical deflections as

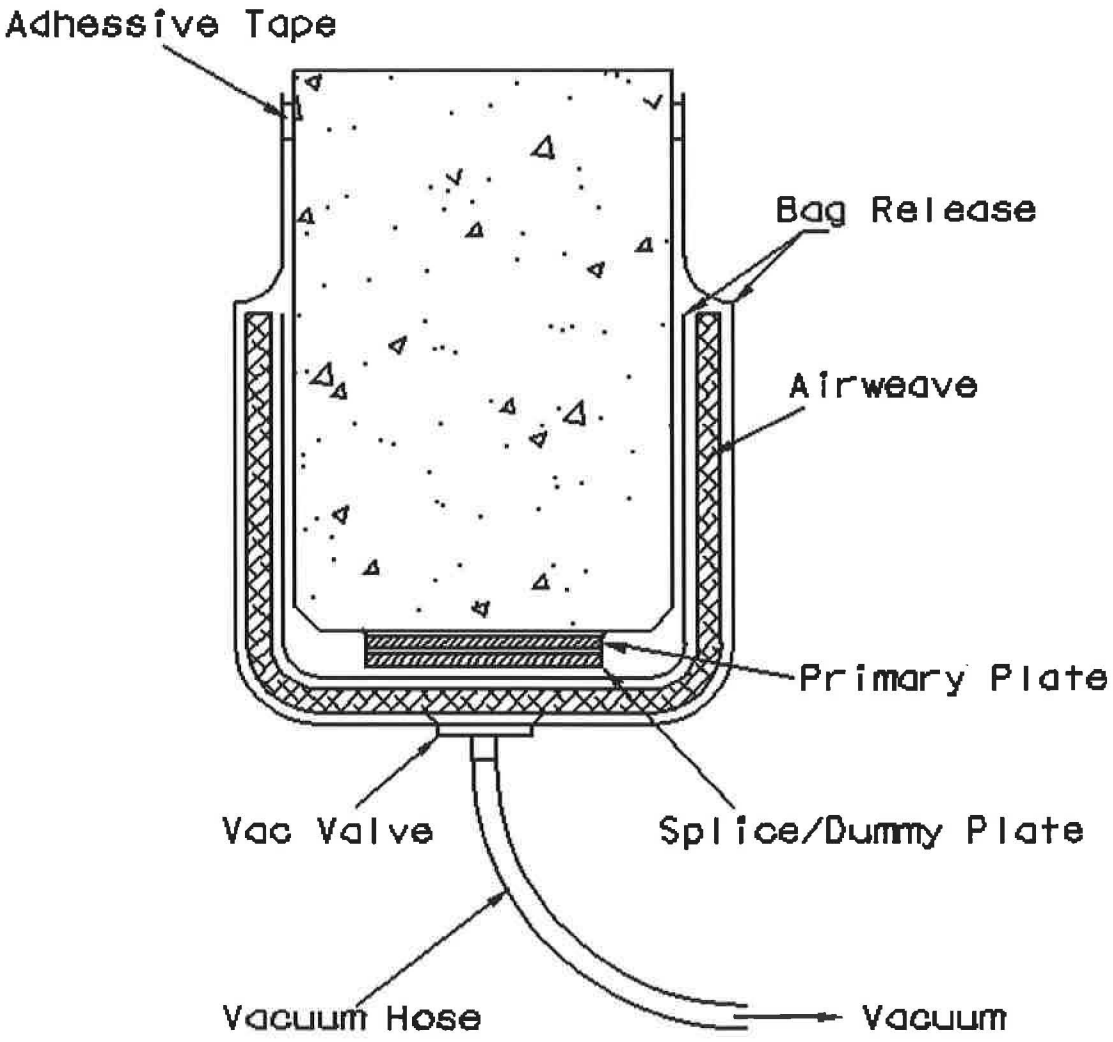

FIGURE 3.4. Vacuum System Used in Application of CFRP Plates

well as longitudinal surface strains at midspan. A hydraulic actuator or ram, with built in load and displacement transducers connected to a electronic controller, was used for load application and ram displacement readings.

The strain gages were self temperature compensating foil gages with polyamide encapsulation and pre-attached wires. All gages used in each test had a nominal resistance of 350 ohms. CFRP surface, rebar, and concrete strain gages had a gauge length of 12.70 mm, 3.18 mm, and 76.20 mm respectively. All gage factors varied from 2.0 to 2.1. Instrumented bars were used to measure longitudinal steel strains at midspan and, for Beams 1 through 4, at a section 1067 mm off-midspan. Two gages were applied to the #6 and #4 instrumented reinforcing bars. The gages were spaced approximately 25.40 mm apart and 12.70 mm off midspan. At the off-midspan location, two gages measured top and bottom reinforcement strains. Each gage was coated with clear silicon rubber and protected with neoprene pad with adhesive backing. Lead wires, attached to the gages, were directed along the top reinforcing steel and extended out of the beam approximately 1.5 m off-midspan, and were protected at the beam surface by clear plastic tubing. Steel reinforcing gage locations and the water proofing technique as well as off-midspan lead wire exit are shown in Figure 3.5.

The LVDTs used for measuring vertical deflections had a dynamic measurement range of approximately +/- 25.4 mm. They were held in place with adjustable clamps attached to a vertical rod welded to a moveable base on the floor. The vertical rod allowed the LVDTs to be adjusted during each test as

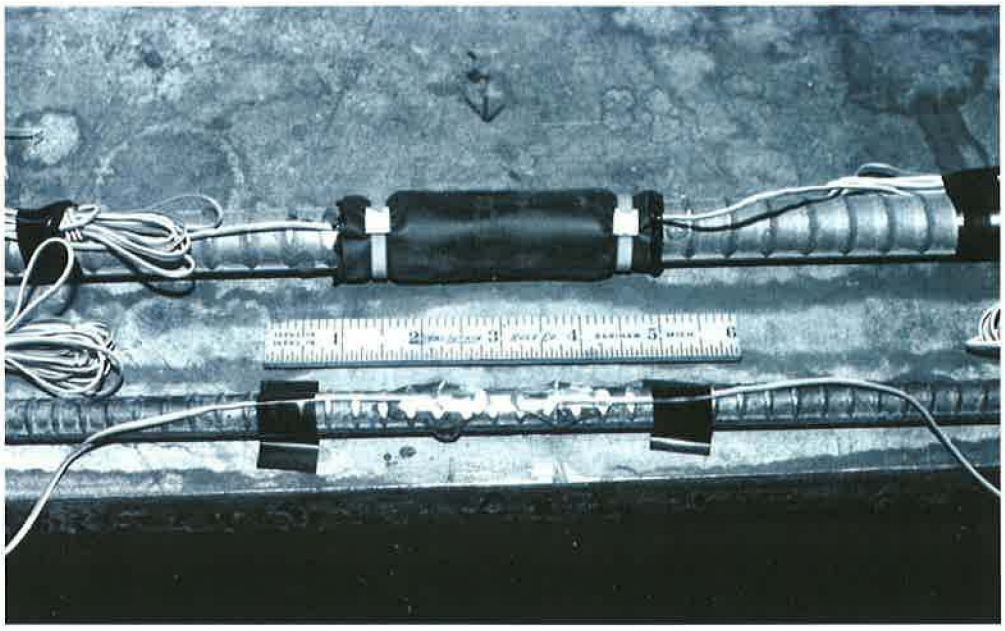

(a)

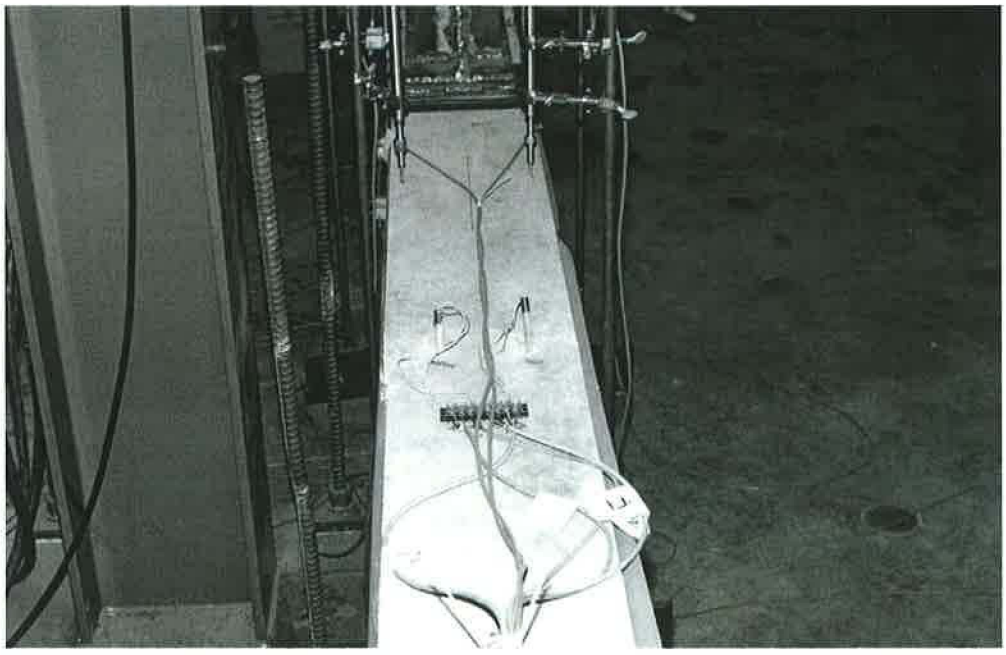

(b)

FIGURE 3.5. (a) Steel Reinforcement Gage Locations and Water Proofing Technique; (b) Off-Midspan Lead Wire Exit

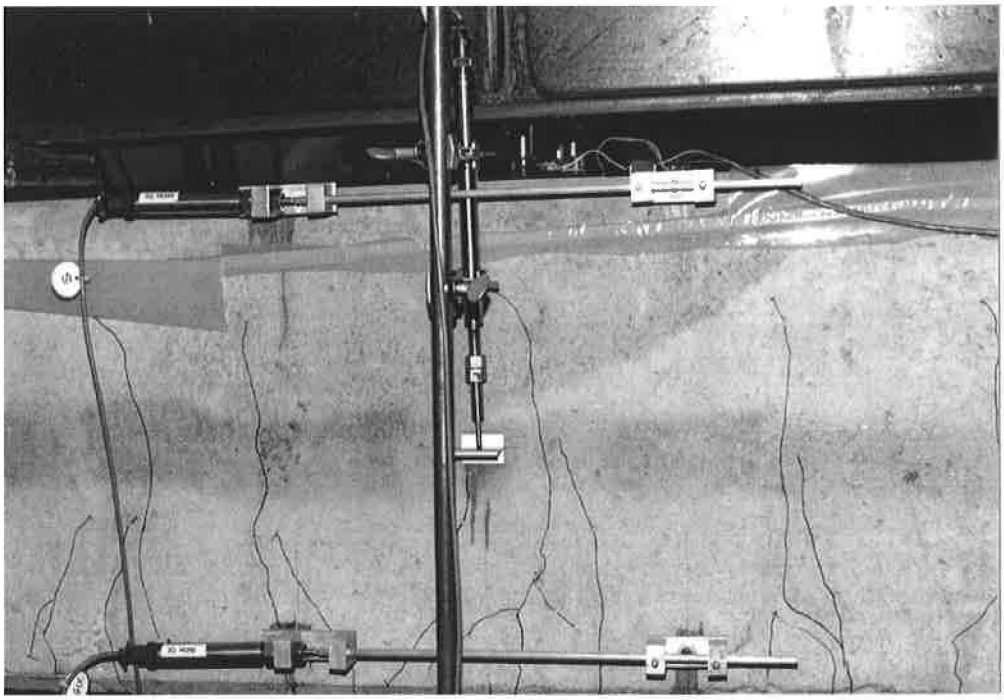

FIGURE 3.6. LVDT Surface Strain Apparatus at Midspan

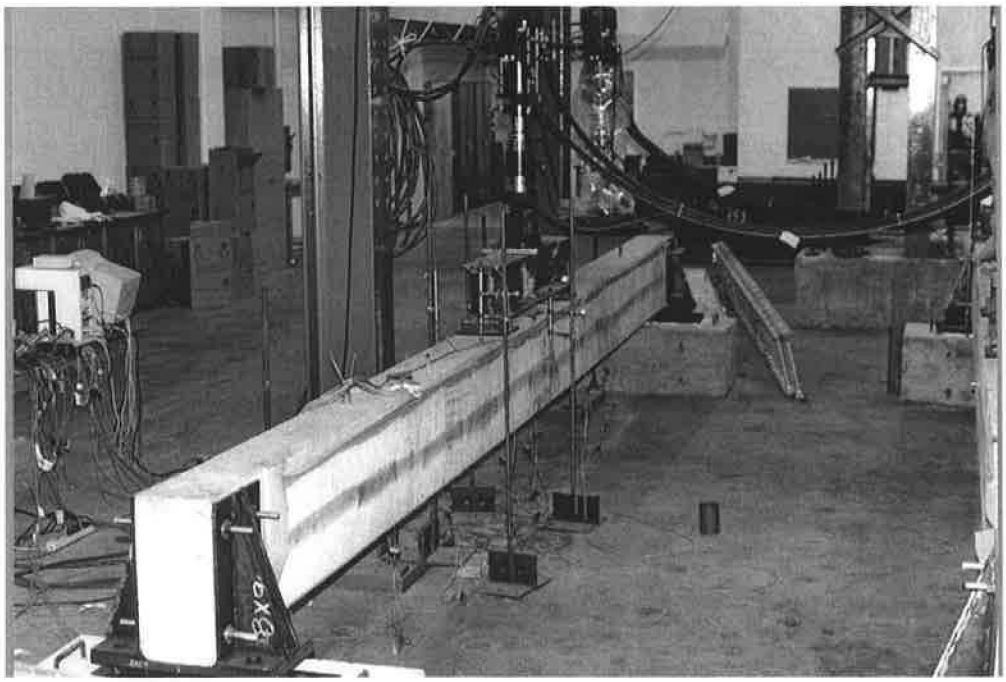

FIGURE 3.7. Typical Beam During Testing

beam deflections exceeded the measurement range of the instrument. The LVDTs used for surface strain measurements had a dynamic measurement range of approximately +/- 6.35 mm. For surface strain measurements, an aluminum apparatus was designed to measure the relative displacement of two points, oriented parallel to the longitudinal axis of the beam, over a gage length equal to the depth of the member, 400 mm. For all tests, surface strain measurements at midspan were taken at the top surface of the beam and the depth of the tension steel. Surface strain readings from the LVDTs at these locations were only used when foil gages reading similar data failed (i.e. bottom steel and top concrete surface strain gages). In Figure 3.6, a photograph of the LVDT surface strain apparatus at midspan is shown.

A photograph of a typical beam taken during testing is shown in Figure 3.7. For load application, a 222 kN capacity ram was used. A full bridge force transducer with a 500 kN capacity along with a LVDT built into the actuator provided precise load and displacement readings during all test. The applied load was transmitted to the beam through a 609.60 mm long stiffened W-section spreader beam. Two 177.80 x 203.20 mm steel plates were welded to the ends of the spreader beam and placed on neoprene pads on the top surface of the specimens to create the two point loading.

Test data were collected using a MEGADAC data acquisition system and a 486-33 personal computer with compatible software (OPTIM (1994)). For various test performed, 6 to 28 channels were used for recording strain gage data. For all tests, 4 channels were used for LVDT vertical deflection data,

2 channels for LVDT surface strain data, and 2 channels were connected to the electronic controller for ram load and displacement data. Additional channels were employed for CFRP and concrete surface strain data. All data recorded by the MEGADAC was automatically transferred to the hard drive of the personal computer. Function keys were used to control the data collection. All data was collected at a sample rate of 25 samples/second/channel.

Data Reduction

Data collected during all tests were processed by the data acquisition system and then transferred to the personal computer hard drive. After each test, backup files where created on a magnetic tape to reduce the amount hard drive disk space taken by the large data files. DADISP (1995) data reduction software, compatible with OPTIM software, assisted in the unit conversions, creation of plots, calculations, and peak strain readings.

CHAPTER FOUR

ANALYTICAL ANALYSIS

Introduction

Reinforced concrete beams are commonly designed using methods and specifications defined by the ACI 318 (ACI 1989) to insure the failure mode is ductile (i.e. results from yielding of the steel reinforcement). Compression failure of the concrete is proceeded by yielding of the steel reinforcement where the area of steel ratio is below a limiting value ($\rho \leq 0.75\rho_b$). The analysis of beams, in accordance to ACI 318, is a fairly simple procedure. Assuming the tension steel yields, and a uniform compressive stress distribution in the concrete equal to 0.85f'c, the strength of the beam can be calculated. For reinforced concrete beams strengthened with Carbon Fiber Reinforced Plastics (CFRPs), the analysis is not as simple. This is because the CFRP remains linear-elastic to failure. The ACI procedure must be discarded in favor of an alternate approach for analyzing beams strengthened with CFRP. The following procedure was developed for doubly reinforced concrete beams strengthened with a unidirectional CFRP plate/s. The procedure is based on force equilibrium at incremented strain levels at the extreme compression face of the concrete. A similar procedure is described by Chajes et al. (1994).

Assumptions

In the development of the analytical procedure, the following assumptions are made concerning the behavior of the beam and CFRP plate/s: (1) plane sections before bending remain plane after bending; (2) stress-strain relationships for all materials are known; (3) no slip between the longitudinal steel and concrete; (4) the adhesive bond between the CFRP plate and concrete beam as well as between CFRP plates is rigid; (5) no shear failure of the concrete adjacent to the bonded CFRP plate; (6) concrete has no tensile capacity; (7) maximum strain in the concrete in compression is 0.003 as specified in ACI 318; and (8) no axial compression is produced by the end bearings.

Analytical Method

The analytical procedure described herein is based on equations derived from theoretical moment-curvature relationships presented in Park and Paulay (1975). The method requires that all cross-sectional dimensions are known as well as the material's stress-strain relationships. The steel rebar is assumed to behave linearly elastic-perfectly plastic where the steel stress (f_s) is given by

$$f_s = E_s \varepsilon_s \quad for\ 0 \le \varepsilon_s < \varepsilon_y \tag{3.1}$$

and

$$f_s = f_y \quad for\ \varepsilon_y \le \varepsilon_s \tag{3.2}$$

where E_s is the elastic modulus of the steel, ε_s is the strain in the steel, and f_y and ε_y are the yield stress and strain of the steel, respectively. The assumption is made that concrete or CFRP fiber failure will occur before tensile fracture of the steel. The specified yield strength of all the rebar used in lab experiments was 414 MPa, with a modulus of elasticity of 200,000 MPa.

The CFRP plate/s used in lab experiments were modeled as linear-elastic to failure. The tensile stress in the plate/s (f_f) is given as

$$f_f = E_f \varepsilon_f \quad \text{for } 0 \le \varepsilon_f < \varepsilon_{fu} \tag{3.3}$$

where E_f is the elastic modulus of the plate, ε_f is the plate strain, and ε_{fu} is the ultimate strain of the CFRP plate. The ultimate stress and modulus for 12K-Unigraphite/E-772 CFRP utilized in lab experiments are 1,517 MPa and 127,691 MPa, respectively.

For the concrete, the modified Hognestad idealized stress-strain relationship was used. This relationship shown in Figure 4.1, consists of a parabola followed by a sloping line, both of which can be described by the following equations:

$$f_c = f_c'' \left[\frac{2\varepsilon_c}{\varepsilon_o} - \left(\frac{\varepsilon_c}{\varepsilon_o} \right)^2 \right] \quad \text{for } 0 \le \varepsilon_c < \varepsilon_o \tag{3.4}$$

and,

$$f_c = f_c'' \left[1 - \frac{0.15}{0.003 - \varepsilon_o} (\varepsilon_c - \varepsilon_o) \right] \quad \text{for } \varepsilon_o \le \varepsilon_c < 0.003 \tag{3.5}$$

where

$$f_c'' = k_3 f_c'$$

$$\varepsilon_o = 2 f_c''/E_c$$

$$k_3 \approx 0.93 \quad \text{for } f_c' \ge 48 \quad \text{[MPa]}$$

$$E_c = 4730 \sqrt{f_c'} \quad \text{[MPa]}$$

in which f_c is the stress in the concrete, f_c' is the cylinder strength, f_c'' is the maximum compressive stress reached in the concrete, k_3 is a strength reduction factor, ε_c is the strain in the concrete, ε_o is the strain at maximum stress in the concrete, ε_{cu} is the maximum strain in concrete at failure (taken to be 0.003 in this analysis), and E_c is the elastic modulus for concrete. The concrete cylinder strength for each beam is tabulated in Chapter Three (Table 3.2).

For a cross section, as shown in Figure 4.2, a procedure was designed and implemented for computer application. The procedure determines the moment-curvature relationship and strain levels at any location in the cross-

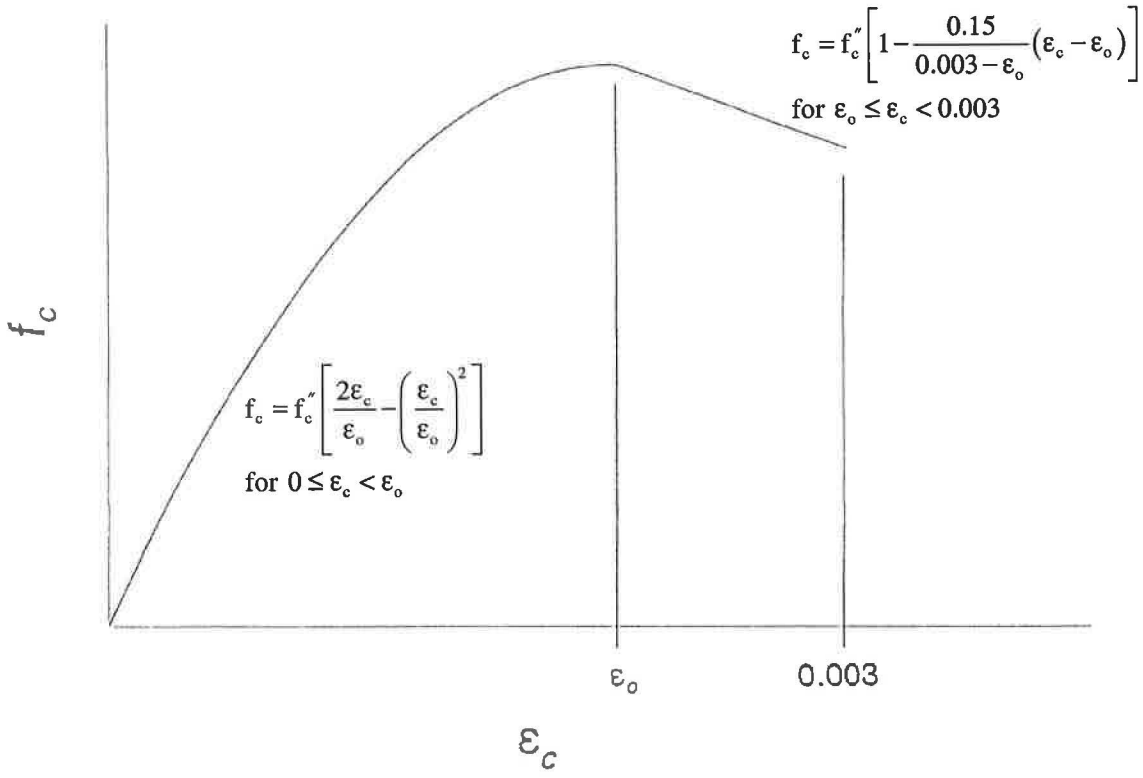

FIGURE 4.1. Hognestad Idealized Stress-Strain Relationship

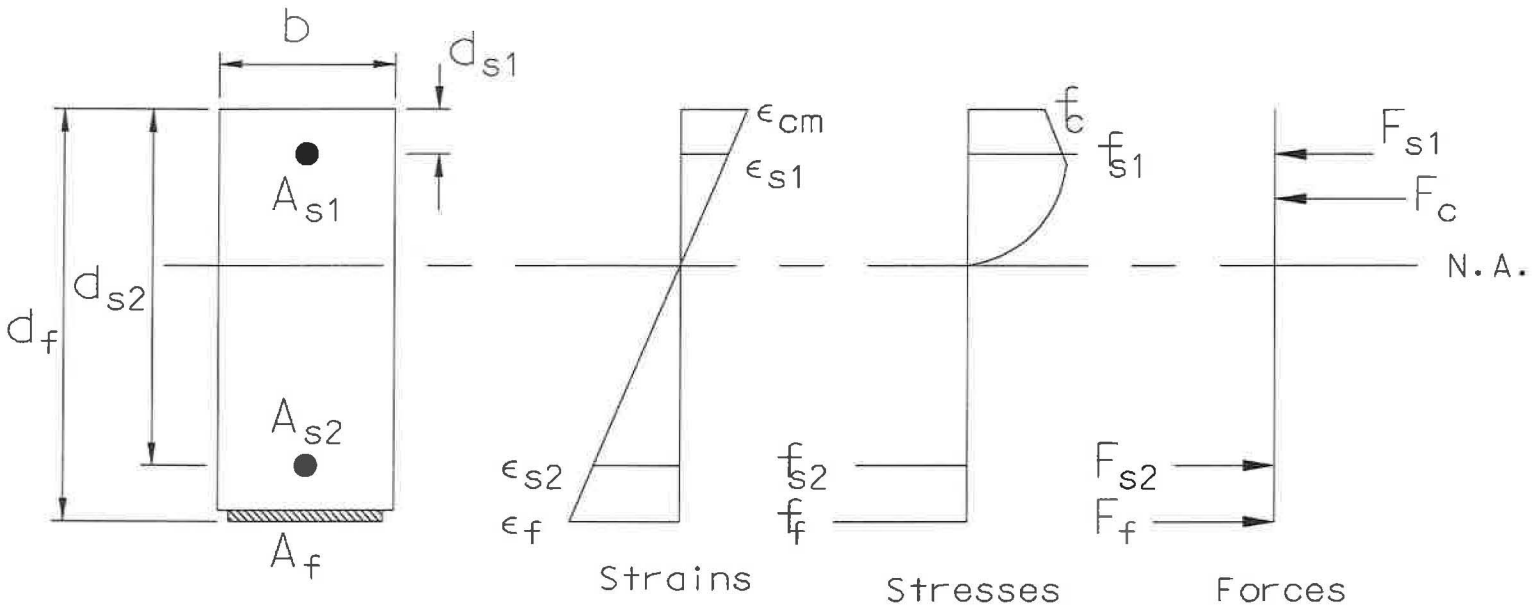

FIGURE 4.2. Internal Strain, Stress, and Force Distribution Through a Cross-Section of the Beam

section. To determine the moment-curvature relationship, the strain level at the extreme compression fiber of the concrete is incremented from 0 to ultimate ($\varepsilon_{cu} = 0.003$) at a set interval. At each value of extreme fiber strain, equilibrium is used to locate the neutral axis and the internal resisting moment and curvature are calculated. For each increment of extreme fiber strain, the stress-strain relationships of the preceding increment are assumed to apply and a derived quadratic equation is solved for force equilibrium, and the depth of compression (neutral axis location) are calculated. This avoids trial and error methods which are difficult to code and can be computationally intensive. After the neutral axis location is calculated, the reinforcement strains are recalculated and the assumptions are checked (i.e. steel before and after yielding). If the assumed stress-strain relationship is incorrect, the quadratic equation is updated and the neutral axis location is recalculated. Once the neutral axis is located, the strain at any depth can be determined by similar triangles. The resisting moment is calculated by summing moments of the force resultants about the neutral axis. The curvature of the section is calculate by dividing the extreme fiber strain of the concrete by the depth to the neutral axis. Failure of the beam is assumed to occur when either the concrete reaches its maximum compressive strain ($\varepsilon_{cu} = 0.003$) at the extreme compression fiber or the CFRP reaches its ultimate tensile strain capacity (ε_{fu}). A computer program was developed with the procedure previously mentioned. The program with definitions of all variables used is listed in Appendix A.

In Figure 4.3, typical theoretical moment-curvature relationships for beam test specimens with and without an applied CFRP primary plate are shown. The plot indicates a substantial increase in ultimate capacity of beams with bonded CFRP primary plates. The plot also shows a decrease in curvature ductility ($\phi u/\phi y$) which coincides with the increased strength. In Figure 4.4, a typical primary plate strain-moment relationship for a continuous plate bonded to the extreme tension face of the beam is shown.

Bending moment capacities at first yield of the steel tension reinforcement and at ultimate failure were calculated for the concrete strengths of each of the beam test specimens. These results are listed in Table 4.1. As shown in Table 4.2, application of the CFRP primary plate produces an increase in theoretical moment capacity of 87 percent and an increase in yield moment of 20 percent.

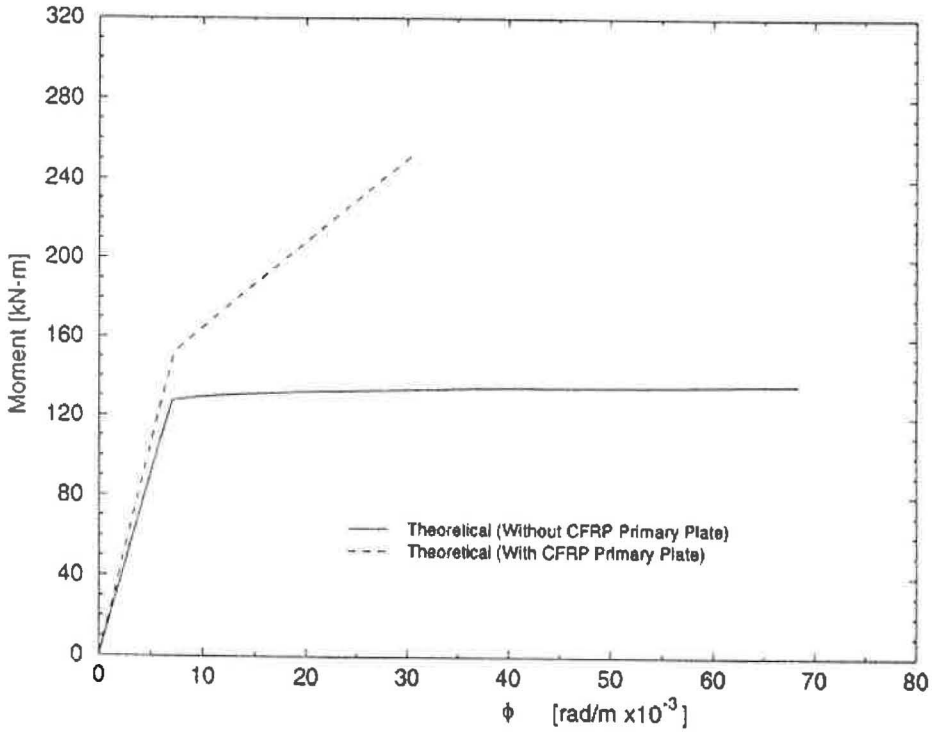

FIGURE 4.3. Typical Theoretical Moment-Curvature Relationships for Beams With and Without an Applied CFRP Primary Plate

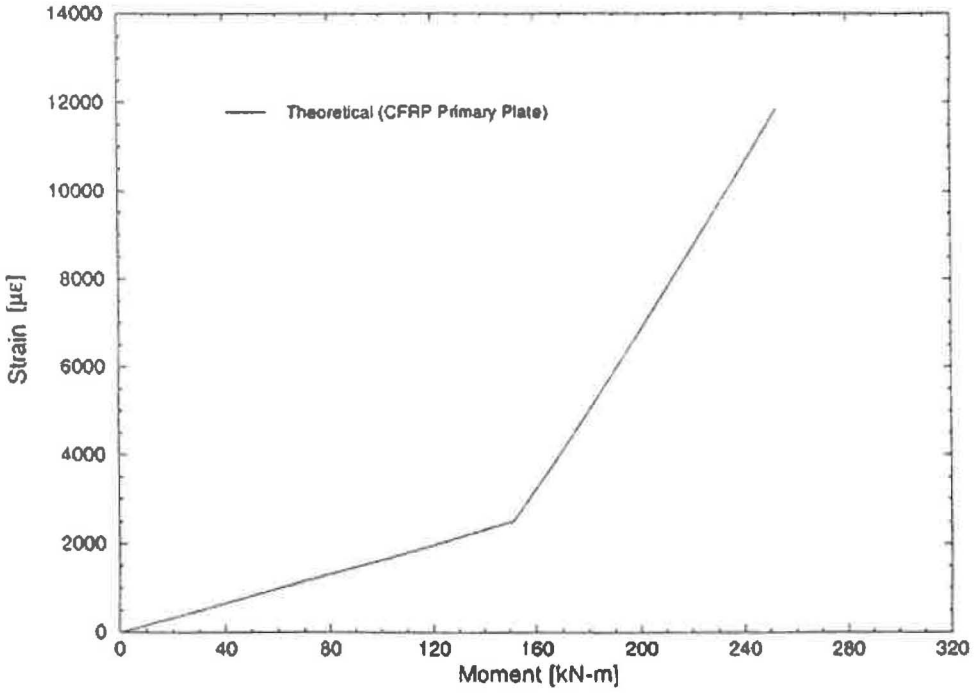

FIGURE 4.4. Typical Theoretical CFRP Primary Plate Strain-Moment Relationship

TABLE 4.1. Results of Theoretical Analysis

Beam	Yield Moment [kN-m]		Ultimate Moment [kN-m]	
	No CFRP	With CFRP	No CFRP[a]	With CFRP[b]
1	127	152	136	254
2	127	152	136	254
3	126	151	136	254
4	127	151	135	253
5	126	152	137	255
6	127	152	136	254
7	126	151	136	254
8	126	151	136	254

[a]Concrete crushing failure.
[b]CFRP Primary Plate tension failure.

TABLE 4.2. Theoretical Average Percent Differences in the Beams With and Without CFRP Primary Plates.

Percent Increase in Yield Strength	20
Percent Increase in Ultimate Strength	87

CHAPTER FIVE

CRACK TEST

Introduction

To provide a better understanding of the behavior of bonded Carbon Fiber Reinforced Plastic (CFRP) primary/splice plates on existing damaged concrete bridge girders, six of the eight beams (Beams 1-4,5,7) were loaded to create significant flexural cracking before the CFRP was applied. Here the test loading used to create the flexural cracking is referred to as a "Crack Test". Details of the Crack Tests and results are provided in this chapter. Two beams (Beams 6 and 8) were left untested and uncracked prior to application of the CFRP and were used as control specimens for comparison of CFRP primary/splice plate performance for uncracked versus pre-loaded beams.

Instrumentation, test procedure, and results for all beam specimens are presented in this chapter. To check the validity of the analytical method for predicting beam behavior, comparisons between experimental and theoretical data are made.

Instrumentation

Two instrumentation schemes were used for collecting test data. In the first scheme, as shown in Figure 5.1, Beams 1 through 4 were instrumented at

two locations, at midspan and 1067 mm off midspan. At midspan, two gages (CN1 and CS1) measured concrete strains on the top surface of the beam, two gages (T1 and T2) measured steel strain at the level of the top reinforcement, and two gages (B1 and B2) measured the steel strain at the level of the tension reinforcement. Vertical deflections were measured on each side of the beam, at mid-height, with two LVDTs (LVDT_N1 and LVDT_S1). This position allowed clearance form the load spreader beam over midspan. Strain measurements were also made using LVDT's mounted on one side of the beams near the top and at the level of the tension reinforcement. Each LVDT was mounted to measure the change in length over a gage length equal to the effective depth of the member.

At the second location, 1067 mm off midspan, two concrete gages (CN2 and CS2) measured the concrete strain on the top surface, and two steel gages (T3 and B3) measured strains at the level of the top and bottom steel reinforcement. The vertical deflection at this location was also measured with two LVDTs positioned at the top of the beam (LVDT_N2 and LVDT_S2). For the second scheme, Beams 5 and 7 were instrumented similarly at midspan, but gages CN2, CS2, T3, and B3 at the section 1067 mm off midspan were omitted. The instrumentation schemes described were consistent for all series of tests (i.e. Fatigue and Ultimate Load Tests). Although Crack Tests were not preformed on Beams 6 and 8, the instrumentation scheme was the same as that of Beams 5 and 7 in subsequent testing.

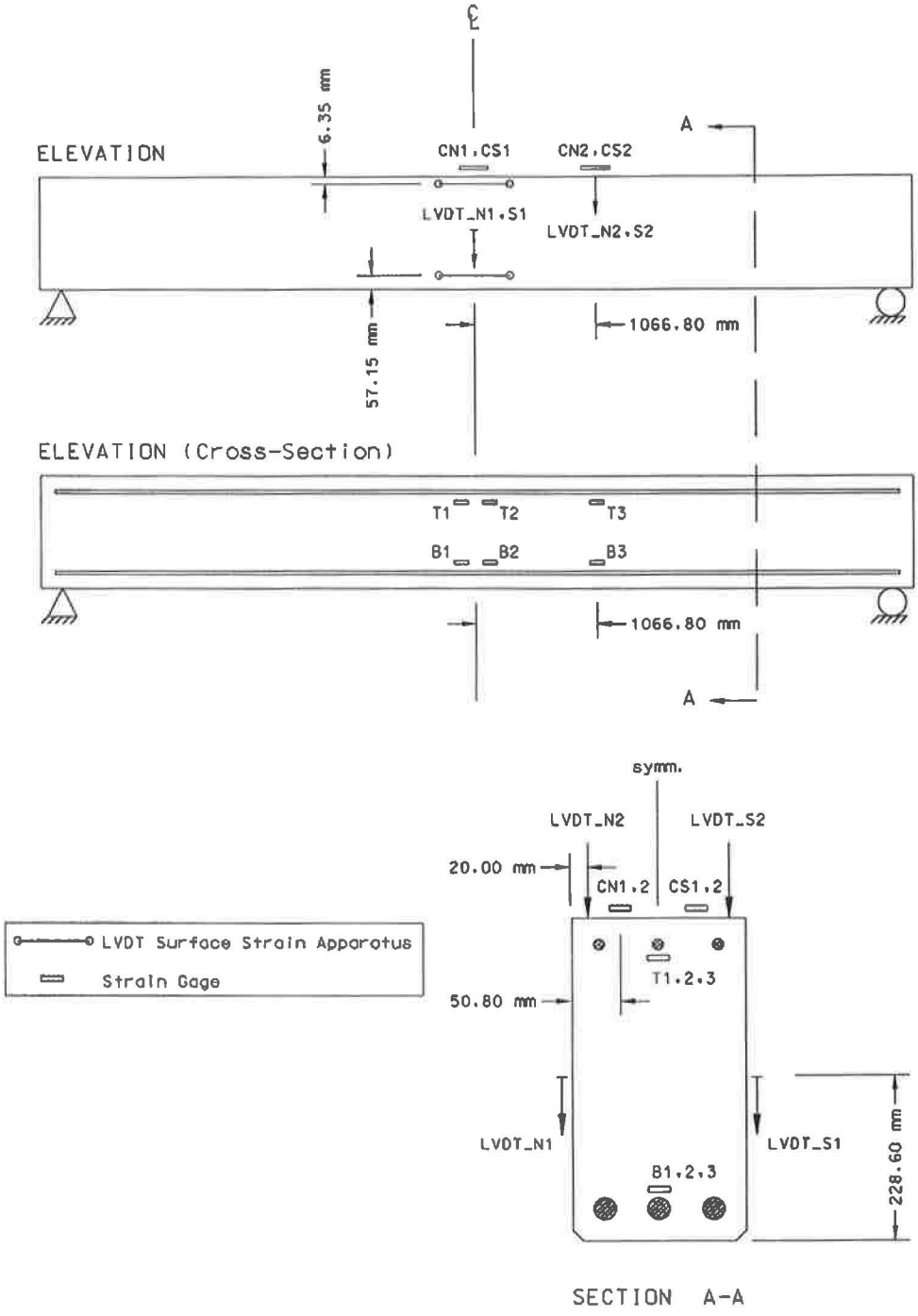

FIGURE 5.1. LVDT and Strain Gage Locations

To obtain accurate and comparable results for all series of tests, the following procedures were used for data reduction. At both instrumented cross sections, the average of the two readings of LVDT deflection as well as those for concrete strain at the top of the beam were used. For reinforcement strains at the top and bottom steel locations at midspan, data from the gage producing the largest overall strain was taken to be the steel strain. Curvature calculations were made using the sum of the top concrete and bottom steel strain data divided by the depth of the member. It should be noted however, that due to the failure of both bottom steel gages during the Crack Test of Beam 4, strain data from the LVDT's at the level of the tension reinforcement was used for curvature calculations for all subsequent series of Beam 4 tests.

Test Procedure

Before load was applied to each test specimen, all instrumentation was initialized. In the initial phase of the Crack Test, the beam was loaded in displacement increments with data provided by the ram's internal LVDT. The displacement increments selected were initially based on preliminary load and displacement calculations of first crack and first yield. The increments were refined slightly for subsequent tests based on an increased knowledge of beam behavior. A typical test began with displacement increments of 2.54 mm up to and just beyond the first sign of cracking. Next, the increments were increased to 5.08 mm and then reverted to 2.54 mm before the anticipated yield point was reached. At 2.54 mm increments, the beam was then loaded to approximately 8.00 mm beyond the first sign of yielding. The additional displacement insured a

well defined crack pattern with openings typical of damaged girders seen in the field. Data collected at the end of each displacement increment and plotted on graph paper was used to aid in the identification of critical points (i.e. first crack and first yield). With the aid of bright lights, all visible cracks were marked at this time.

After the maximum desired deflection was reached, the beam was then unloaded to a deflection of 22.86 mm. Using this deflection as a starting point, five cycles of loading to a maximum displacement of 35.56 mm were applied. The load cycles were applied to more clearly develop the flexural cracks and dislodge any loose concrete which might have been produced during the initial loading.

After the five load cycles, the beam was unloaded. Approximately 24 hrs after testing, allowing time for the beam to rebound completely, LVDT residual deflection data were collected. All Crack Tests were reasonably identical with the exception of Beam 1. In this case, the beam was initially loaded in displacement increments just prior to the yield point. The test was stopped prematurely and unloaded because it was unclear whether the yield point was reached. The beam was reloaded in a second test to the desired deflection beyond first yield. Some residual deflection was evident after first loading and was accounted for in the data reduction.

Results

A typical plot of the load-deflection relationship, at midspan, for the initial static loading of each beam can be seen in Figure 5.2. The three dashed

sloping lines, connecting the minimum points at the end of each deflection increment, represent the stiffness or the true static load response at various load stages. Each stage can be defined by the following: (1) before initial cracking; (2) after cracking or service load range; and (3) after first yield. The load and deflection, at first yield for each test specimen, were determined by the intersection of slopes (2) and (3). The plot also illustrates the extent of displacement beyond first yield. The load-deflection behavior during the cyclic loading was also investigated (see Figure 5.3). The dashed line in Figure 5.3, represents the service load stiffness for the damaged beam after the initial static loading. In Table 5.1, the experimental displacement, load, and moment at first yield for each test specimen is listed. In addition to experimental results, theoretical yield moments are presented as well as the percent differences between the two. From the results, an average percent difference of -0.8 was calculated.

The service load stiffnesses for each test specimen are listed in Table 5.2. From the results, an average stiffness of 1.90 kN/mm was calculated for the initial static loading beyond the cracking moment (stage 2 in Figure 5.2). For the cyclic loading, the average service load stiffness was 2.73 kN/mm. The results of the two loadings indicate that the stiffness from the cyclic loading was significantly larger than the stiffness from the initial static loading.

The effects of loading the beams to first yield are illustrated by the maximum and residual deflections obtained. In Table 5.3, those results are presented. The consistencies obtained for each test specimen resulted in similar

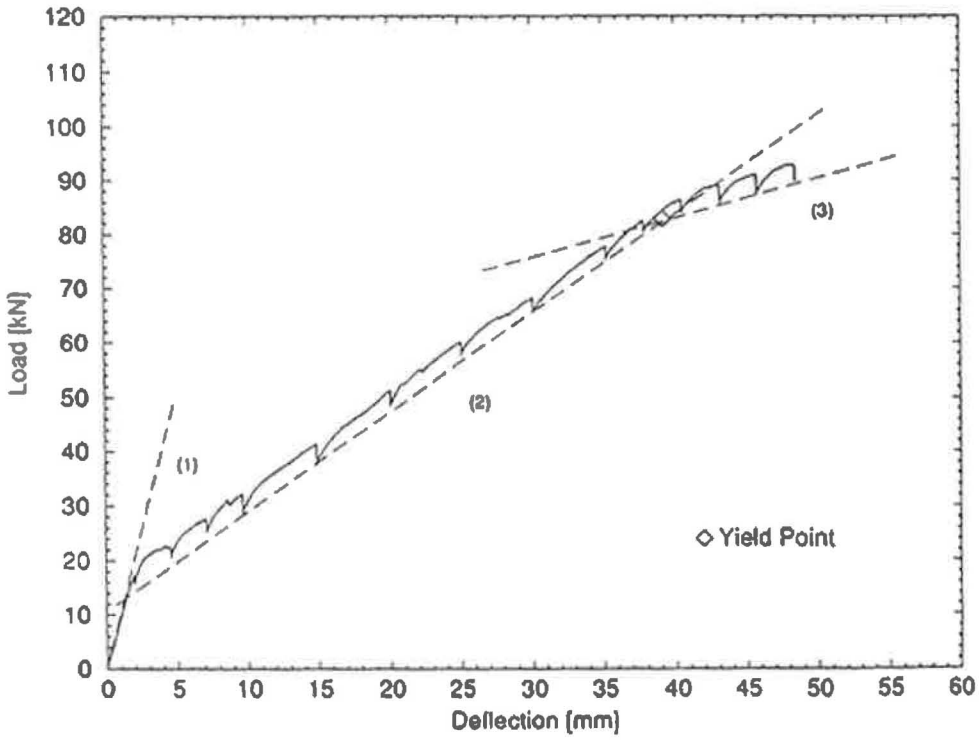

FIGURE 5.2. Typical Load-Deflection Relationship at Midspan During Initial Loading

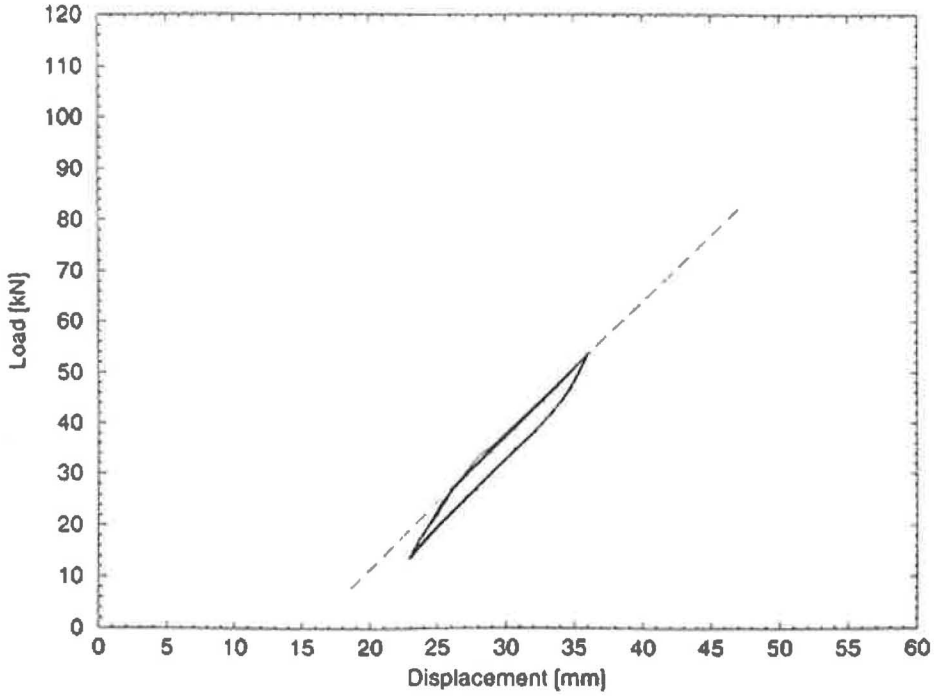

FIGURE 5.3. Typical Load-Deflection Relationship at Midspan During Cyclic Loading After Initial Damage

TABLE 5.1. Experimental and Theoretical Results at First Yield for Crack Test

Beam	Experimental			Theoretical	Moment Percent Difference
	Displacement [mm]	Load [kN]	Moment [kN-m]	Moment [kN-m]	
1	37[a]	82[b]	125[b]	127	-1.6
2	37	84	128	127	0.8
3	38	82	125	126	-0.8
4	40	82	125	127	-1.6
5	39	81	123	126	-2.4
7	39	83	127	126	0.8

[a]Data reflects beam behavior during the second test plus residual data from first.
[b]Data reflects beam behavior during the second test.

TABLE 5.2. Service Load Stiffness from Crack Test

Beam	Stiffness Initial Static Loading [kN/mm]	Stiffness Cyclic Loading [kN/mm]
1	2.07[a]	2.65[b]
2	2.00	2.90
3	1.87	2.78
4	1.80	2.67
5	1.83	2.74
7	1.83	2.64

[a]Service load stiffness of first test.
[b]Service load stiffness of second load test (cyclic loading).

crack distributions. In Figure 5.4, a typical crack pattern after testing is illustrated.

Moment-curvature and bottom steel strain-moment relationships, at midspan, were also investigated. Typical plots of experimental data along with theoretical results can be seen in Figures 5.5. In the figures, distortion in data following the yield moment was attributed to the relative position of crack sections to instrumentation. Although the true behavior of the beams after first yield was not established, the results shown in Figure 5.4 indicate the ability of the computer program of Appendix A to reasonably predict steel reinforcement and beam behavior up to the yield moment. Some of the discrepancies seen in the plots can be attributed to theoretical assumption that the concrete has no tensile capacity.

TABLE 5.3. Maximum Deflections from Crack Test and Residual Deflections After 24 Hours

Beam	Maximum Deflection [mm]	Residual Deflection [mm]
1	47[a]	13
2	45	15
3	46	16
4	45	15
5	49	17
7	49	17

[a]Data reflects beam behavior during the second test plus residual deflection from the first.

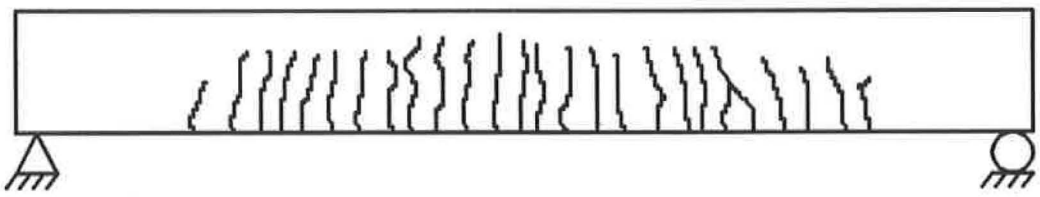

FIGURE 5.4. Typical Crack Pattern After Crack Test

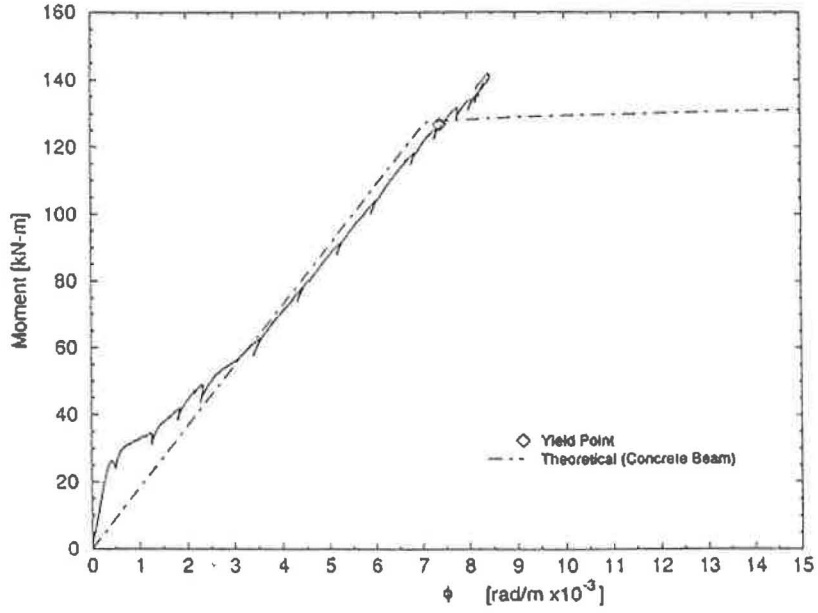

(a)

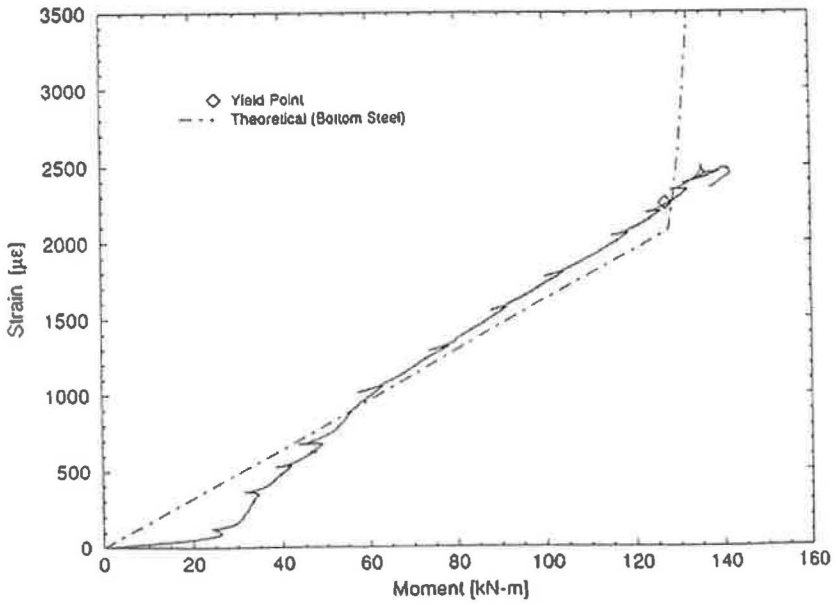

(b)

FIGURE 5.5. (a) Typical Experimental and Theoretical Moment-Curvature Relationships (Crack Test); (b) Typical Experimental and Theoretical Bottom Steel Strain-Moment Relationships (Crack Test)

CHAPTER SIX

FATIGUE AND ULTIMATE LOAD TESTS

Introduction

The previous chapter provided important information on the preliminary tests which were conducted on six of the eight beam specimens. These tests were preformed in order to simulate damage in overloaded concrete girders, as seen in the field, to deduce whether or not the performance of such beams can be enhanced with application of Carbon Fiber Reinforced Plastic (CFRP) primary and splice plates. In this chapter, results from tests of the six damaged and two undamaged beams strengthened with CFRP primary and splice plates, as well as the performance of the plates themselves, is discussed.

During the planning of the beam tests, the bond between the concrete and CFRP was believed to be the most critical concern. The bond between the primary and splice plates was not a significant concern based on discussions with representatives from the composite industry. Thus, tests were initially designed to focus on the effect of fatigue on the adhesive bond between the primary plate and concrete surface at crack locations of damaged girders. After initial Fatigue Tests of Beams 1 and 2, it became apparent that the adhesive bond between the primary and splice plate does, in fact, pose a problem.

Because of this, subsequent Ultimate Load Tests were designed to determine the initial cause of splice plate debonding as well as beam behavior prior to and after initial signs of debonding.

Fatigue Test (FT)

CFRP Primary/Splice Plate Layout and Instrumentation

External reinforcement used for flexural strengthening during fatigue testing of Beams 1 and 2 consisted of a primary plate, on the extreme tension face of each specimen, with a butt joint at midspan and a 610 mm long splice plate centered over the joint as shown in Figure 6.1.

In addition to the instrumentation scheme and data reduction techniques described in Chapter Five, six gages were used for CFRP surface strain measurements. The CFRP surface strain gage locations for Beams 1 and 2 are illustrated in Figure 6.1.

Test Procedure

For Beam 1, the Fatigue Test consisted of an initial slow loading of the specimen, by manually using the digital ram controller, to a ram displacement of 20.32 mm and then unloading to a displacement of 2.54 mm. These values are the maximum and minimum ram displacements in the Fatigue Tests and were manually applied first for an instrumentation check. Once all instrumentation had been evaluated, the beam was displaced to 8.89 mm and then cycled 11.43 mm above and below this point to provide a 17.78 mm sine wave amplitude. The system was operated in displacement control mode to insure a constant

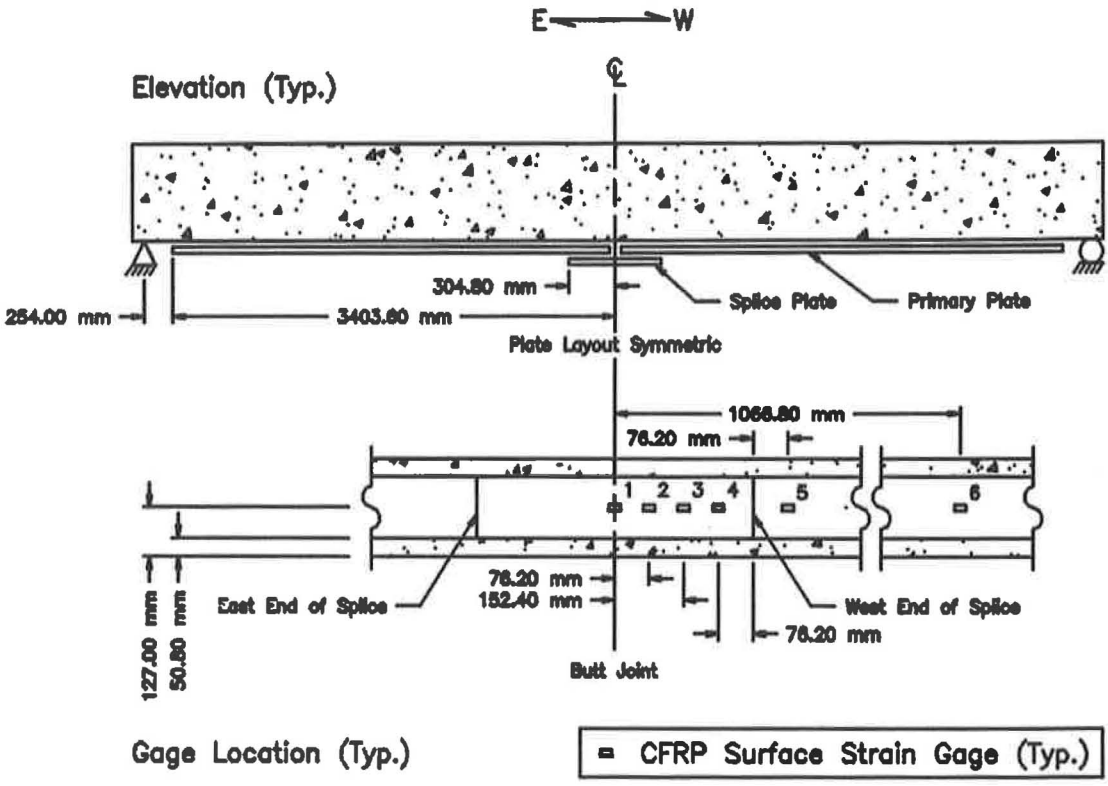

FIGURE 6.1. CFRP Plate Layout and Gage Locations, Beams 1 and 2 (FT)

amplitude of specimen deflections, at a frequency of 0.25 Hz. The load in the ram cycled between approximately 6 kN and 68 kN throughout the test with corresponding steel strains in the bottom reinforcement, at midspan, of 156 με and 1196 με, respectively. The maximum steel strain level was 58 percent of the required yield strain, indicating a load range well within the service load conditions. Data collected during the initial loading, and periodically during the Fatigue Test, was used to monitor beam, primary and splice plate behavior.

At approximately 8000 cycles, the first indication of splice plate debonding was seen with surface strain levels on the splice over the butt joint (CFRP 1) of approximately zero. Visual inspection of the splice plate revealed that complete splice plate debonding did in fact occur from the east end of the plate to the butt joint. Thus, testing was discontinued and the specimen was unloaded. The maximum strain in the bottom steel reinforcement, at midspan, during the cyclic loading after complete debonding was 1412 με, approximately 68 percent of the yield strain.

During the initial manual loading of Beam 2, to a ram displacement of 20.32 mm, the first indications of splice plate debonding were seen at the west end of the plate, at which point CFRP surface strain levels began to drop to approximately zero at gage locations CFRP 4 and CFRP 3 (see Figure 6.1). Hence, the fatigue test was never started, and the beam specimen was unloaded. The maximum applied load was 74 kN at the initial deflection of 20.32 mm and the strain in the bottom steel reinforcement at midspan was 1236 με, approximately 60 percent of the yield strain of the steel.

Results

For Beam 1 (FT), complete splice plate debonding occurred at the east end of the splice at approximately 8000 cycles. Although debonding occurred at the end opposite the instrumentation, the test did provide important information pertaining to beam, primary and splice plate behavior.

In Figure 6.2, experimental CFRP strain-moment relationships, on and off the splice plate, before complete debonding, as well as the theoretical primary plate relationship are shown. The results indicate maximum normal strain levels on the end of the splice (CFRP 4) and off the splice (CFRP 5) of 1011 με and 2189 με, respectively. The difference in the strain levels on and off the splice was 1178 με. The moment at the end of the splice, for the maximum load of 68 kN, was 103 kN-m. Using this moment, the theoretical primary plate strain at the end of the splice was 1682 με. At the butt joint (CFRP 1), the maximum normal strain was 2057 με, approximately 17 percent of the ultimate strain capacity of the plate (ε_{fu}).

In Figure 6.3, the load-deflection relationship at midspan is shown. A service load stiffness of 2.70 kN/mm was determined for the beam taking the slope of the dashed line in Figure 6.3. Experimental and theoretical moment-curvature relationships at midspan were also considered (see Figure 6.4).

After visual inspection of the debonded splice plate, it was determined that adhesive failure occurred at the primary plate/adhesive interface. The visual inspection also revealed that a paper label 50 mm by 100 mm was on the surface of the splice plate, near the corner of the splice plate and approximately

25 mm from the edge. The label was accidently left on the plate during installation. Hence, the label essentially created a void in the adhesive layer. The label was believed to be the sole cause for the failure at that time. However, the debonding behavior of Beam 1 with the label was not significantly different from the behavior of subsequent tests. A detailed illustration of the complete splice plate failure mode is shown in Figure 6.5.

The first indication of splice plate debonding for Beam 2 (FT) was seen at the west end of the plate at a total load of 65 kN and a beam deflection of 17 mm at midspan. No indication of splice plate debonding was seen at the opposite end of the splice plate or butt joint.

CFRP strain histories for gage locations on and off the splice are shown in Figure 6.6. The plot clearly indicates the time of initial debonding, and shows that due to debonding the strain levels at CFRP 4 and eventually CFRP 3 dropped to zero.

CFRP strain-moment relationships, up to the first sign of debonding, for gages CFRP 1 through 5 are shown in Figure 6.7. In addition to the experimental relationships, the theoretical primary plate relationship is also presented. The normal strain levels at initial debond on the splice (CFRP 4) and off the splice (CFRP 5) were 870 με and 1226 με, respectively, corresponding to a moment at the end of the splice of 99 kN-m. The difference in normal strain on and off the splice at the first sign of debonding was 356 με. At the moment for which debonding occurred, the theoretical primary plate strain was 1617 με. The

strain at the butt joint (CFRP 1), at the first sign of debonding was 2003 με, approximately 17 percent of the ultimate strain capacity of the plate.

In Figure 6.8, the load-deflection relationship at midspan is shown. From the plot, no indication of beam yielding was seen during the loading. The service load stiffness before splice plate debonding was 3.50 kN/mm. Experimental and theoretical moment-curvature relationships at midspan are shown in Figure 6.9.

It was determined, after visual inspection of the partially debonded splice plate, that adhesive failure at the primary plate/adhesive interface controlled the failure of the splice for Beam 2 (FT) just as in Beam 1 (FT).

Although the tests on Beam 1 and 2 were not conclusive for determining the fatigue effects on the adhesive bond layer between the primary plate and concrete surface at crack locations, they did provide important information on splice plate behavior and identified a potential mode of splice failure (i.e. adhesive failure at the primary plate/adhesive interface). Subsequent testing, presented in the following section, was designed to focus on the factors contributing to splice plate debonding as well as beam behavior prior to and after the first signs of debonding.

Splice plate debonding was determined to be a result of the difference in normal strains occurring on the splice plate and off the splice, on the primary plate, at the end of the splice. Since there is a high normal strain in the primary plate and zero normal strain in the splice plate, at the end of the splice, large shear stresses are created in the adhesive at the primary plate/adhesive interface. This behavior was confirmed by the tests described in the following

section, and the stresses necessary to cause debonding were shown to occur even without the presence of a butt joint (i.e. dummy plates). In the following section, a significant amount of data regarding the normal strains on the splice plate and off the splice, on the primary plate, at the ends of splice/dummy plates are presented. Summarization of this data is presented in Chapter Eight.

There was no apparent damage to the primary plates of Beam 1 and 2 as a result of the initial tests, and the maximum steel strain levels reached during the initial tests were less than 70 percent of the yield strain. Hence, splice plate repairs were made to permit subsequent testing (i.e. ultimate load tests). For Beam 1, the east end of the splice plate was reattached after all residual adhesive was removed. In the case of Beam 2, the splice plate as well as all residual adhesive was removed and a 914 mm splice reattached.

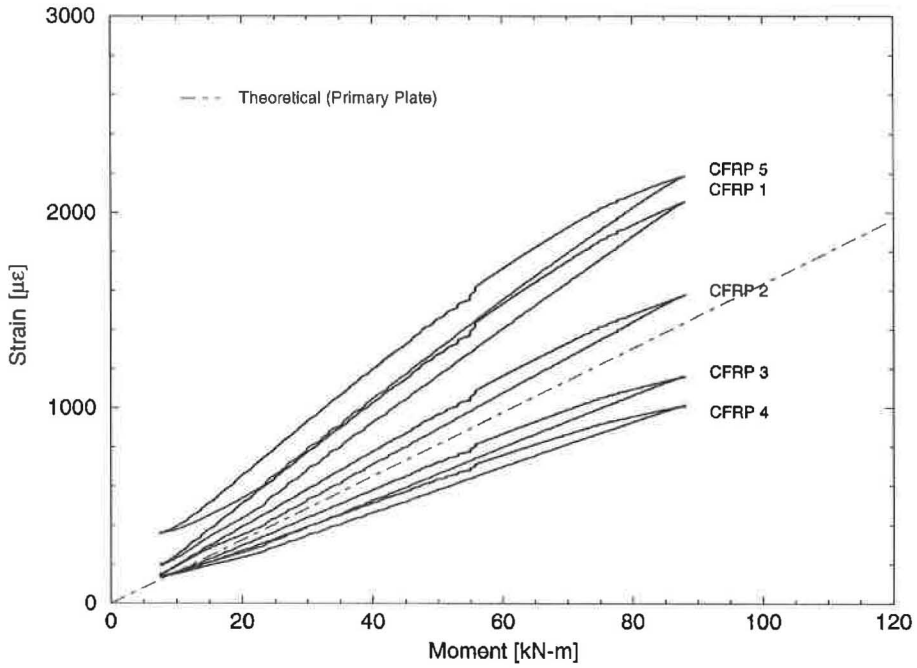

FIGURE 6.2. CFRP Strain-Moment Relationships at Gage Locations On and Off the Midspan Splice Plate, Beam 1 (FT)

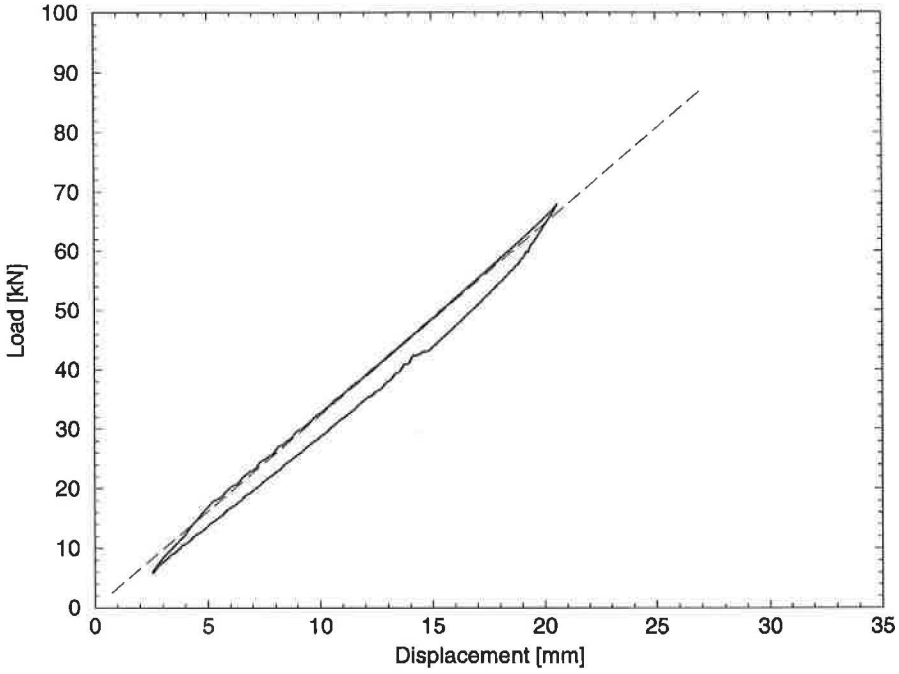

FIGURE 6.3. Load-Deflection Relationship at Midspan, Beam 1 (FT)

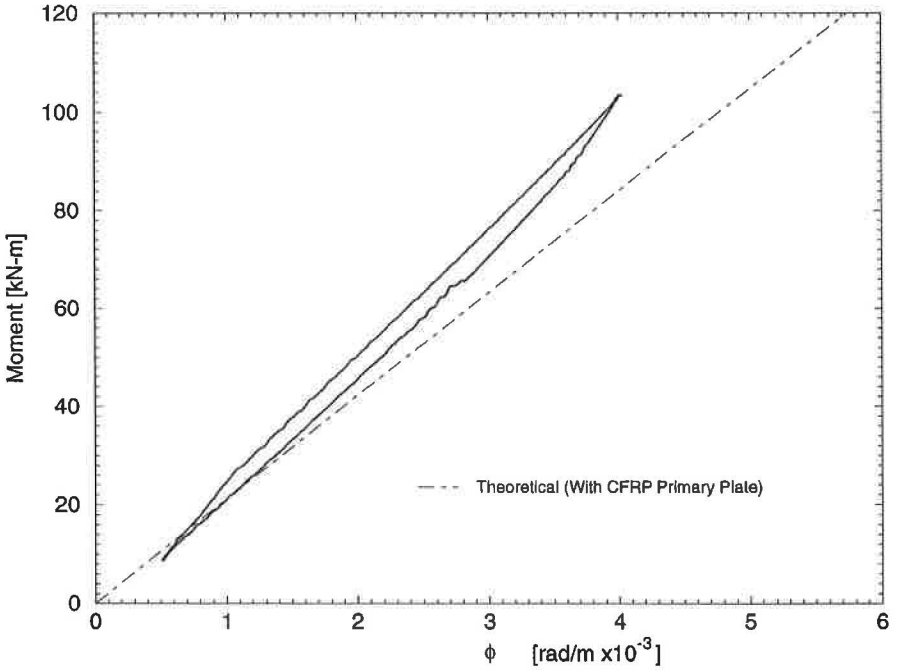

FIGURE 6.4. Moment-Curvature Relationships at Midspan, Beam 1 (FT)

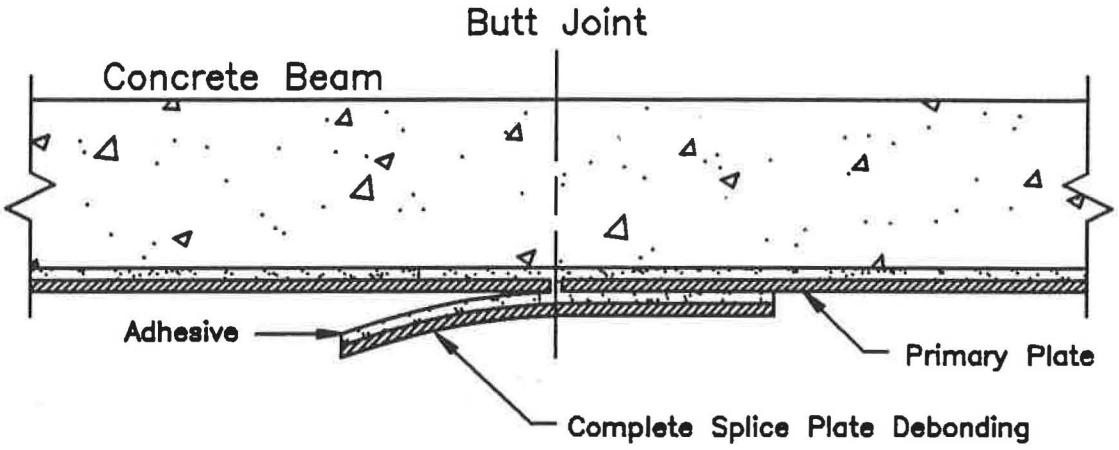

FIGURE 6.5. Illustration of the Complete Splice Plate Debonding Failure Mode

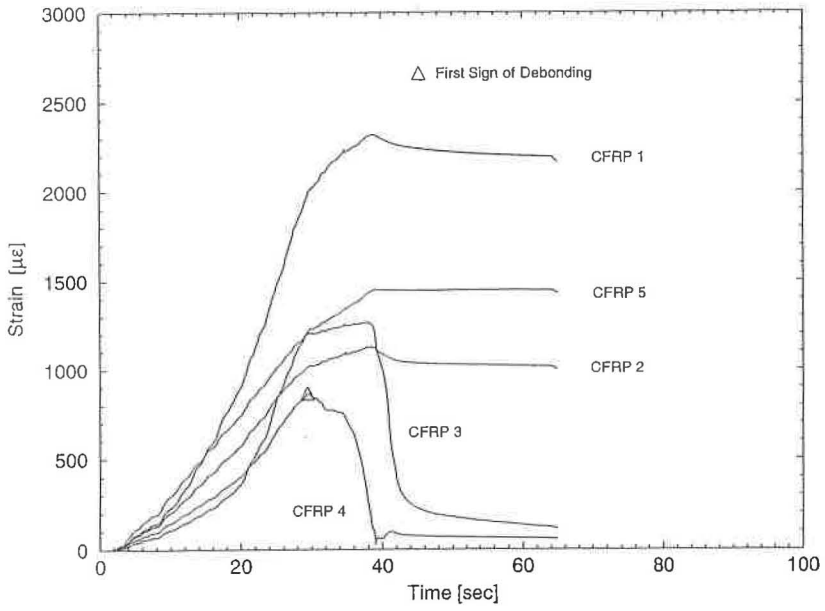

FIGURE 6.6. CFRP Strain Histories at Gage Locations On and Off the Midspan Splice Plate, Beam 2 (FT)

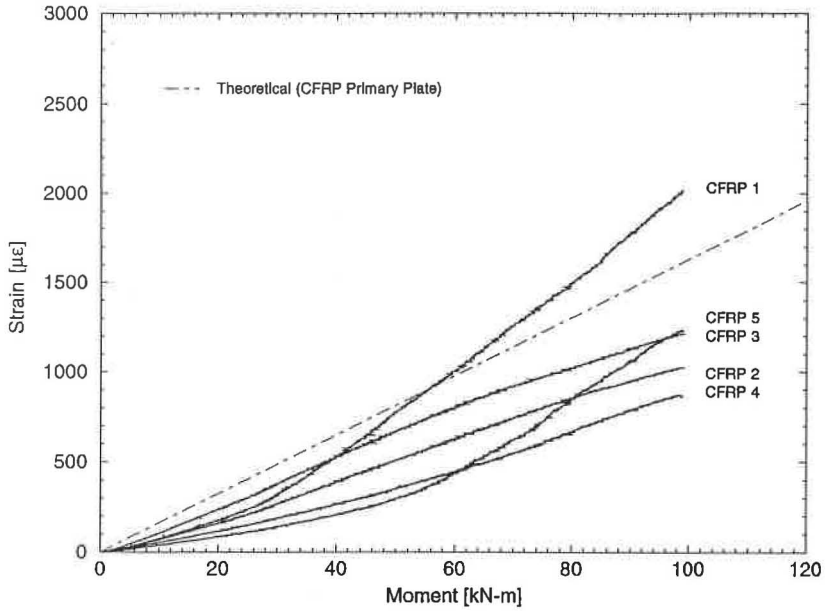

FIGURE 6.7. CFRP Strain-Moment Relationships at Gage Locations On and Off the Midspan Splice Plate, Beam 2 (FT)

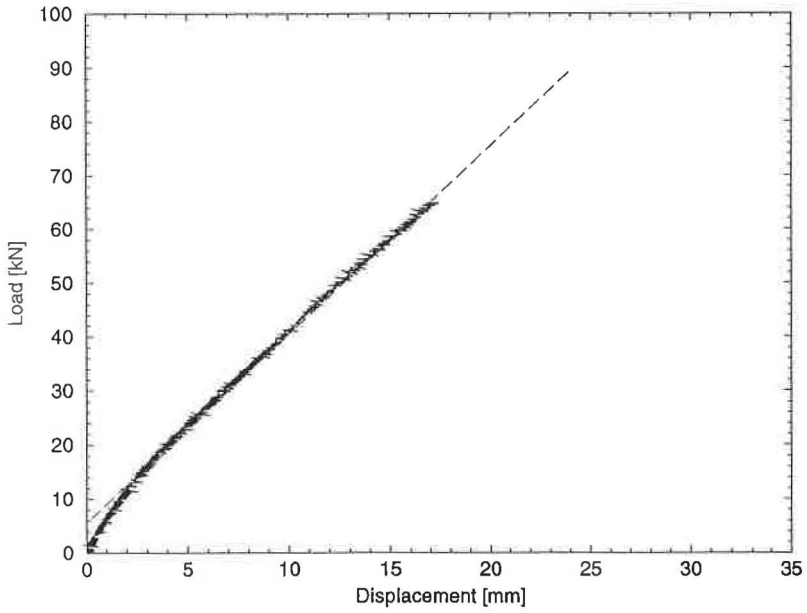

FIGURE 6.8. Load-Deflection Relationship at Midspan, Beam 2 (FT)

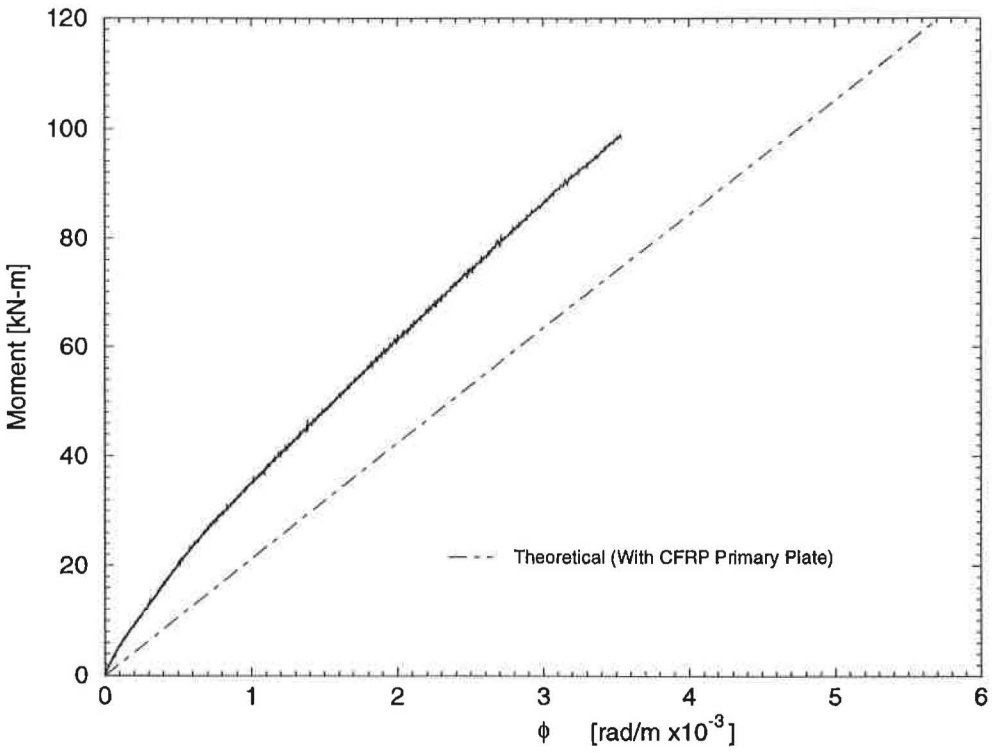

FIGURE 6.9. Moment-Curvature Relationships at Midspan, Beam 2 (FT)

Ultimate Load Test (ULT)

CFRP Primary/Splice/Dummy Plate Layout and Instrumentation

Three CFRP primary and splice plate layouts were used for flexural strengthening of Beams 1 through 8 for the Ultimate Load Tests as shown in Figures 6.10 through 6.19. In the first two layouts, the plate selection was similar to that of the Fatigue Tests, with Beam 1 having a 610 mm long and Beam 2 and 3 having a 914 mm long splice plate at midspan. The third layout, for Beams 4 through 8, consisted of a primary plate, on the extreme tension face of each beam specimen, with two butt joints at 1702 mm on either side of midspan. In

addition, two splice plates with lengths of 610 mm covered the two joints. A 914 mm long dummy plate, centered at midspan, was used in the first of two Ultimate Load Tests (ULT 1) conducted on Beams 4 and 6.

All CFRP primary and splice plates were applied with the carbon fibers oriented parallel to the longitudinal axis of the beam except for Beam 8. For Beam 8, as a result of the positioning of the vacuum valves, both splice plates were sightly misaligned from the primary plates as shown in Figure 6.19. Consideration was given to the possibility that problems of this nature could occur during field applications. Therefore, the misaligned plates were not repaired and subsequently tested.

In addition to the instrumentation schemes used in the Crack Tests, CFRP surface strain gages were employed during all Ultimate Load Tests. Throughout testing, modifications were continuously made to primary and splice plate layouts, and to gage locations as a result of increased knowledge of splice plate behavior. Surface strain gage locations for all tests are illustrated in Figures 6.10 through 6.19.

Test Procedure

Each specimen was loaded in displacement increments measured by the rams's internal LVDT with the loading system operated in displacement control mode. The increments used ranged from 2.54 mm to 12.70 mm. This was dependent upon the behavior of the beam, whether or not the beam was initially damaged during Crack Tests, and the measurement range of the of the LVDTs used in beam deflection readings. Testing continued until gage readings and/or

visual inspection identified indications of beam failure. The beam specimen was then unloaded, and approximately 24 hours after testing residual deflection data collected.

Four possible primary beam failure modes were considered during testing. Those modes are: (1) concrete compression failure; (2) tension failure of the CFRP primary and/or splice plate; (3) adhesive failure between the primary plate and concrete; and (4) complete adhesive failure between the splice and primary plate (see Figure 6.5). Only the third and fourth primary failure modes were observed during testing. In reduction of the test data, the first sign of splice plate debonding was considered to be failure of the splice. Although the first sign of splice debonding was not always immediately followed by complete debonding, it was assumed that initial signs of debonding would represent the practical failure of the bridge beam subjected to cyclic loading.

A total of ten ultimate load tests were conducted on the eight beam specimens, one for Beams 1-3,5,7,8 and two for Beams 4 and 6. In Table 6.1, a summary of the testing sequence, test designation, CFRP plate layout, surface strain gage locations, beam condition before testing, and primary beam failure mode are given.

TABLE 6.1. Summary of Ultimate Load Tests

Beam	Test	CFRP Layout/ Gage Locations	Beam Initial Condition[a]	Primary Beam Failure Mode
1	ULT	Figure 6.10	Cracked	Complete Splice Plate Debonding
2	ULT	Figure 6.11	Cracked	Complete Splice Plate Debonding
3	ULT	Figure 6.12	Cracked	Complete Splice Plate Debonding
4	ULT 1	Figure 6.13	Cracked	No Failure, Debonding of Dummy Plate
	ULT 2	Figure 6.14	Cracked	Primary Plate Tension Failure
5	ULT	Figure 6.15	Cracked	Complete Splice Plate Debonding
6	ULT 1	Figure 6.16	Uncracked	No Failure, Debonding of Dummy Plate
	ULT 2	Figure 6.17	Cracked[b]	Complete Splice Plate Debonding
7	ULT	Figure 6.18	Cracked	Complete Splice Plate Debonding
8	ULT	Figure 6.19	Uncracked	Complete Splice Plate Debonding

[a]Cracked - Initial damage produced during crack test.
[b]Cracked during ULT 1.

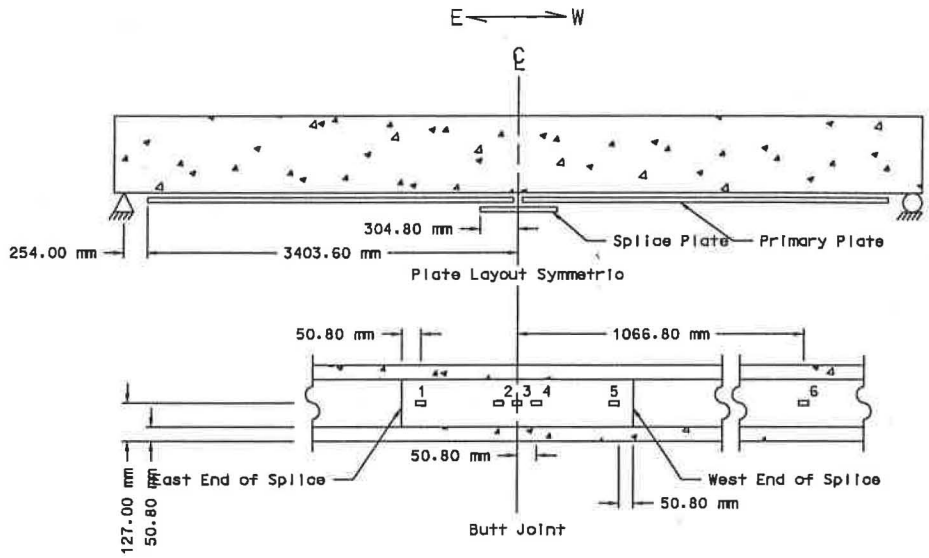

FIGURE 6.10. CFRP Plate Layout and Gage Locations, Beam 1 (ULT)

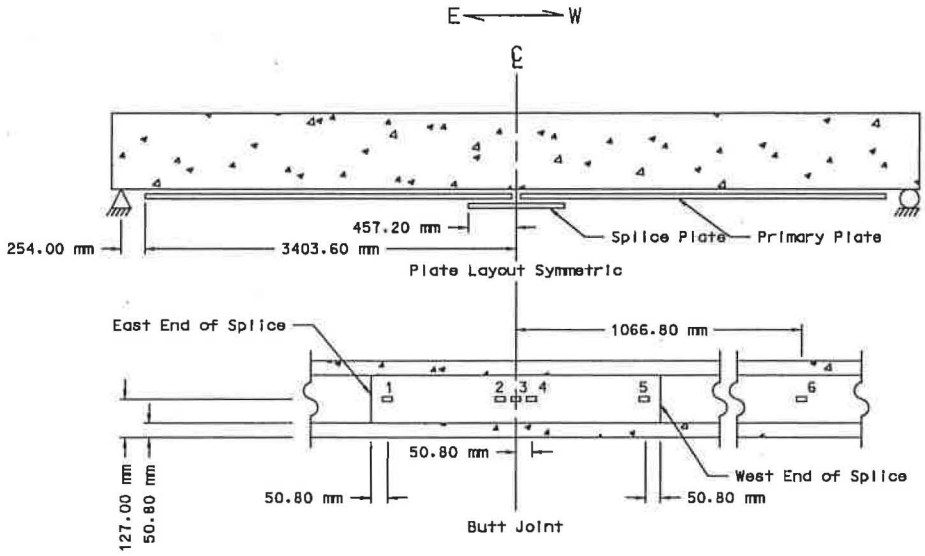

FIGURE 6.11. CFRP Plate Layout and Gage Locations, Beam 2 (ULT)

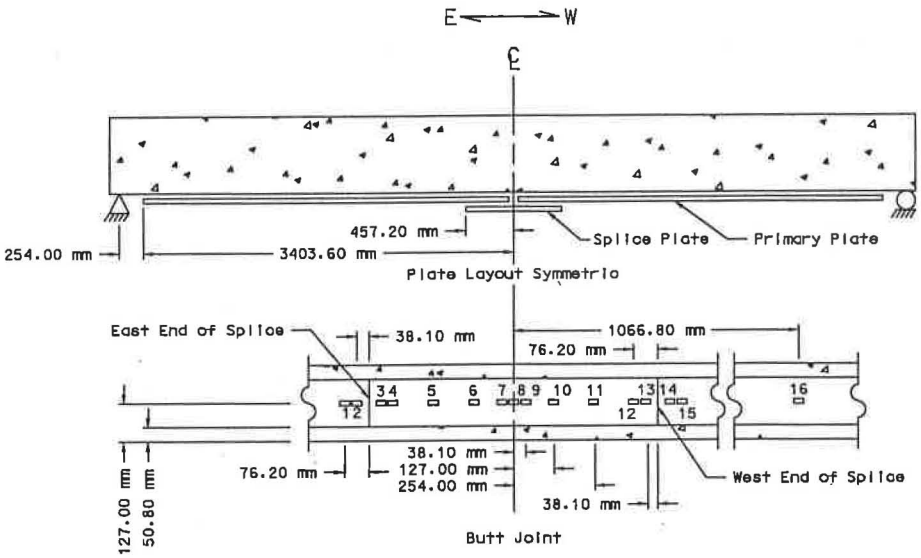

FIGURE 6.12. CFRP Plate Layout and Gage Locations, Beam 3 (ULT)

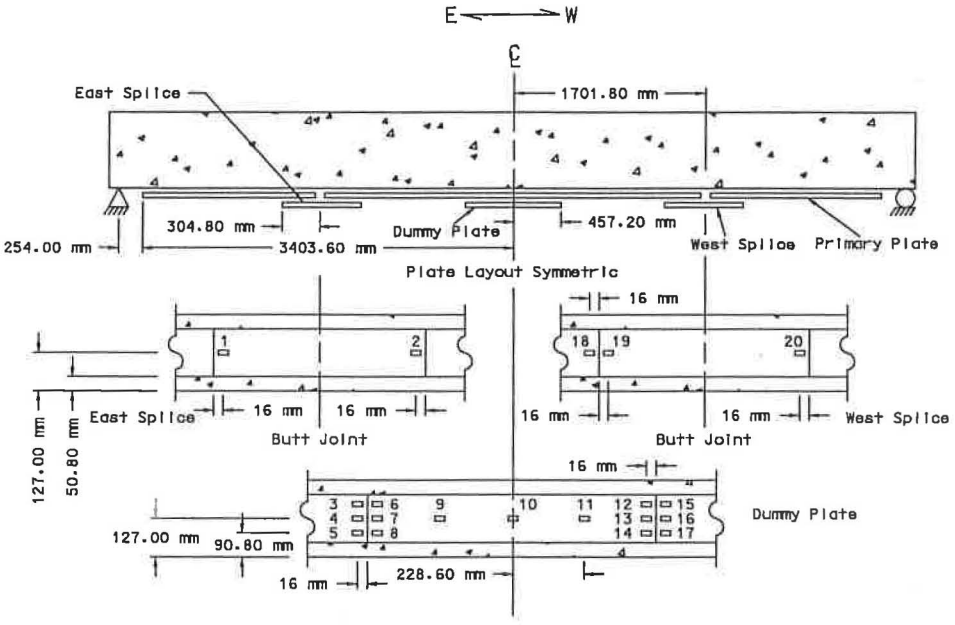

FIGURE 6.13. CFRP Plate Layout and Gage Locations, Beam 4 (ULT 1)

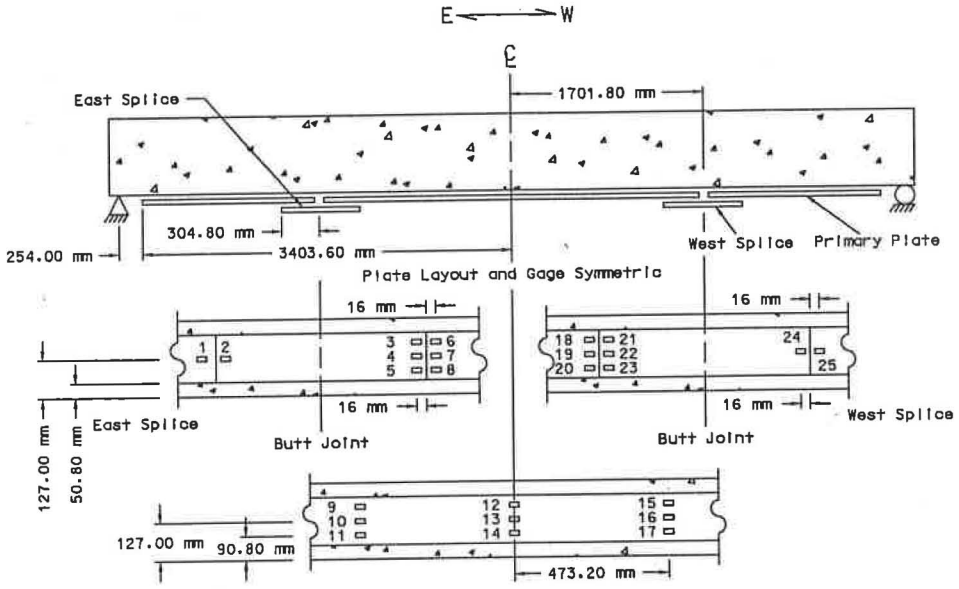

FIGURE 6.14. CFRP Plate Layout and Gage Locations, Beam 4 (ULT 2)

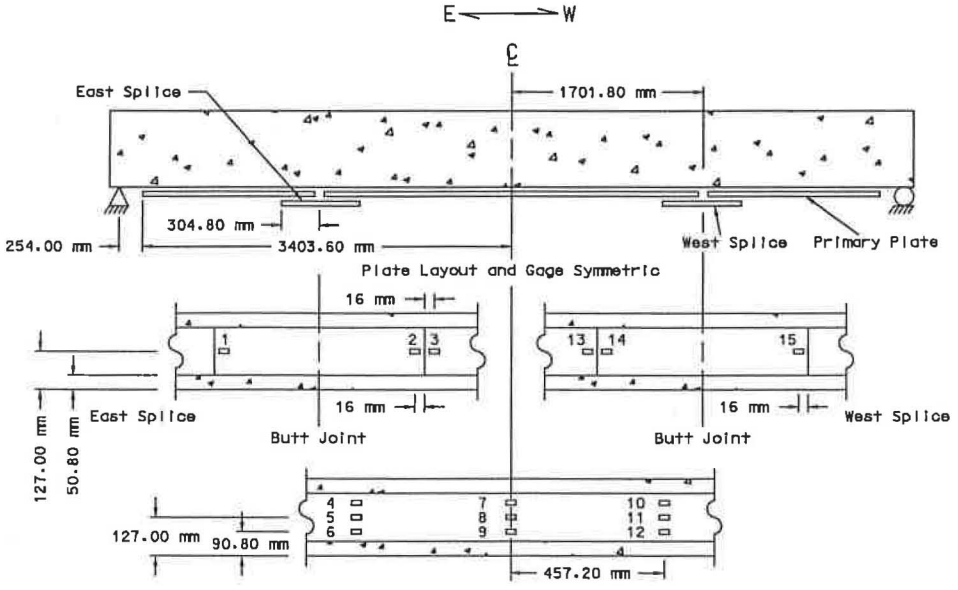

FIGURE 6.15. CFRP Plate Layout and Gage Locations, Beam 5 (ULT)

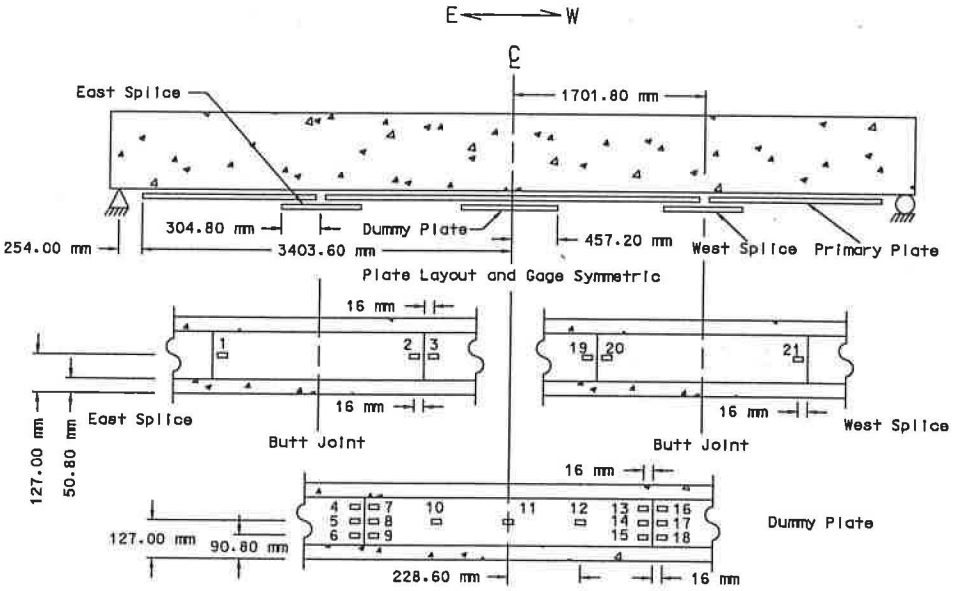

FIGURE 6.16. CFRP Plate Layout and Gage Locations, Beam 6 (ULT 1)

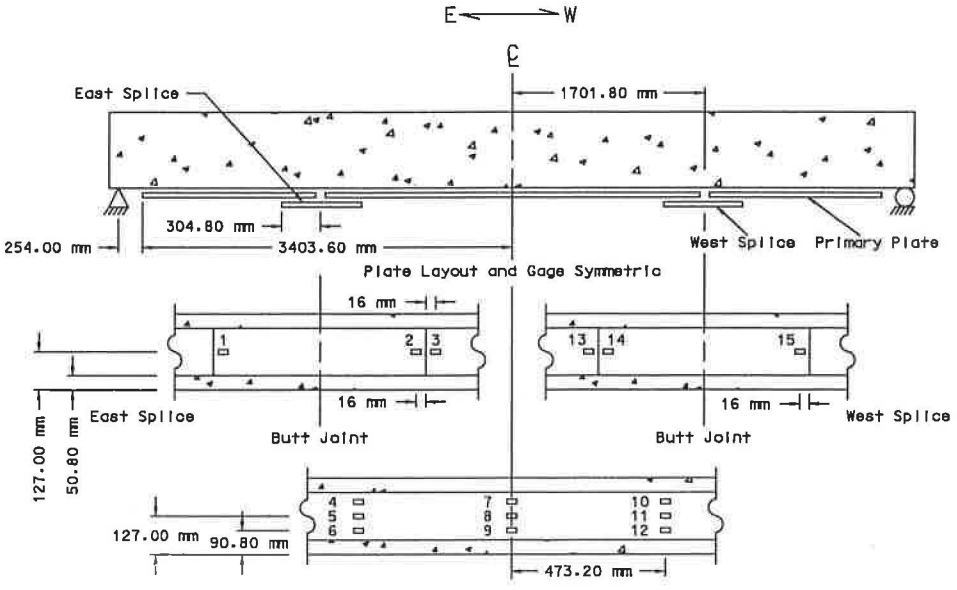

FIGURE 6.17. CFRP Plate Layout and Gage Locations, Beam 6 (ULT 2)

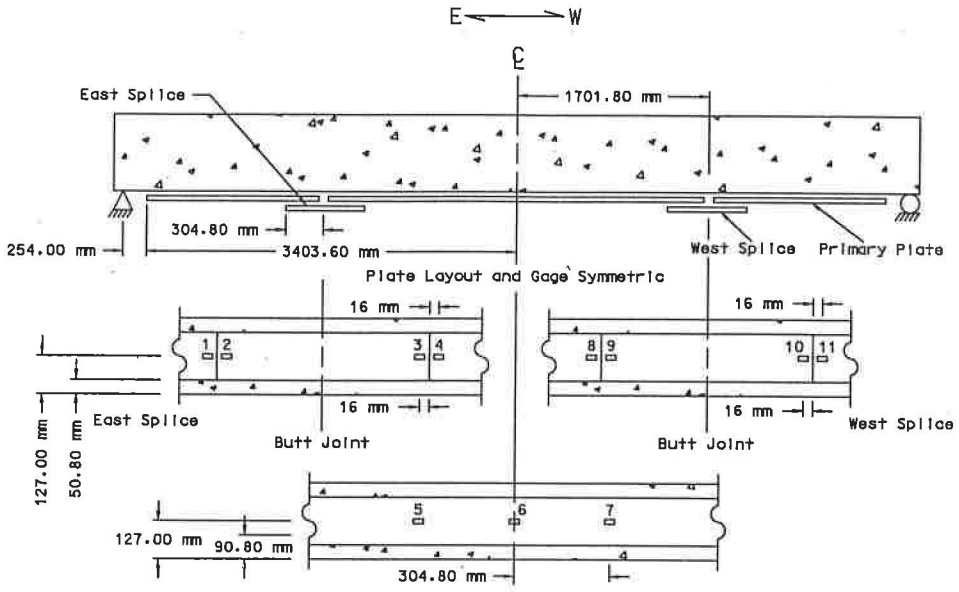

FIGURE 6.18. CFRP Plate Layout and Gage Locations, Beam 7 (ULT)

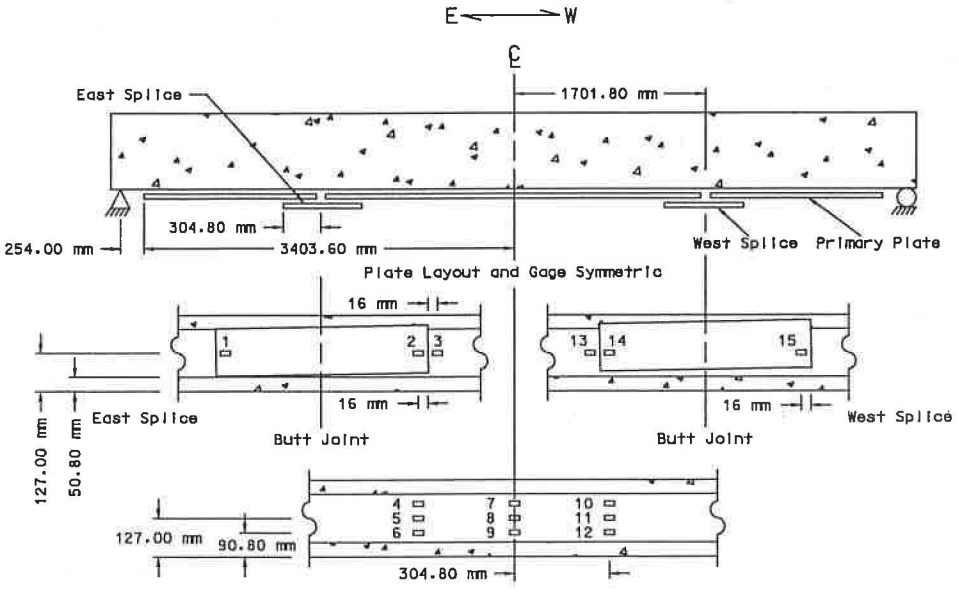

FIGURE 6.19. CFRP Plate Layout and Gage Locations, Beam 8 (ULT)

Results

The results of the ultimate load tests are presented in the following sections in the sequence in which they were conducted.

Beam 1 (ULT)

The first indication of splice plate debonding occurred at the east end of the midspan splice at a beam deflection of 34 mm and a total load of 108 kN. Complete debonding followed at a deflection of 48 mm and a load of 119 kN. This was accompanied by a loud noise which turned out to be fairly typical for all succeeding tests.

In Figure 6.20, CFRP strain histories at gage locations along the splice are shown. The plot clearly indicates the first sign of splice plate debonding at the east end (CFRP 1) and the point of complete debonding (CFRP 3). Some initial signs of splice plate debonding were also seen at the west end of the splice (CFRP 5) before complete debonding occurred. The maximum strain measured at the butt joint (CFRP 3) was 5182 με, approximately 44 percent of the ultimate strain capacity of the splice plate. In Figure 6.21, the strain distribution along the splice at first debond is shown.

For all gage locations along the splice, experimental CFRP strain-moment relationships, up to the first sign of debonding, are shown in Figure 6.22. Along with the experimental results in Figure 6.22, the theoretical primary plate relationship is also presented. At the first sign of debonding, the normal strain at the east end of the splice (CFRP 1) was 2313 με. The moment at the end of the

splice, at first debond, was 165 kN-m. Using the same moment, the theoretical primary plate strain was determined to be 3606 με.

In Figure 6.23, the load-deflection relationship at midspan indicates beam yielding did occur before complete splice plate debonding. Using the dashed lines shown in Figure 6.23, the load and deflection at yield were determined to be 100 kN and 31 mm. The moment at yield was 152 kN-m. A service load stiffness of 3.13 kN/mm was determined from the slope of the dashed line before beam yielding. In Figure 6.24, experimental and theoretical moment-curvature relationships at midspan are shown. The residual deflection of the beam 24 hours after loading was 16.43 mm.

It was determined after visual inspection of the splice plate that adhesive failure at the primary plate/adhesive interface controlled the failure mode of the splice. In Figure 6.25, a photo of the midspan splice plate of Beam 1 (ULT) removed after complete debonding is shown. The photo represents a typical completely debonded splice plate observed throughout testing. As can be seen in Figure 6.25, the adhesive remained with the splice plate after debonding as a result of adhesive failure occurring at the primary plate/adhesive interface.

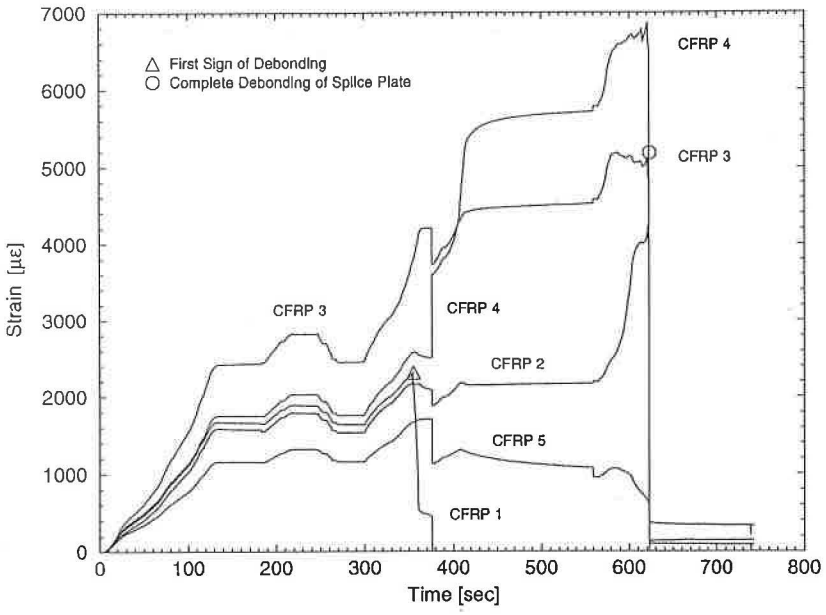

FIGURE 6.20. CFRP Strain Histories, Beam 1 (ULT)

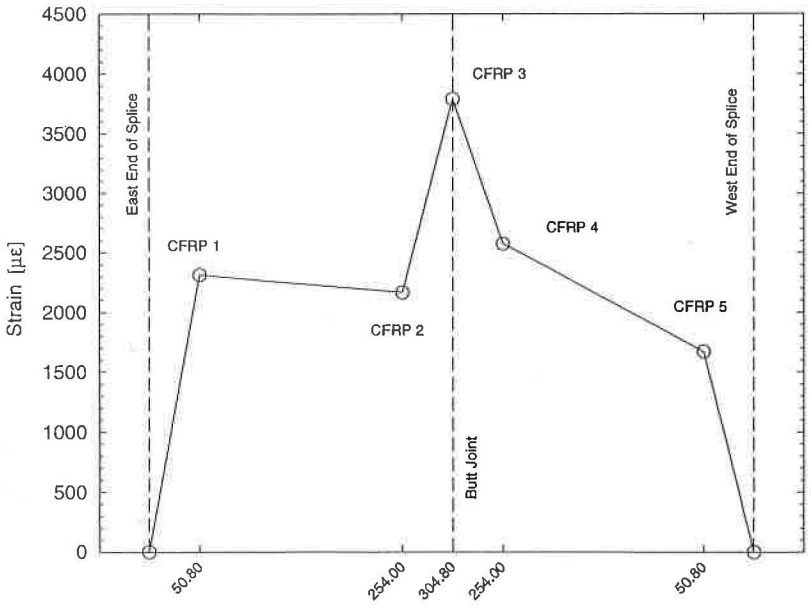

FIGURE 6.21. Splice Plate Strain Distribution at First Sign of Debonding, Distances Measured from the End of the Splice Plate [mm], Beam 1 (ULT)

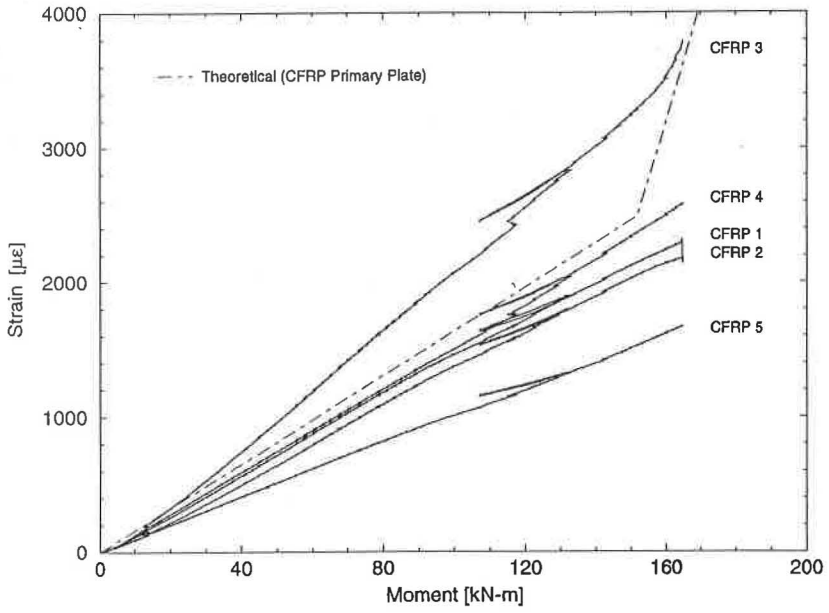

FIGURE 6.22. CFRP Strain-Moment Relationships, Beam 1 (ULT)

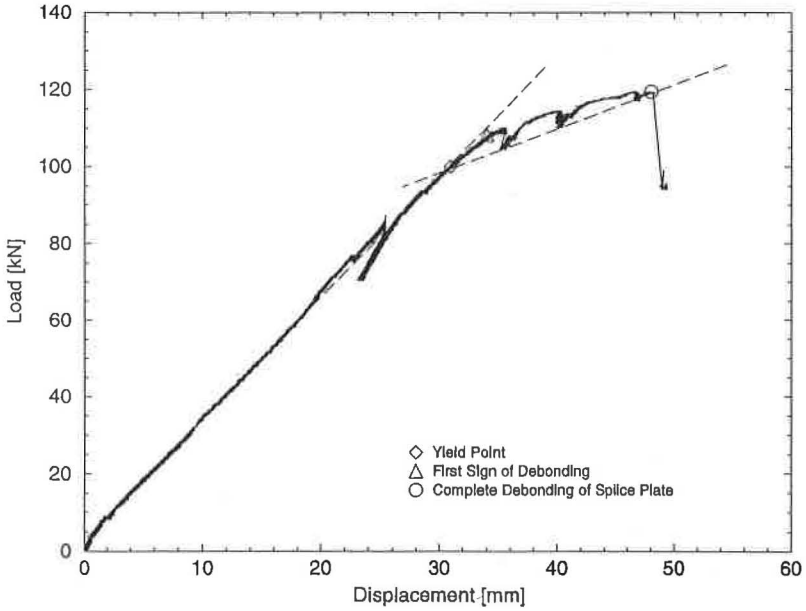

FIGURE 6.23. Load-Deflection Relationship at Midspan, Beam 1 (ULT)

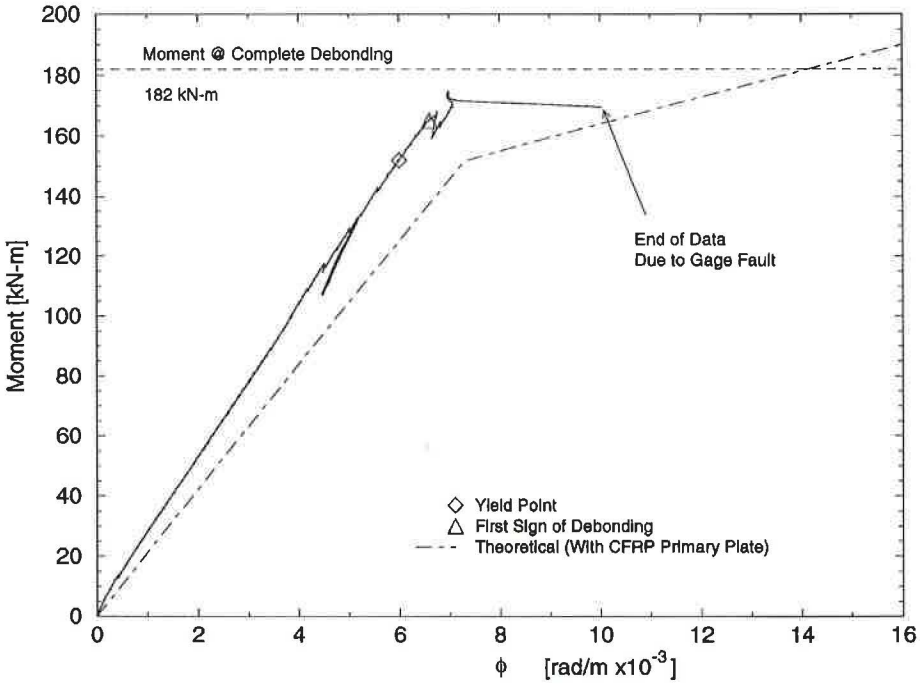

FIGURE 6.24. Moment-Curvature Relationships at Midspan, Beam 1 (ULT)

FIGURE 6.25. Splice Plate After Complete Debonding

BEAM 2 (ULT)

Similar to the situation for the 610 mm long splice plate used in Beam 1 (ULT), initial splice plate debonding also occurred for the 914 mm long splice used in Beam 2 (ULT) followed by complete debonding. The first indication of splice debonding occurred at the west end of the midspan splice plate at a beam deflection of 20 mm and a total load of 74 kN. At a beam deflection of 39 mm and a load of 116 kN, complete debonding occurred. In contrast to the preceding test, as a result of complete debonding of the splice plate, some primary plate debonding from the concrete surface was seen at the butt joint.

In Figure 6.26, the CFRP strain histories at gage locations along the splice are shown. The maximum strain level seen by the splice plate at the butt joint was 4280 με, approximately 36 percent of the ultimate strain capacity of the plate. The strain distribution along the splice, at the first sign of debonding, can be seen in Figure 6.27.

Experimental CFRP strain-moment relationships, for gage locations along the splice, up to the first sign of debonding, as well as the theoretical primary plate relationship are shown in Figure 6.28. The normal strain at the west end of the splice (CFRP 5), at the first sign of debonding, was 1021 με, corresponding to a moment of 112 kN-m. The theoretical primary plate strain at the point of initial debonding was 1831 με.

In Figure 6.29, the load-deflection relationship is shown. From Figure 6.29, it is observed that yielding of the reinforcing steel did occur before complete splice plate debonding at a load of 109 kN and a beam deflection of

32 mm. The midspan moment at yield was 166 kN-m. A service load stiffness of 3.27 kN/mm was determined from the slope of the dashed line before yielding.

After visual inspection of the splice plate, it was determined that adhesive failure at the primary plate/adhesive interface controlled the failure of the splice plate. As was mentioned earlier, some primary plate debonding also occurred. In an attempt to further test primary plate behavior, the beam was loaded beyond the point of complete debonding to a beam deflection of approximately 64 mm. The test was stopped when no additional load could be applied due to a plastic hinge forming at the butt joint. As a result of the additional loading, a longitudinal concrete shear failure pattern was seen at the depth of the bottom steel reinforcement around the butt joint and at the end of the debonded primary plate (see Figure 6.31). Although the degree of this type of secondary failure varied for the Ultimate Load Test of Beam 1-3, the figure represents a typical shear failure pattern seen around butt joints after complete debonding of a midspan splice plate. Residual deflection data were not collected because the beam was loaded well beyond the beams primary failure mode.

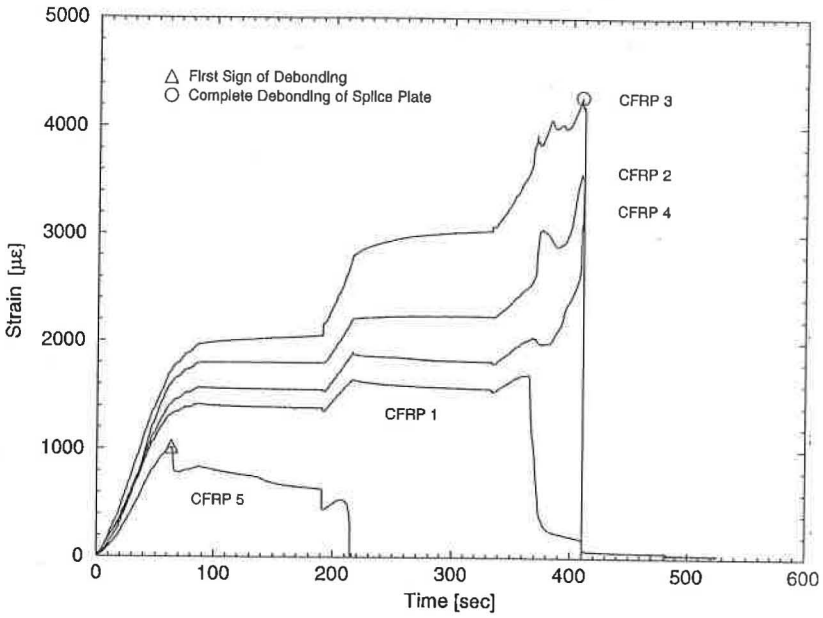

FIGURE 6.26. CFRP Strain Histories, Beam 2 (ULT)

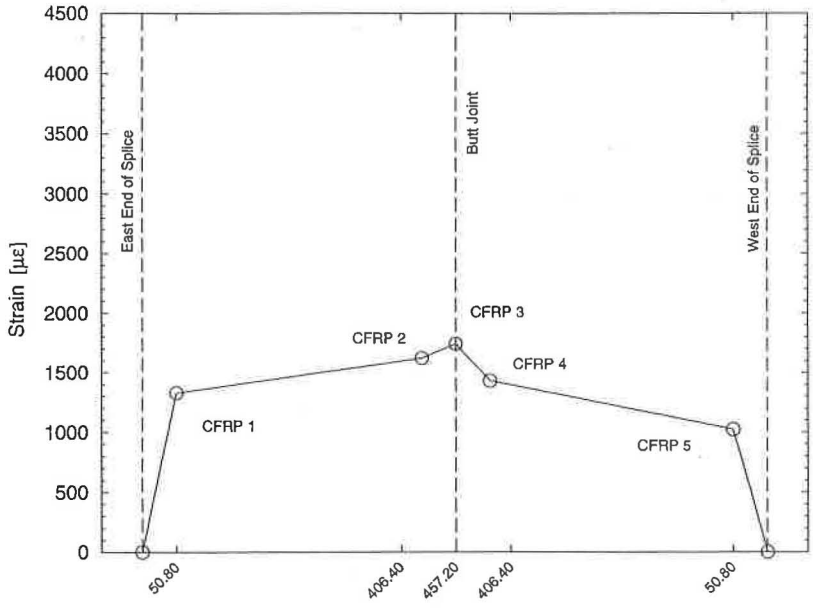

FIGURE 6.27. Splice Plate Strain Distribution at First Sign of Debonding, Distances Measured from the End of the Splice Plate [mm], Beam 2 (ULT)

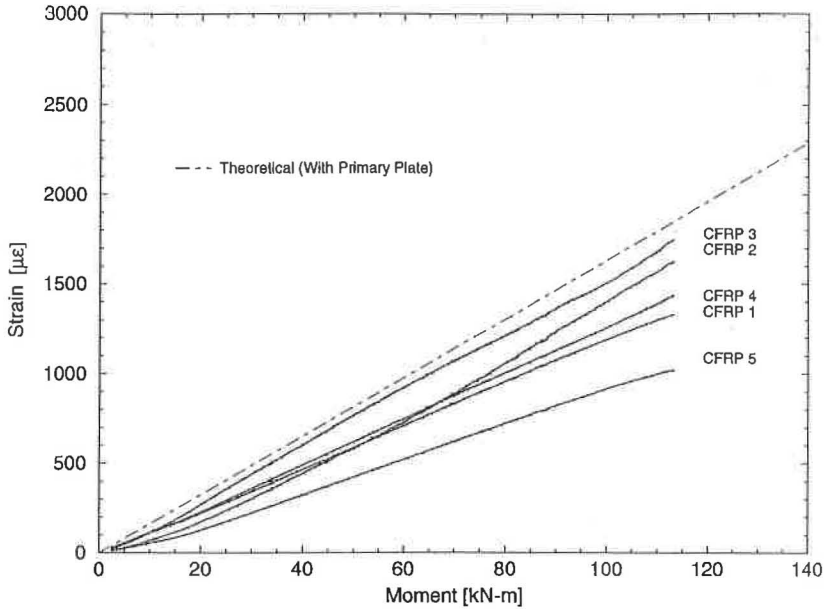

FIGURE 6.28. CFRP Strain-Moment Relationships, Beam 2 (ULT)

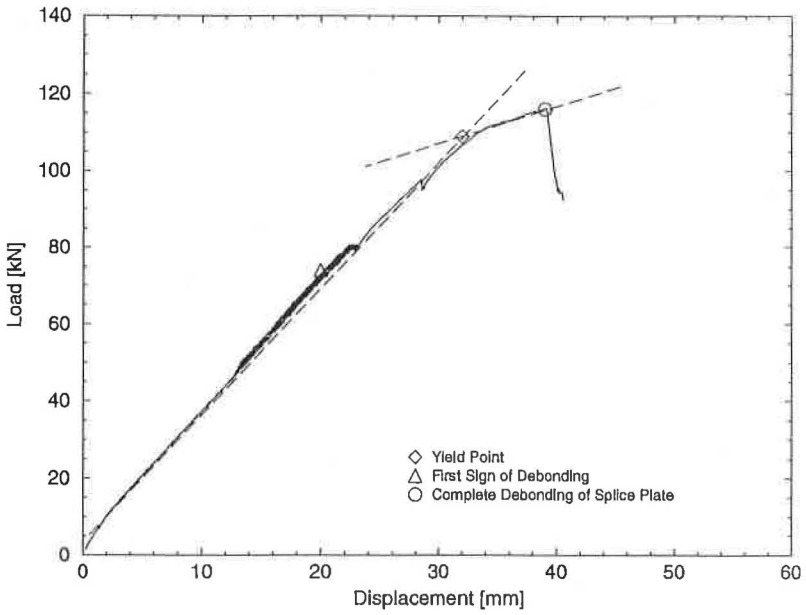

FIGURE 6.29. Load-Deflection Relationship at Midspan, Beam 2 (ULT)

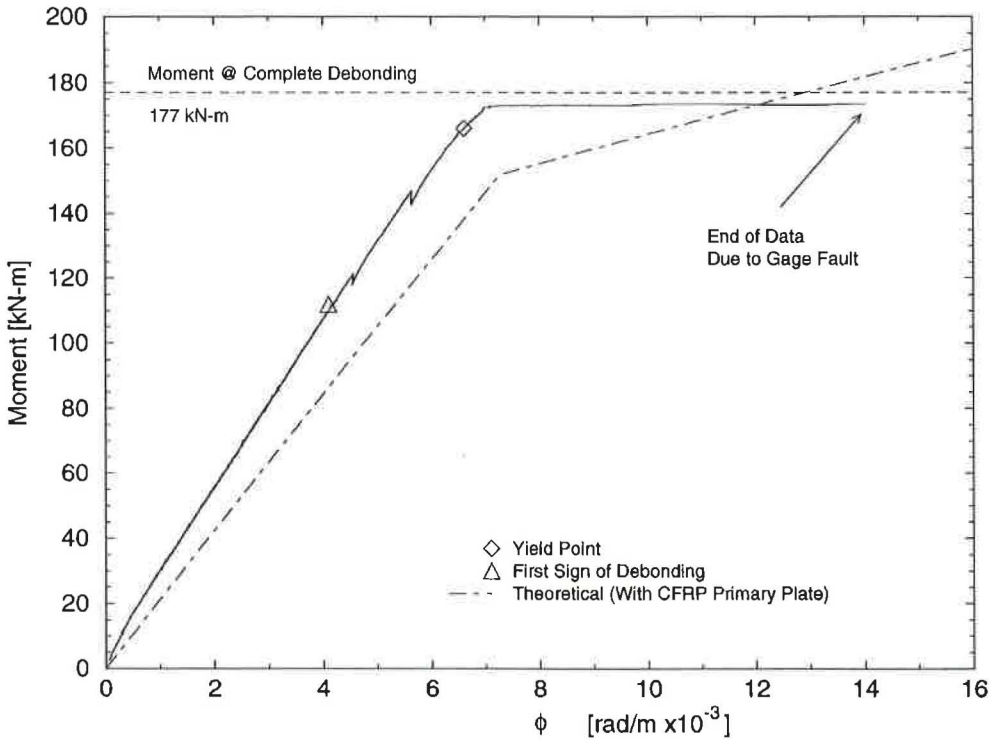

FIGURE 6.30. Moment-Curvature Relationships at Midspan, Beam 2 (ULT)

FIGURE 6.31. Typical Concrete Shear Failure Pattern After Complete Splice Debonding

Beam 3 (ULT)

In appreciation of the results of the previous two Ultimate Load Tests and fatigue tests, gage locations on the primary plate just off the splice (CFRP 1,2 and 14,15) were selected to measure normal primary plate strains at first debond (see Figure 6.12).

As was seen in the previous two Ultimate Load Tests, complete debonding of the midspan splice plate also controlled the failure mode of Beam 3. The first sign of splice plate debonding was noticed at the west end of the plate at a load of 80 kN and a beam deflection of 23 mm. Complete debonding ensued at a load of 82 kN and a deflection of 24 mm.

Strain histories from gage locations on the splice and just off the splice, on the primary plate, (CFRP 2,3,13,14) as well as over the butt joint (CFRP 8) are shown in Figure 6.32. The maximum strain recorded at the butt joint was 2699 με, approximately 23 percent of the ultimate strain capacity of the plate. The strain distribution at first debond, for gage locations on and off the splice, can be seen in Figure 6.33.

CFRP strain-moment relationships, up to the first sign of debonding, for gage locations at the west end of the splice (CFRP 13 and 14) are shown in Figure 6.34. In addition to the experimental relationships, the theoretical primary plate relationship is also shown in Figure 6.34. The normal strain at initial debond for gages CFRP 13 and 14 were 1329 με and 2301 με, respectively. The difference in strain at the west end of the splice and just off splice, on the

primary plate, was 972 με. At initial debond, the moment at the end of the splice was 122 kN-m. The theoretical primary plate strain at this moment was 1654 με.

From the load-deflection relationship in Figure 6.35, no indication of beam yielding was observed before complete splice debonding. A service load stiffness of 3.00 kN/mm was determined from the plot. Experimental and theoretical moment-curvature relationships at midspan are shown in Figure 6.36.

Similar to the scenarios observed in the previous two Ultimate Load Tests as well as fatigue tests, adhesive failure at the primary plate/adhesive interface controlled the failure of the midspan splice. The residual deflection 24 hours after testing was 1.30 mm.

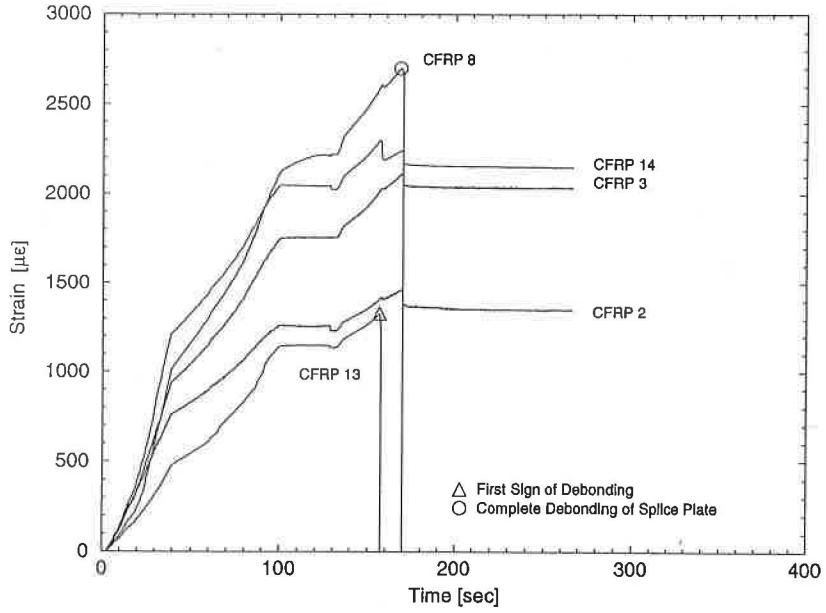

FIGURE 6.32. CFRP Strain Histories, Beam 3 (ULT)

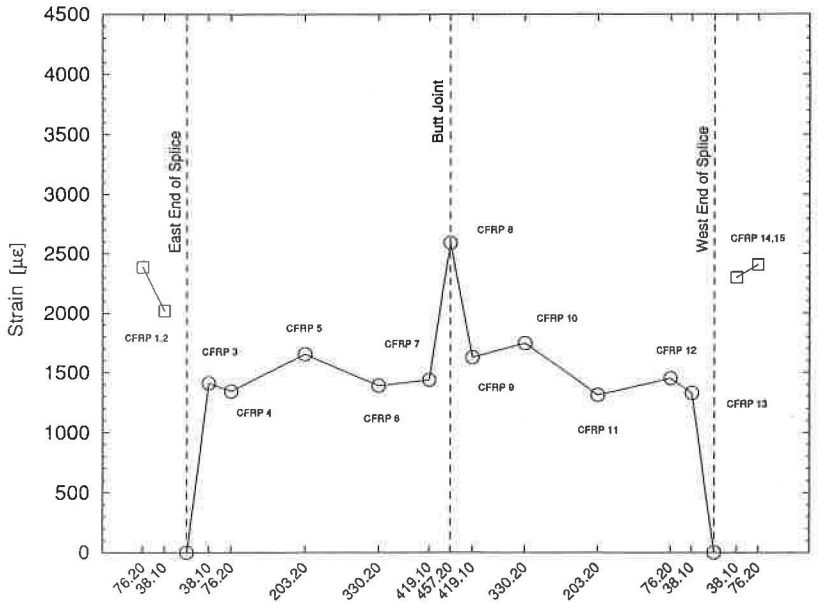

FIGURE 6.33. Splice/Primary Plate Strain Distribution at First Sign of Debonding, Distances Measured from the End of the Splice [mm], Beam 3 (ULT)

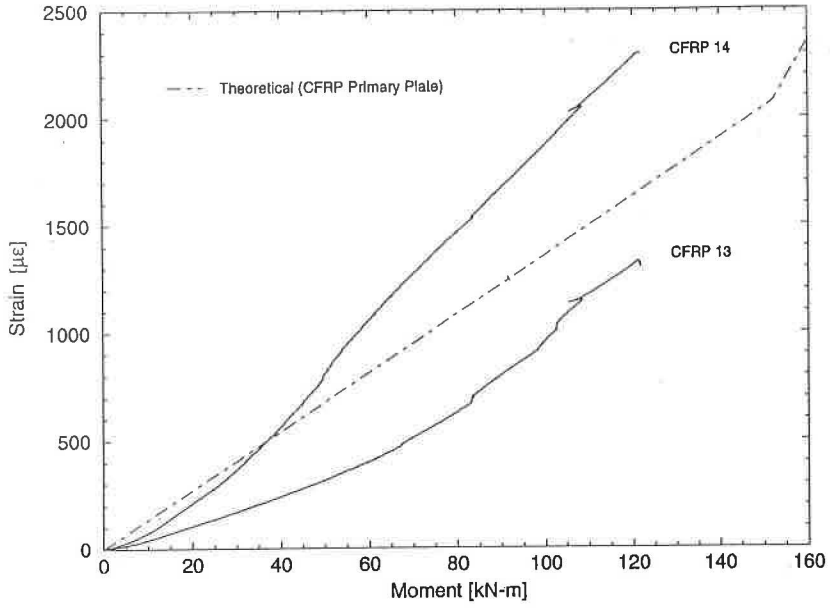

FIGURE 6.34. CFRP Strain-Moment Relationships at Gage Locations On and Off the West End of the Splice Plate, Beam 3 (ULT)

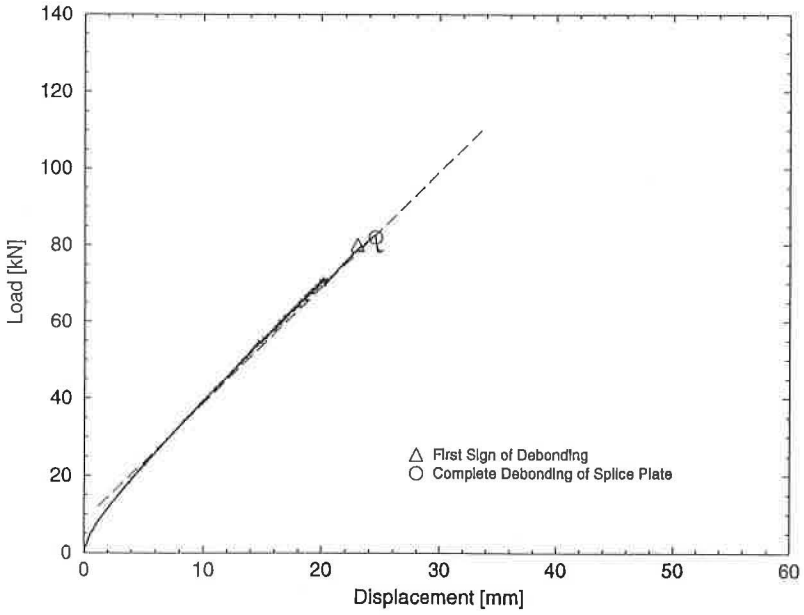

FIGURE 6.35. Load-Deflection Relationship at Midspan, Beam 3 (ULT)

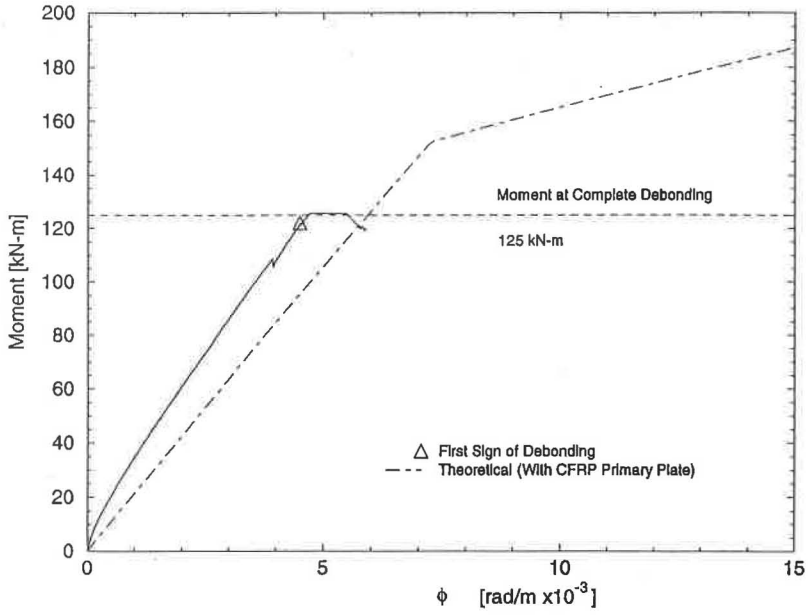

FIGURE 6.36. Moment-Curvature Relationships at Midspan, Beam 3 (ULT)

Beam 4 (ULT 1)

Two splice plates approximately located at the beam third points, as shown in Figure 6.13, were used for Beam 4. The splice plate lengths were 610 mm. By moving the splice plates from the critical region around midspan, the intent was to increase the beam's capacity before initial and/or complete debonding occurred. A 914 mm long dummy plate was applied at midspan to determine if splice plate debonding would in fact occur without a butt joint. Testing continued until complete dummy plate debonding occurred.

At a deflection of 15 mm and a total load of 54 kN, the first indication of dummy plate debonding was seen at the west end of the plate. Complete debonding followed at a deflection of 26 mm and a load of 84 kN. No signs of initial debonding were seen at the east and west splice plates during the test.

CFRP strain gages on the splice/dummy plates, as well as on the primary plates were placed 16 mm off the end of the splice/dummy plates and employed during Beam 4 (ULT 1), and all subsequent tests. By placing the gages as close to the end of the splice/dummy plate as possible, a clearer understanding of the true strain levels observed at the ends of the plates at initial debond was obtained (see Figure 6.13). The average of any transverse line of gages was considered the actual normal strain at their respective locations.

The strain histories for gage locations at the end of the dummy plate and just off the dummy plate, on the primary plate, are shown in Figure 6.37. From the plot, the first sign of dummy plate debonding at the west end of the plate was followed shortly by initial debonding of the east end. The strain distribution for gage locations on and off the ends dummy plate, at first debond, is shown in

Figure 6.38.

Strain-moment relationships on the west end of the dummy plate and on the primary plate, up to the first sign of debonding, as well as the theoretical primary plate relationship are shown in Figure 6.39. The average normal strain at initial debond at the end of the dummy plate and on the primary plate was 835 με and 2668 με, respectively. The difference in strains at the point of debonding was 1833 με. The moment at the end of the splice for which debonding occurred was 82 kN-m. Using this moment, the theoretical primary plate strain at the end of the splice at initial debond was 1340 με.

In Figure 6.40, the load-deflection relationship is shown. No indication of beam yielding was evident before complete debonding of the dummy plate. A service load stiffness of 2.97 kN/mm was determined from the dashed line shown in Figure 6.40. Experimental and theoretical moment-curvature relationships at midspan are shown in Figure 6.41.

Similar to the observations for the midspan splice plate for Ultimate Load Tests of Beam 1 through 3, adhesive failure at the primary plate/adhesive interface controlled the failure of the dummy plate. Based on the results of Beam 4 (ULT 1), it was concluded that splice plate debonding was not controlled by the butt joint, but rather by the normal strain differences occurring at the end of the splice plate and just of the splice in the primary plate. The residual deflection after the initial test on Beam 4 was 1.23 mm. With the exception of a few hair line cracks forming between the initial cracks created during the Crack Test of Beam 4, no additional damage to the beam or primary and splice plates was observed.

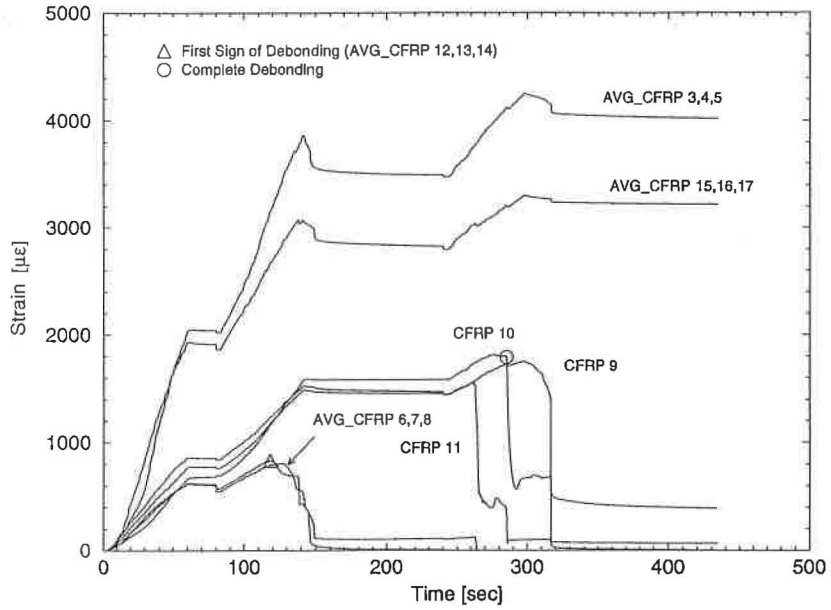

FIGURE 6.37. CFRP Strain Histories at Gage Locations On and Off the Dummy Plate, Beam 4 (ULT 1)

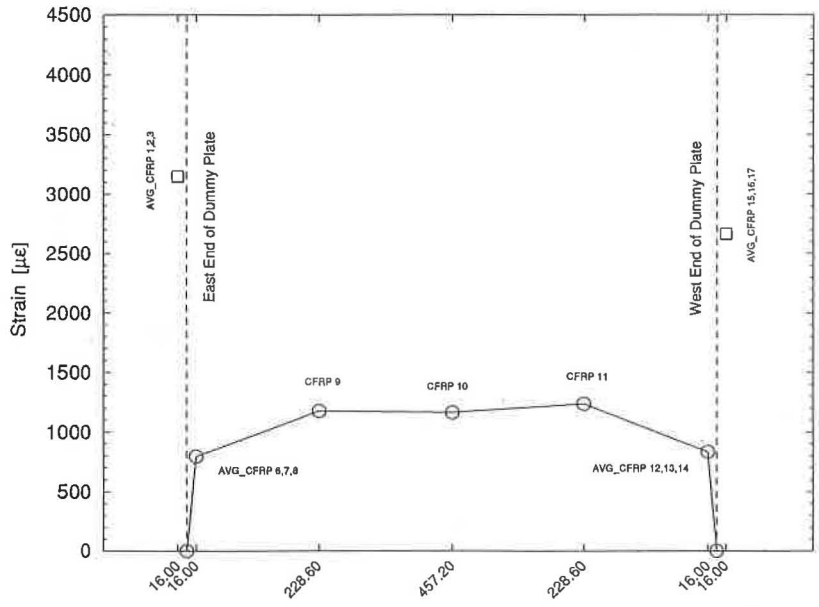

FIGURE 6.38. Dummy/Primary Plate Strain Distribution at First Sign of Debonding, Distances Measured from the Ends of the Dummy Plate [mm], Beam 4 (ULT 1)

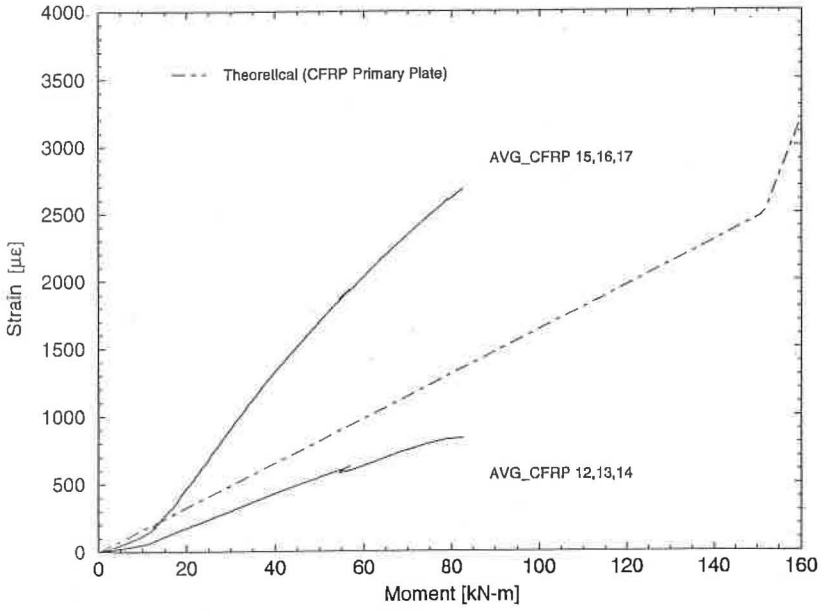

FIGURE 6.39. CFRP Strain-Moment Relationships at Gage Locations On and Off the West End of the Dummy Plate, Beam 4 (ULT 1)

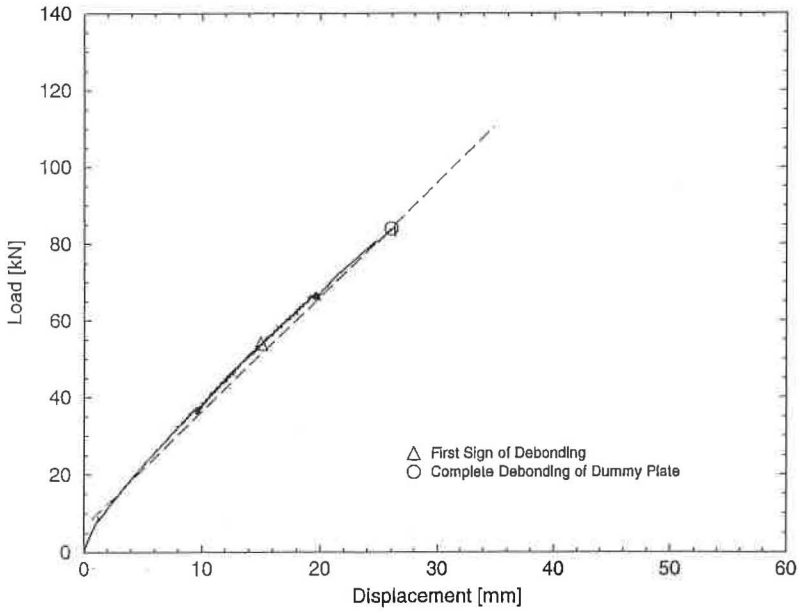

FIGURE 6.40. Load-Deflection Relationship at Midspan, Beam 4 (ULT 1)

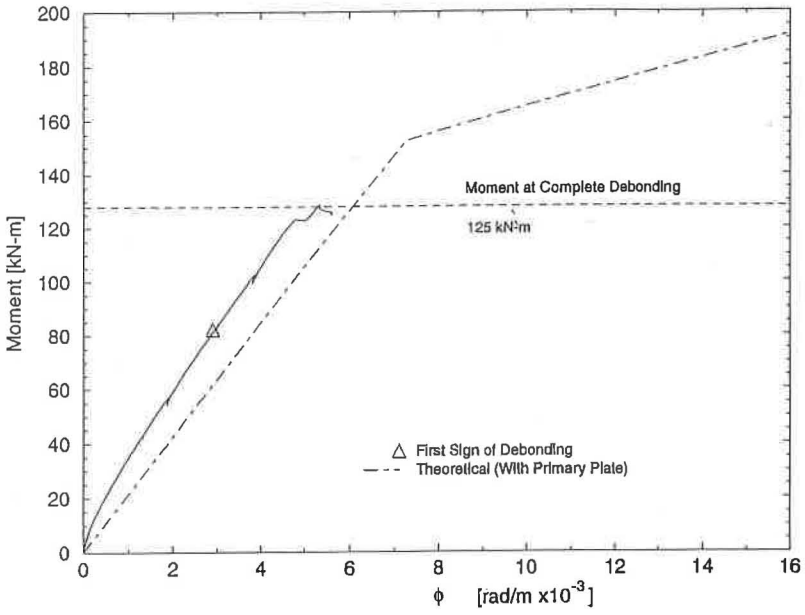

FIGURE 6.41. Moment-Curvature Relationships at Midspan, Beam 4 (ULT 1)

Beam 4 (ULT 2)

After the initial Ultimate Load Test, Beam 4 (ULT 1), the beam was unloaded and the dummy plate as well as all residual adhesive removed for a second test, Beam 4 (ULT 2).

During the second Ultimate Load Test of Beam 4, initial debonding occurred at the interior ends at both splice plate locations. At a beam deflection of 31 mm and a total load of 100 kN, the first sign of debonding occurred at the west splice plate. Initial debonding of the east splice plate followed at a beam deflection of 32 mm and a total load of 102 kN. In contrast to the preceding ultimate load tests with splice plates at midspan, primary plate tension failure occurred over gage locations CFRP 9 through 11 (see Figure 6.14). The average strain level at failure for gages CFRP 9 through 11 was 7909 με, approximately 67 percent of the ultimate strain capacity of the plate. The failure of the primary plate, at strain levels well below that of the ultimate, may have occurred as a result of damage to the plate from surface sanding conducted for strain gage application. The beam deflection and load at the time of failure were 53 mm and 120 kN, respectively. The ultimate moment was 183 kN-m. Although premature failure of the primary plate did occur, the performance of the beam was enhanced with the relocation of the splice plates.

In the data analysis, it was assumed that the behavior of each splice plate acted independent of the other due to their relative locations. Therefore, strain levels at the end of the splice and just off the splice, on the primary plate, at initial debond for both splices were considered. In Figures 6.42 and 6.43, CFRP

strain histories for gage locations at the end of the splice and off the splice, on the primary plate, for the west and east splices are shown respectively.

In Figures 6.44 and 6.45, experimental average strain-moment relationships, up to the first sign of debonding, at gage locations at the end of the splice and off the splice, on the primary plate, for the interior ends of the west and east splice plates are shown. In addition to the experimental results, the theoretical primary plate relationship is presented. At the first sign of debonding, the average normal strains at the end of the splice and off the splice, on the primary plate, at the interior end of the west splice plate were 581 με and 1693 με, respectively. The calculated moment at the interior end of the splice at debonding was 113 kN-m. The difference in strain on and off the plate was 1112 με. At the moment for which debonding occurred, the theoretical primary plate strain at the end of the splice was 1850 με. For the east splice plate, the normal strain levels at the end of the splice and off the splice, on the primary plate, at the interior end of the plate were 822 με and 2189 με, respectively. The calculated moment at the interior end of the splice at debonding was 115 kN-m. The difference in strain for the east splice plate at initial debond was 1367 με. At the moment for which debonding occurred, the theoretical primary plate strain was 1883 με.

In Figure 6.46, experimental average primary plate strains at gage locations in the constant moment region, up to primary plate tension failure, are shown. The plot illustrates the computer program's ability to accurately predict

CFRP primary plate strains. Some of the dissimilarities may be attributed to damage created during surface preparations.

In Figure 6.47, the load-deflection relationship at midspan is shown. The plot indicates a pronounced yield zone before tension failure of the primary plate. From dashed lines in Figure 6.47, it was determined that beam yielding occurred at a deflection of 30 mm and a load of 97 kN. The moment at first yield was 148 kN-m. Prior to beam yielding, a service load stiffness of 3.03 kN/mm was calculated. Experimental and theoretical moment-curvature relationships are shown in Figure 6.48. Figure 6.48 also provides an initial indication of the computer program's ability to accurately predict reinforced concrete beam behavior with externally applied CFRP primary and splice plates.

After visual inspection of the two splice plates, it was determined that adhesive failure at the primary plate/adhesive interface controlled the initial debonding of the plates. At the location of primary plate tension failure, a shear failure pattern similar to that seen at the butt joints of midspan splice plates of Beams 1 through 3 (ULT) was observed (see Figure 6.49). The residual deflection, 24 hours after testing, created by the loading and eventual failure of the primary plate was 19.71 mm.

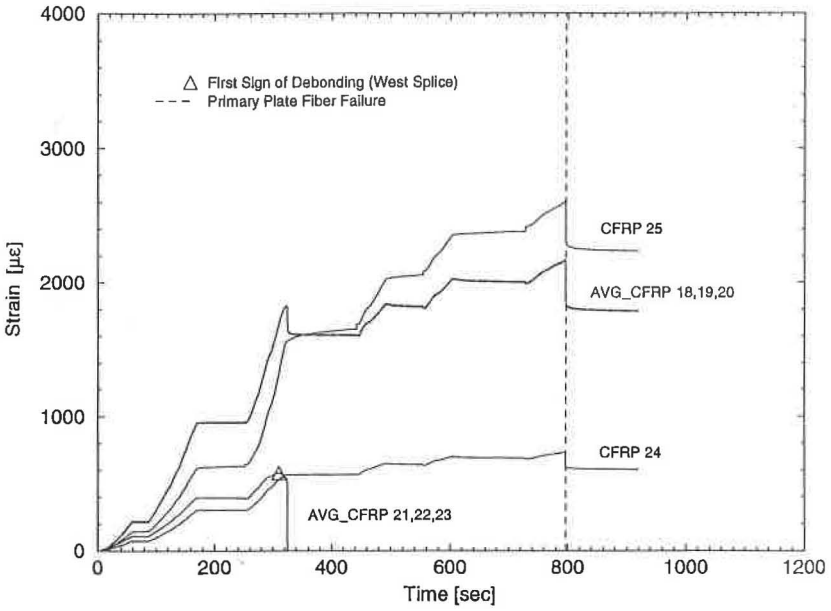

FIGURE 6.42. CFRP Strain Histories at Gage Locations On and Off the West Splice Plate, Beam 4 (ULT 2)

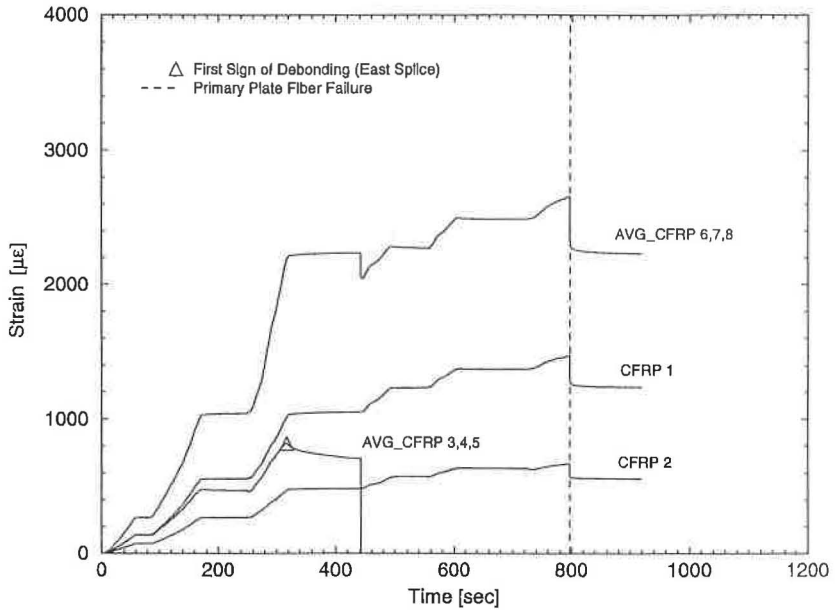

FIGURE 6.43. CFRP Strain Histories at Gage Locations On and Off the East Splice Plate, Beam 4 (ULT 2)

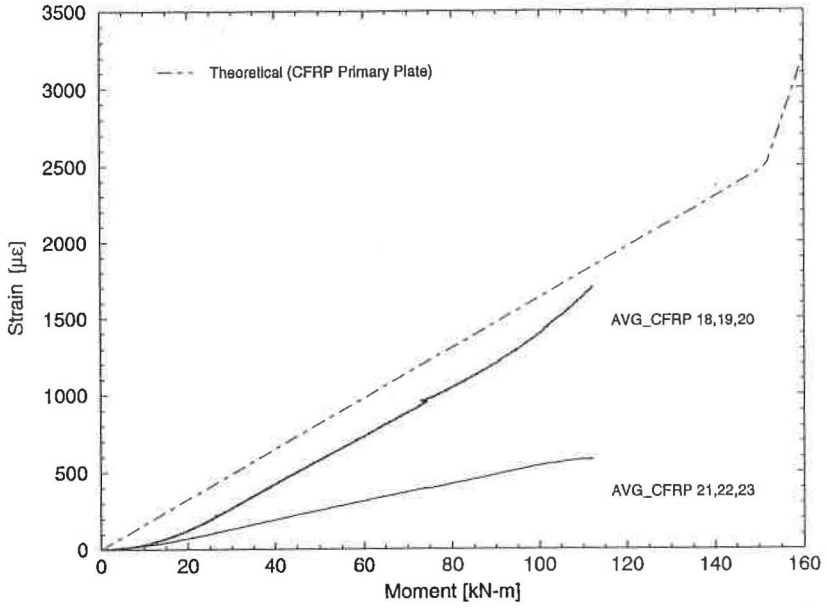

FIGURE 6.44. CFRP Strain-Moment Relationships at Gage Locations On and Off the Interior End of the West Splice Plate, Beam 4 (ULT 2)

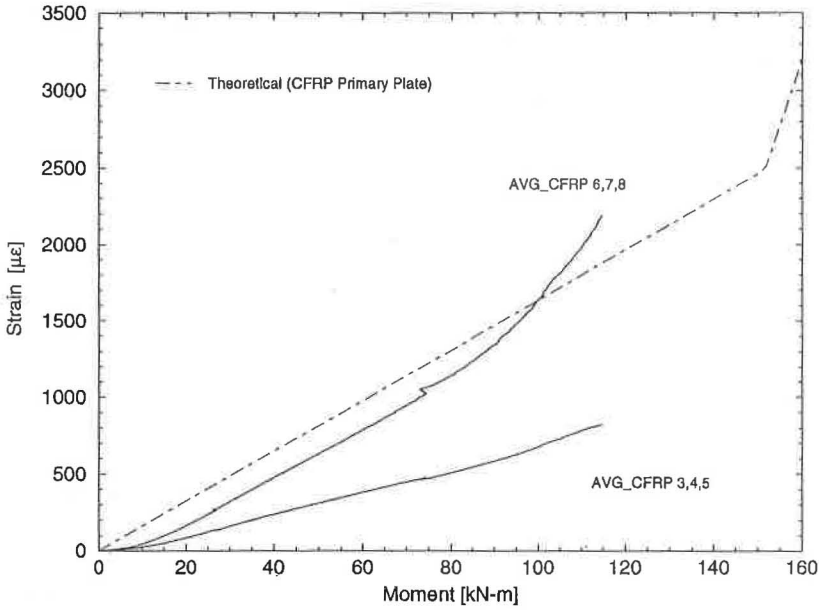

FIGURE 6.45. CFRP Strain-Moment Relationships at Gage Locations On and Off the Interior End of the East Splice Plate, Beam 4 (ULT 2)

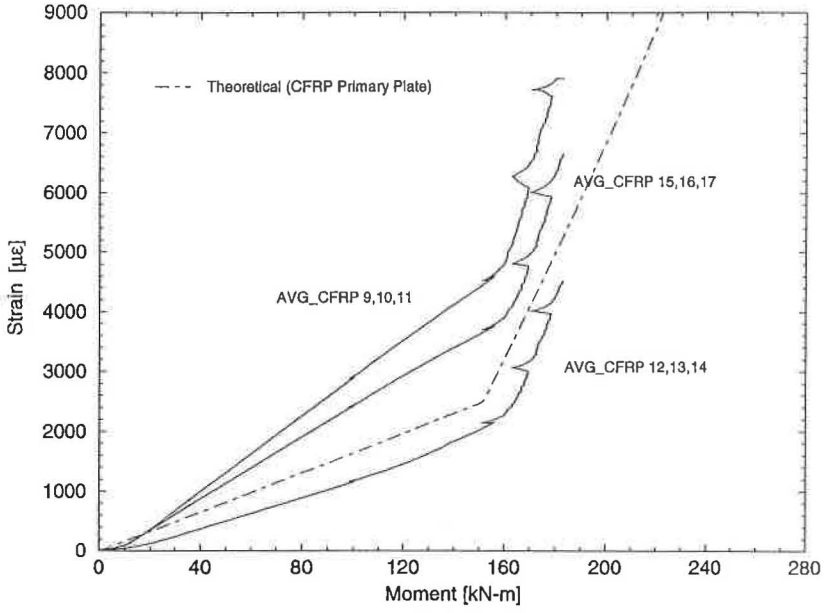

FIGURE 6.46. CFRP Strain-Moment Relationships from Primary Plate Gage Locations in the Constant Moment Region, Beam 4 (ULT 2)

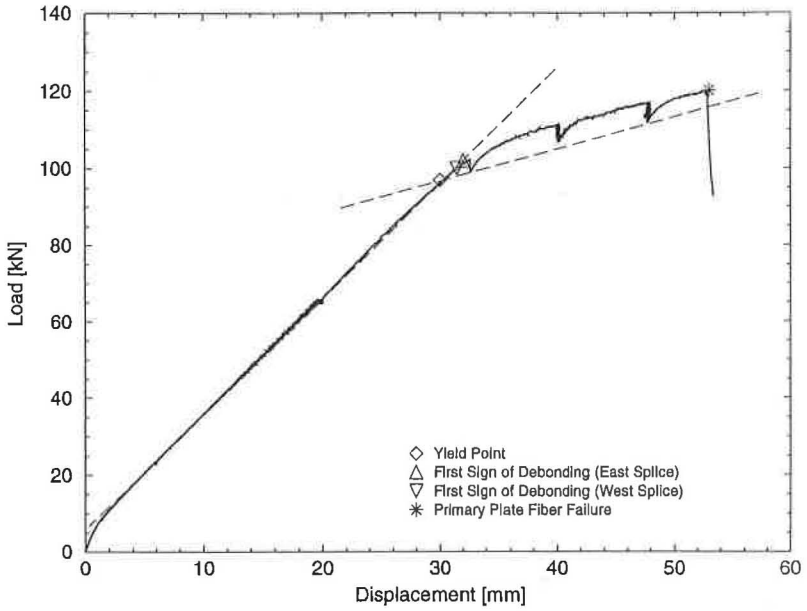

FIGURE 6.47. Load-Deflection Relationship at Midspan, Beam 4 (ULT 2)

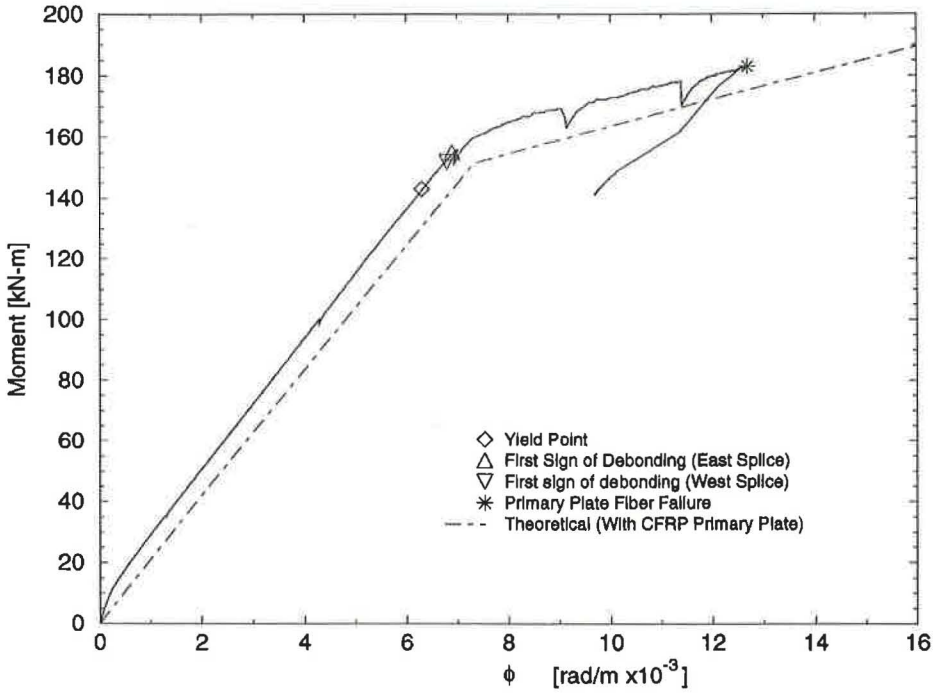

FIGURE 6.48. Moment-Curvature Relationships at Midspan, Beam 4 (ULT 2)

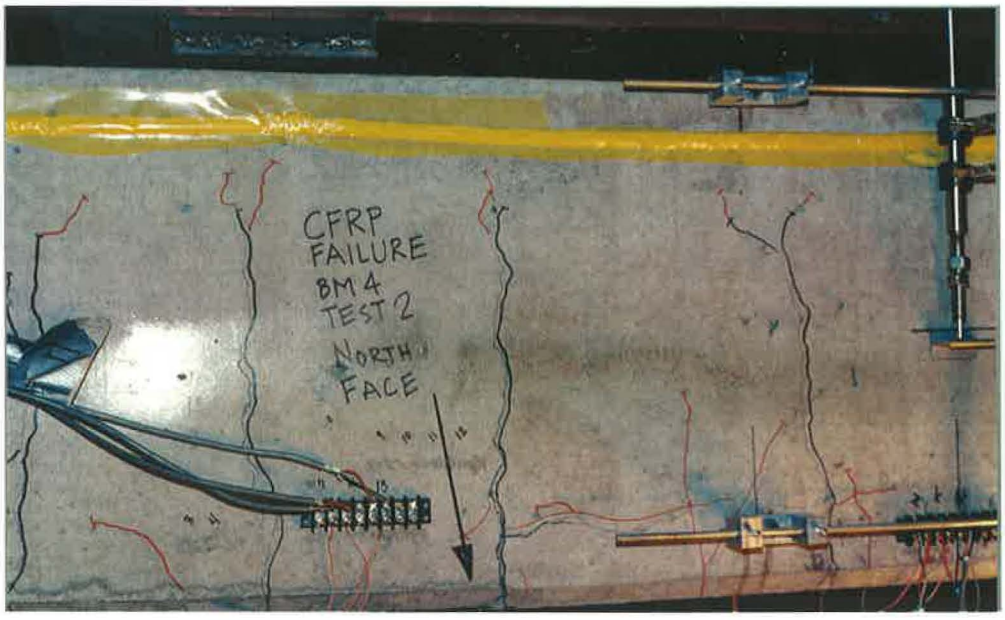

FIGURE 6.49. Shear Failure Pattern After Tension Failure of the Primary Plate, Beam 4 (ULT 2)

Beam 5 (ULT)

The primary and splice plate selection for Beam 5 (ULT) was the same as that used in the second Ultimate Load Test of Beam 4, and is typical for all subsequent beam strengthening tests.

Similar to observations for Beam 4 (ULT 2), initial splice plate debonding occurred at the interior ends of the two plates. Initial debonding of the east and west plates occurred simultaneously at a beam deflection of 36 mm and a total load of 108 kN. In contrast however, complete splice plate debonding did occur at the interior end of the west plate before primary plate tension failure. The load and deflection at complete debonding was 127 kN and 63 mm, respectively. In addition to complete debonding of the splice plate, initiating at the butt joint of west splice plate, and extending approximately 635 mm to east of midspan, primary plate debonding also occurred immediately following splice failure.

In Figure 6.50 and 6.51, CFRP strain histories for gage locations at the end of the splice plates and off the splices, on the primary plates, are shown. The plots indicate the initial signs of debonding occurred at the interior ends of the east and west splice plates with strain levels at CFRP 2 and 14 dropping to zero.

In Figures 6.52 and 6.53, CFRP strain-moment relationships for gage locations at the end of the splice plate and off the splice, on the primary plate, at the interior ends of the east and west plates, respectively, are shown. In addition to the experimental results, the theoretical primary plate strain relationship is also shown. For the east splice at initial debond, the normal strains at the end of the

splice and off the splice, on the primary plate, at initial debond were 656 με and 1744 με, respectively. The difference in strain at the first sign of debonding was 1088 με. For the west splice plate, the normal strains at the end of the splice and off the splice, on the primary plate, at initial debond were 791 με and 2173 με, respectively. The difference in strain at the end of the west splice plate was 1382 με. The calculated moment at the ends of the splices, where debonding occurred, was 122 kN-m. At this moment, the theoretical primary plate strain was 1821 με.

In Figure 6.54, experimental average primary plate strain-moment relationships at gage locations in the constant moment region, up to complete debonding of the west plate, as well as the theoretical relationship are shown. Compared to the results of the primary plate relationships presented for Beam 4 (ULT 2), the results seen in Figure 6.54 for Beam 5 (ULT) indicate a fairly consistent level of agreement between the experimental and theoretical results.

The load-deflection relationship for Beam 5 (ULT) is shown in Figure 6.55. The plot indicates the yield plateau consistent with Beam 4 (ULT 2). At a load of 103 kN and a deflection of 33 mm, the first indication of beam yielding was observed. The moment at first yield was determined to be 157 kN-m. Prior to yielding, a service load stiffness of 2.80 kN/mm was calculated. The experimental and theoretical moment-curvature relationships are shown in Figure 6.56.

Again, adhesive failure at the primary plate/adhesive interface controlled the initial debonding of the east splice and complete debonding of the west. In the case of primary plate debonding, adhesive failure at the primary plate/adhesive interface was seen. In Figure 6.57, a photo of both the west splice plate after complete debonding and the extent of primary plate debonding to the east of midspan are shown. The residual deflection 24 hours after testing was 28.09 mm.

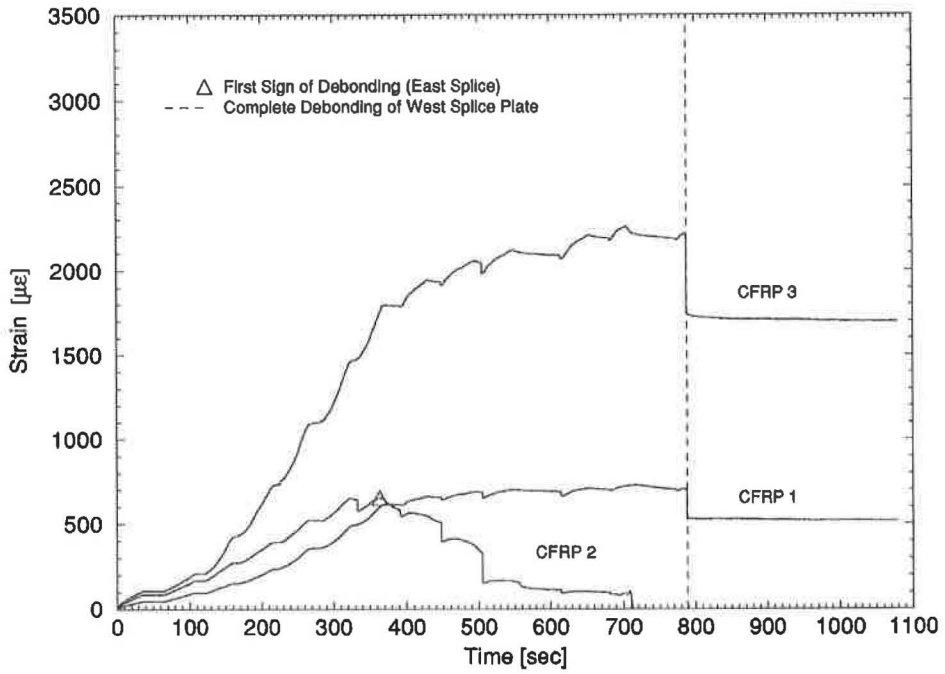

FIGURE 6.50. CFRP Strain Histories at Gage Locations On and Off the East Splice Plate, Beam 5 (ULT)

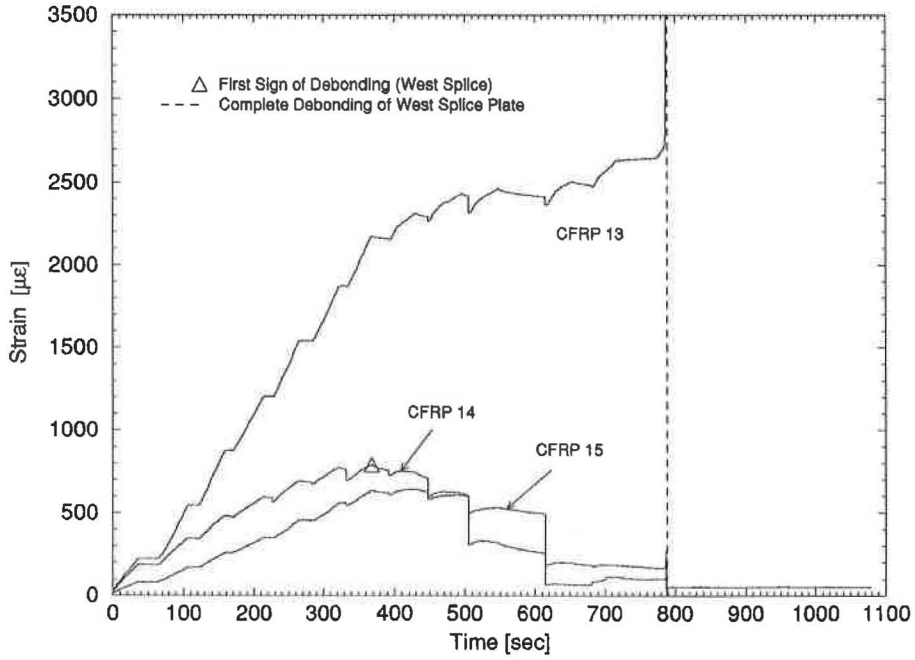

FIGURE 6.51. CFRP Strain Histories at Gage Locations On and Off the West Splice Plate, Beam 5 (ULT)

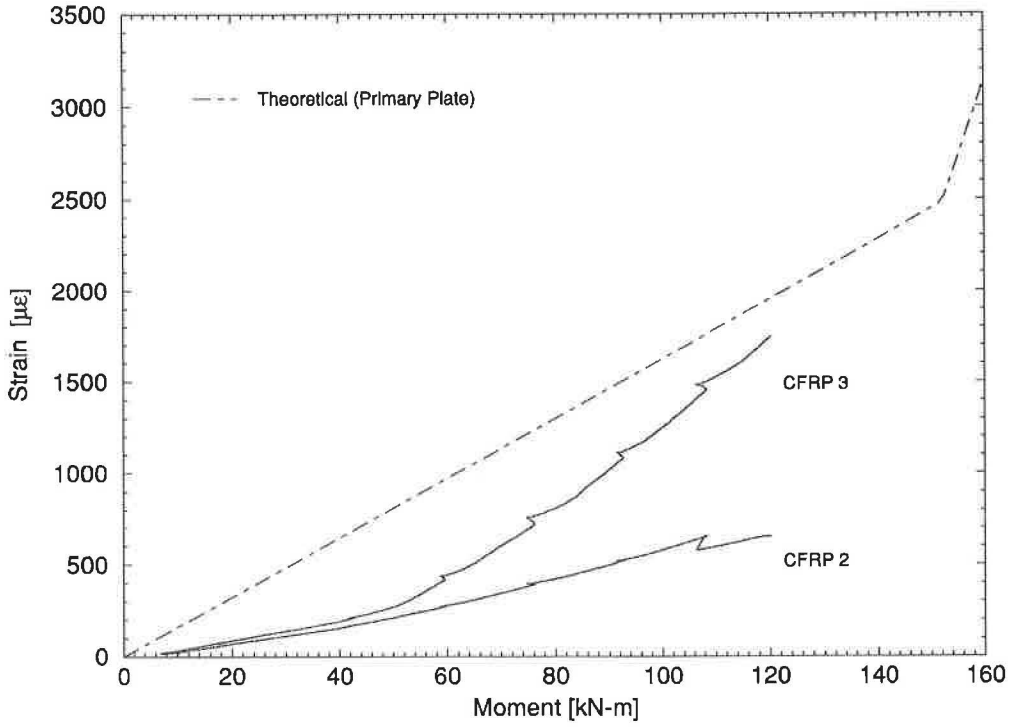

FIGURE 6.52. CFRP Strain-Moment Relationships at Gage Locations On and Off the Interior End of the East Splice Plate, Beam 5 (ULT)

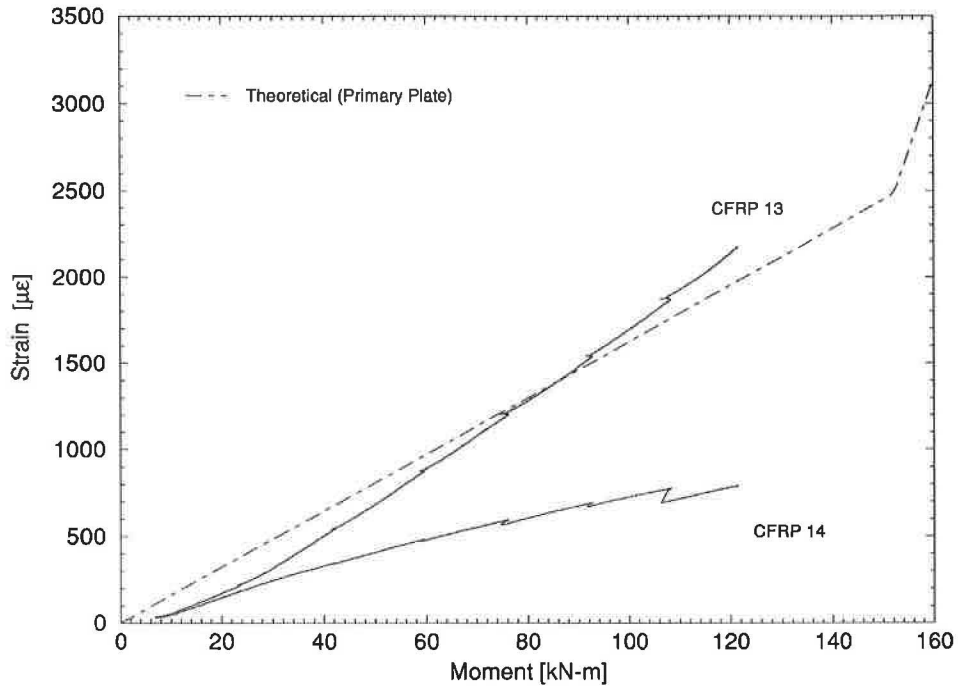

FIGURE 6.53. CFRP Strain-Moment Relationships at Gage Locations On and Off the Interior end of the West Splice Plate, Beam 5 (ULT)

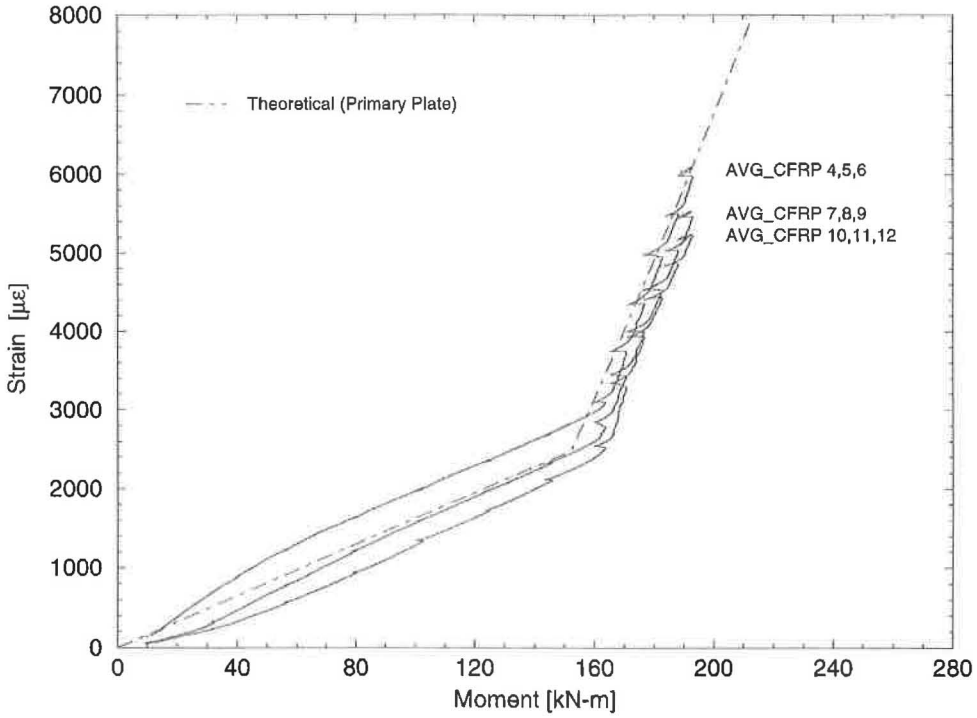

FIGURE 6.54. CFRP Strain-Moment Relationships from Primary Plate Gages in the Constant Moment Region, Beam 5 (ULT)

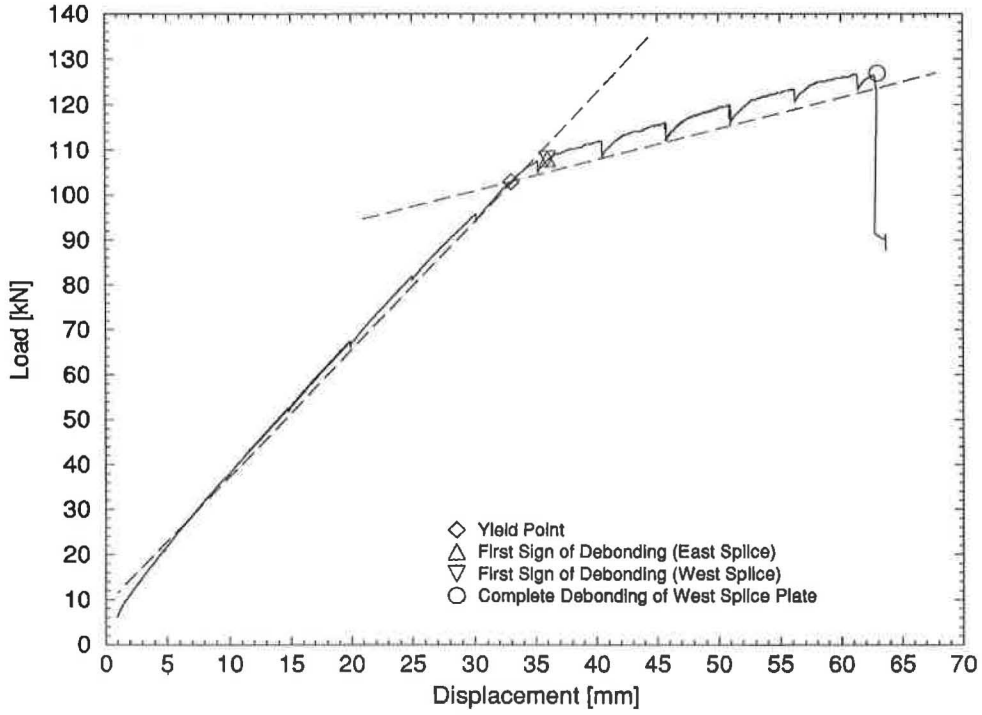

FIGURE 6.55. Load-Deflection Relationship at Midspan, Beam 5 (ULT)

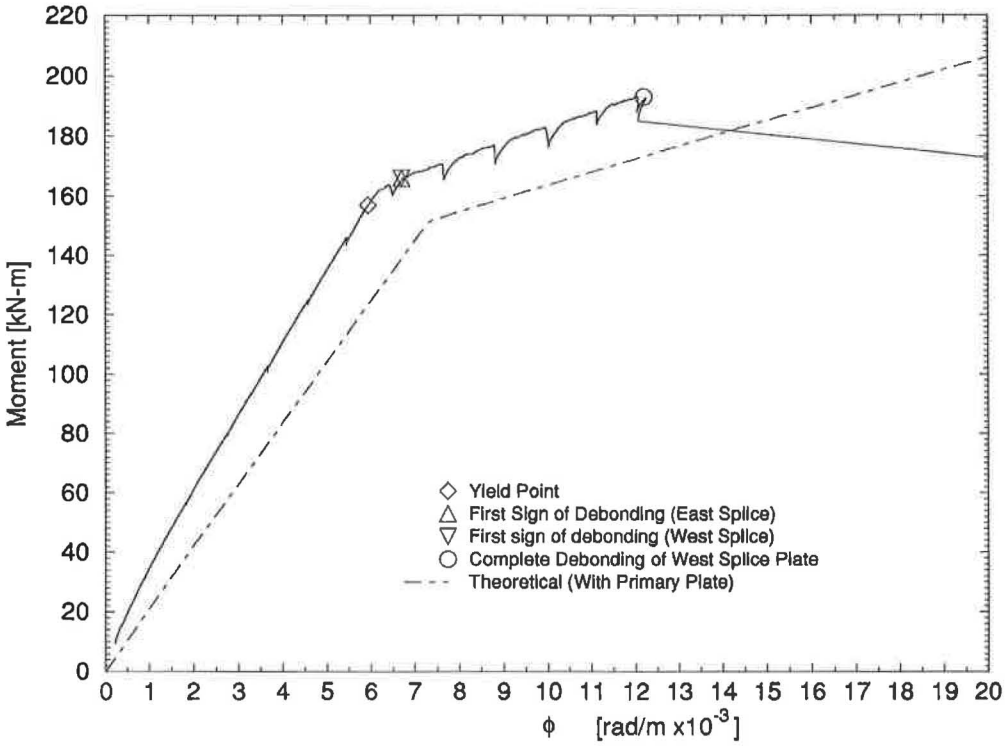

FIGURE 6.56. Moment-Curvature Relationships at Midspan, Beam 5 (ULT)

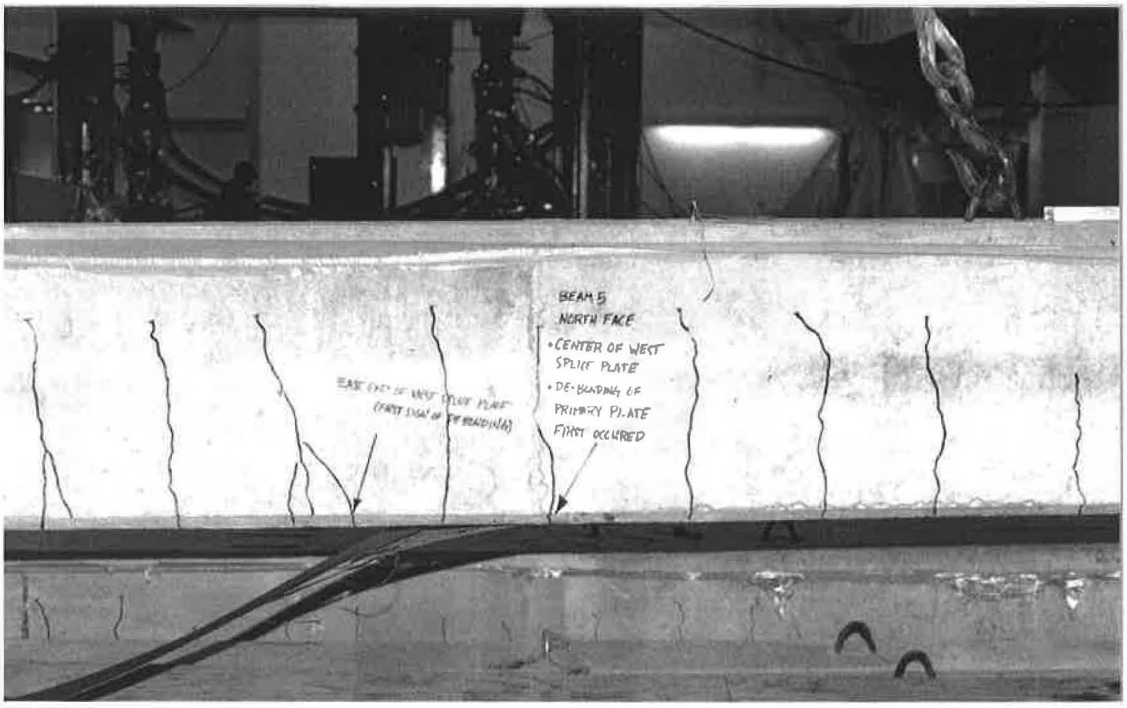

FIGURE 6.57 Beam 5, West Splice Plate and Primary Plate after Debonding

Beam 6 (ULT 1)

Similar to the first Ultimate Load Test of Beam 4, a 914 mm long dummy plate positioned at midspan was used for the initial test of Beam 6 (see Figure 6.16). However, Beam 6 was the first undamaged beam tested. In contrast to the results observed for Beam 4 (ULT 1), initial signs of splice plate debonding did occur at the interior end of the east splice plate before complete debonding of the dummy plate.

At a deflection of 18 mm and a total load of 57 kN, the first indication of dummy plate debonding occurred at both ends of the plate simultaneously. Subsequently, at a deflection of 24 mm and a total load of 69 kN, the first sign of splice plate debonding occurred at the east plate with complete debonding of the dummy plate immediately following.

CFRP strain histories at gage locations at the end of the dummy plate and off the dummy plate, on the primary plate, are shown in Figure 6.58. In Figure 6.59, CFRP strain histories at gage locations at the end of the east splice plate and off the splice, on the primary plate, are shown. The strain distribution at gage locations at the end of the dummy plate and off the dummy plate, on the primary plate, at the time of initial debonding can be seen in Figure 6.60.

With debonding of the dummy plate occurring simultaneously at both ends, strain levels at the ends of the dummy plate and off the dummy plate, on the primary plate, were considered. In Figure 6.61, average strain-moment relationships, up to the first sign of debonding, at the ends of the dummy plate and off the dummy plate, on the primary plate, as well as the theoretical primary plate relationship are shown. The average normal strains at initial debond on the east and west ends of the dummy plate were 865 με and 622 με, corresponding to average normal strains in the primary plate of 1942 με and 1826 με,

respectively. The strain differences observed at the east and west end of the dummy plate were 1077 με and 1204 με, respectively. The moment at first debond at the ends of the dummy plate was 87 kN-m. At this moment, the theoretical primary plate strain was 1418 με.

In Figure 6.62, CFRP strain-moment relationships at the interior end of the east splice plate and off the splice plate, on the primary plate, up to the first sign of debonding, as well as the theoretical primary plate strain relationship are shown. Normal strains at the interior end of the splice and off the splice, on the primary plate, were 543 με and 1690 με, respectively. The difference in strain observed at the interior end of the east splice at initial debond was 1147 με. The moment at the end of the splice at which debonding occurred was 78 kN-m. At the point of initial debonding, the theoretical primary plate strain at the interior end of the east splice was 1271 με.

From the load-deflection relationship, no indication of beam yielding was evident before complete debonding of the dummy plate (see Figure 6.63). The service load stiffness before complete debonding, using the dashed line for the slope, was 2.08 kN/mm. Experimental and theoretical moment-curvature relationships are shown in Figure 6.64.

Adhesive failure for both the completely debonded dummy plate and the partially debonded splice plate occurred at the primary plate/adhesive interface. Residual deflection resulting from the initial load test of the undamaged beam was 7.34 mm. The crack distribution after testing was similar to that of typical crack patterns observed after Crack Tests. With no indication of complete splice plate debonding, the dummy plate was removed along with all residual adhesive for a second test, Beam 6 (ULT 2).

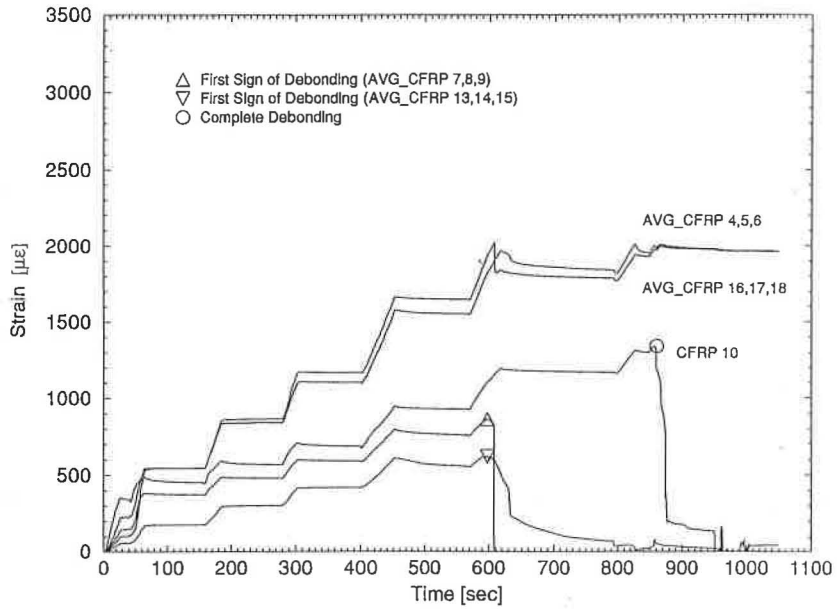

FIGURE 6.58. CFRP Strain Histories at Gage Locations On and Off the Dummy Plate, Beam 6 (ULT 1)

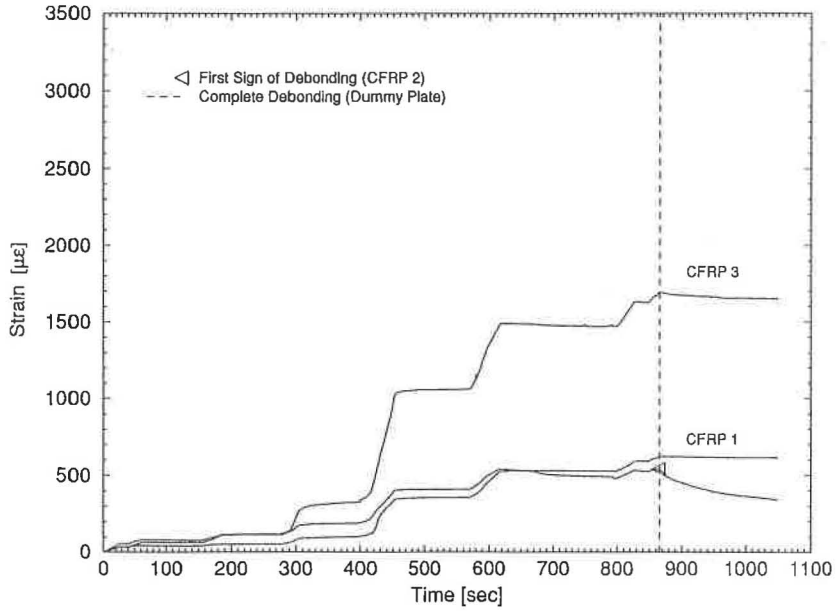

FIGURE 6.59. CFRP Strain Histories at Gage Locations On and Off the East Splice Plate, Beam 6 (ULT 1)

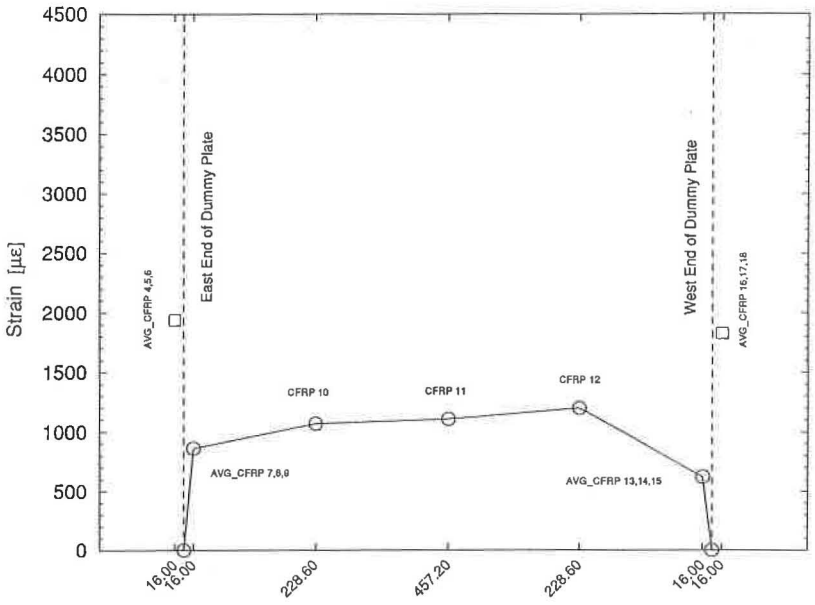

FIGURE 6.60. Dummy/Primary Plate Strain Distribution at First Sign of Debonding, Distances Measured from the Ends of the Dummy Plate [mm], Beam 6 (ULT 1)

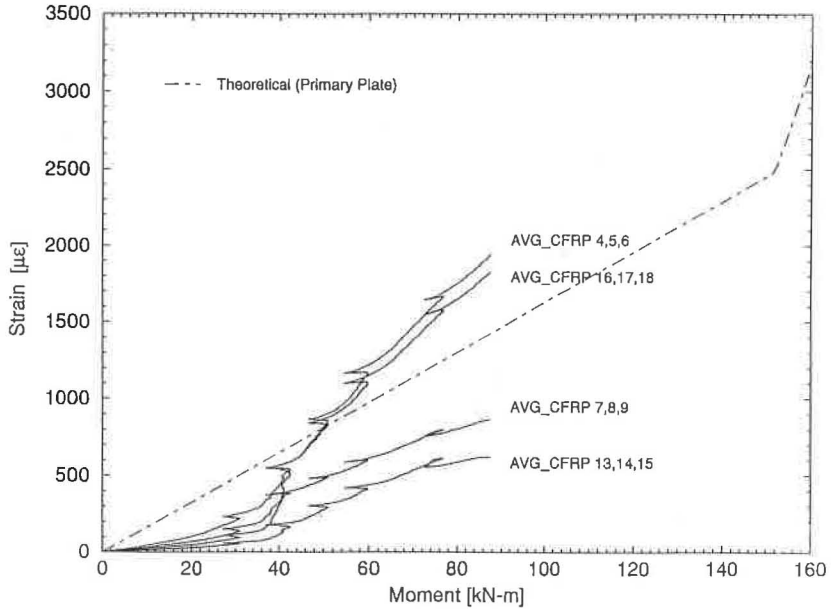

FIGURE 6.61. CFRP Strain-Moment Relationships at Gage Locations On and Off the Ends of the Dummy Plate, Beam 6 (ULT 1)

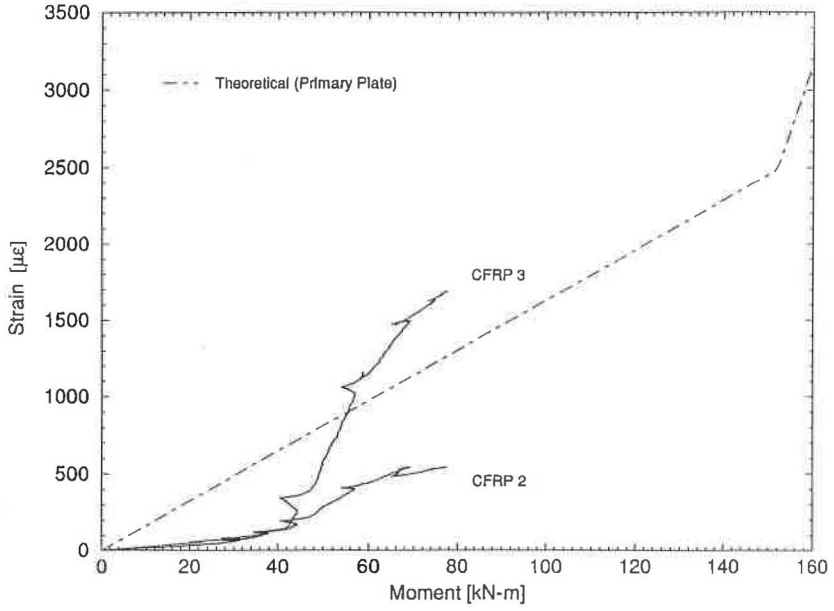

FIGURE 6.62. CFRP Strain-Moment Relationships at Gage Locations On and Off the Interior End of the East Splice Plate, Beam 6 (ULT 1)

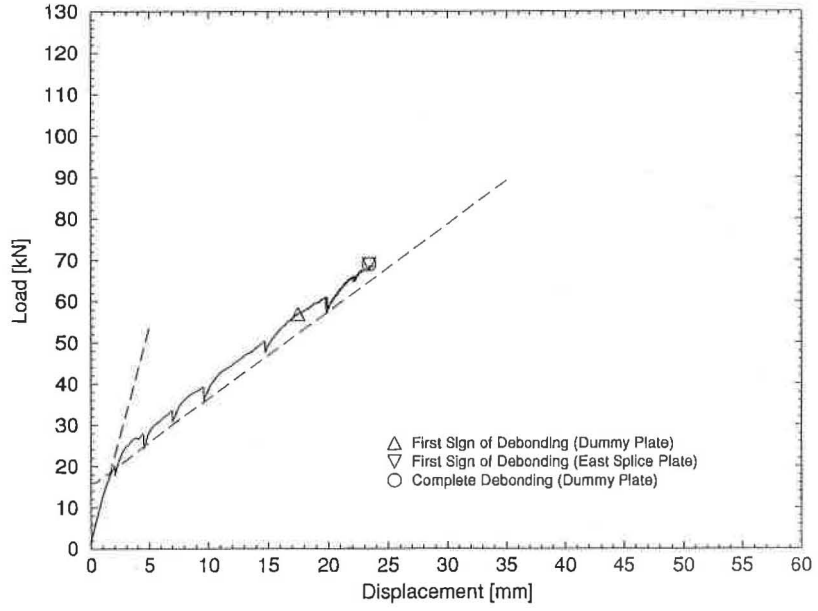

FIGURE 6.63. Load-Deflection Relationship at Midspan, Beam 6 (ULT 1)

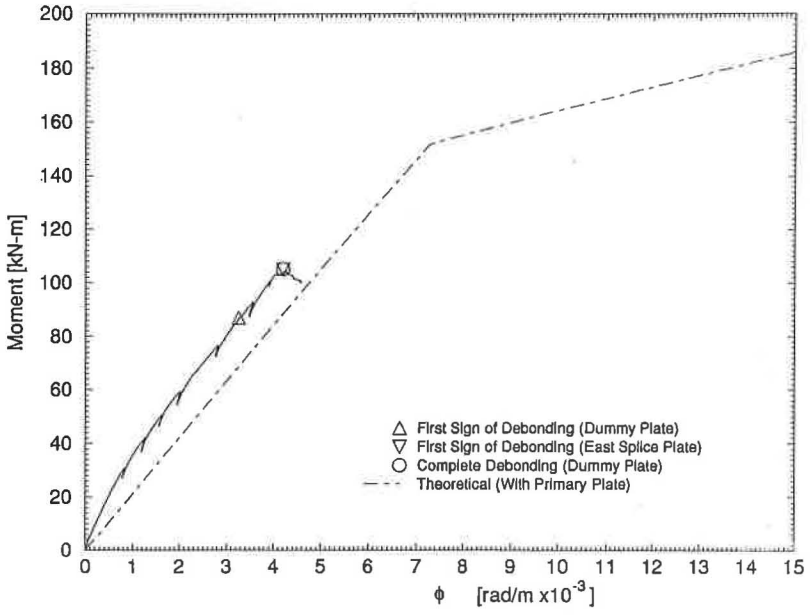

FIGURE 6.64. Moment-Curvature Relationships at Midspan, Beam 6 (ULT 1)

Beam 6 (ULT 2)

Recognizing that initial splice plate debonding occurred at the interior end of the east splice plate during the first Ultimate Load Test of Beam 6, the objective of this test was to identify when or if splice plate debonding would occur at the west splice plate, and what beam failure mode would control.

At a deflection of 20 mm and a load of 75 kN, the first indication of splice plate debonding occurred at the interior end of the west splice plate. Complete debonding at the interior end of the west splice plate followed at a deflection of 28 mm and a load of 95 kN. CFRP strain histories from gage locations at the interior end of the west splice plate and off the splice, on the primary plate, can be seen in Figure 6.65.

For the west splice plate, at the initial sign of debonding, the normal strain levels at the the end of the splice and off the splice, on the primary plate, were 468 με and 1281 με, respectively (see Figure 6.66). The difference in strain levels observed at the end of the splice was 813 με. The moment at the interior end of the plate at the first sign of debonding was 85 kN-m, corresponding to a theoretical primary plate strain of 1385 με. In Figure 6.67, experimental average primary plate strains at gage locations in the constant moment region, as well as the theoretical primary plate relationships are shown. Figure 6.67 indicates that the theoretical analysis accurately predicts primary plate strains.

The load-deflection relationship is shown in Figure 6.68. A service load stiffness of 3.20 kN/mm was determined from the plot in Figure 6.68. No indication of beam yielding was seen before complete debonding of the west

splice plate. The experimental moment-curvature relationship, along with the theoretical relationship, is shown in Figure 6.69.

After visual inspection of the west splice plate, it was determined that adhesive failure at the primary plate/adhesive interface controlled the failure of the plate. As in Beam 2 (ULT), Beam 6 (ULT 2) was loaded beyond the point of beam failure to a deflection at midspan of approximately 81 mm, during which time complete debonding of the east splice plate occurred. No indication of concrete compression failure or primary plate debonding was observed with the additional load. However, as a result of the increased deflection, a longitudinal shear failure pattern at the depth of the bottom flexural reinforcement, originating at the butt joints of the east and west splice plates, was observed (see Figure 6.70). Although the degree of this type secondary failure mode varied for Ultimate Load Tests of Beams 4 through 8, the photo represents a typical crack pattern observed around splice plate, at third point locations, after complete debonding. Residual deflection data was not collected because the beam was loaded well beyond its primary failure mode.

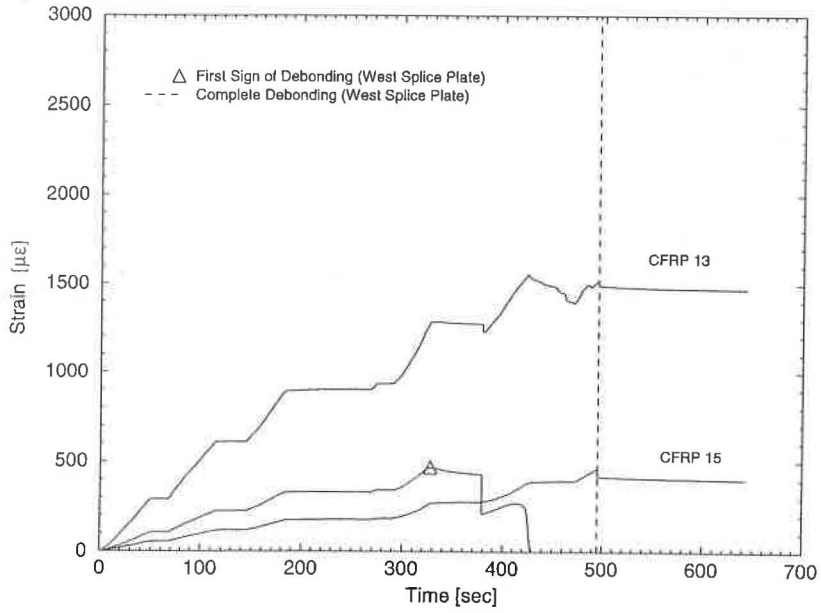

FIGURE 6.65. CFRP Strain Histories at Gage Locations On and Off the West Splice Plate, Beam 6 (ULT 2)

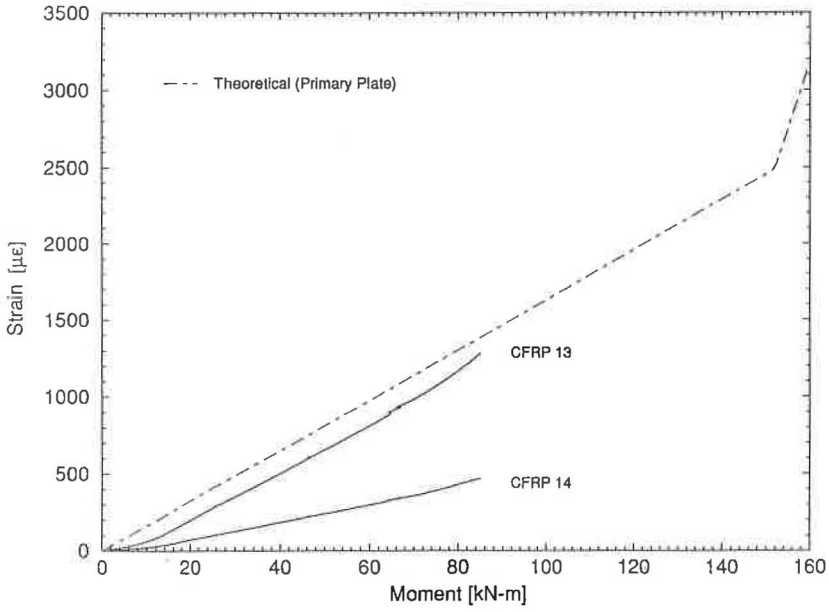

FIGURE 6.66. CFRP Strain-Moment Relationships at Gage Locations On and Off the Interior End of the West Splice Plate, Beam 6 (ULT 2)

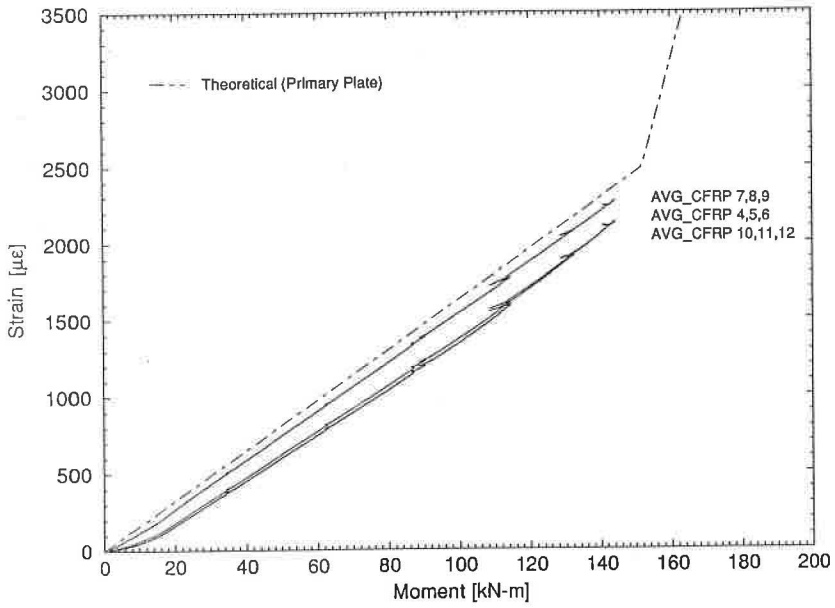

FIGURE 6.67. CFRP Strain-Moment Relationships from Primary Plate Strain Gages in the Constant Moment Region, Beam 6 (ULT 2)

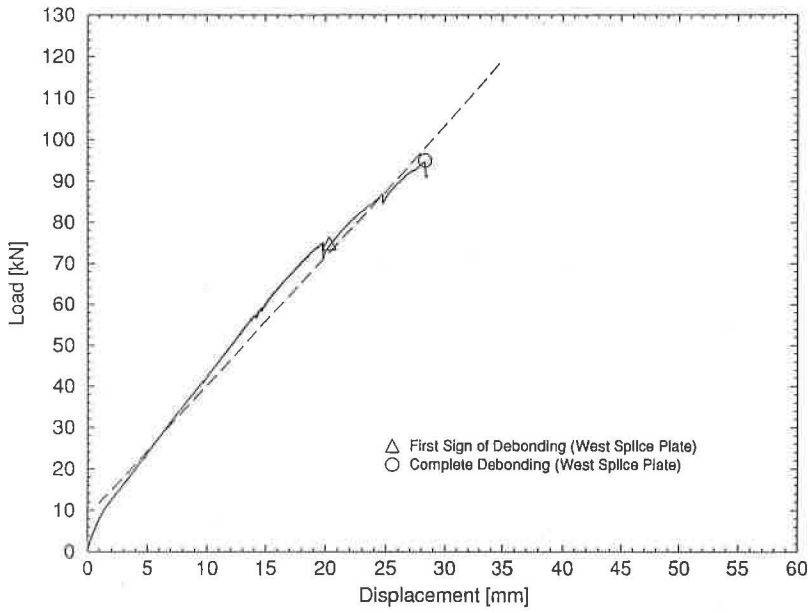

FIGURE 6.68. Load-Deflection Relationship at Midspan, Beam 6 (ULT 2)

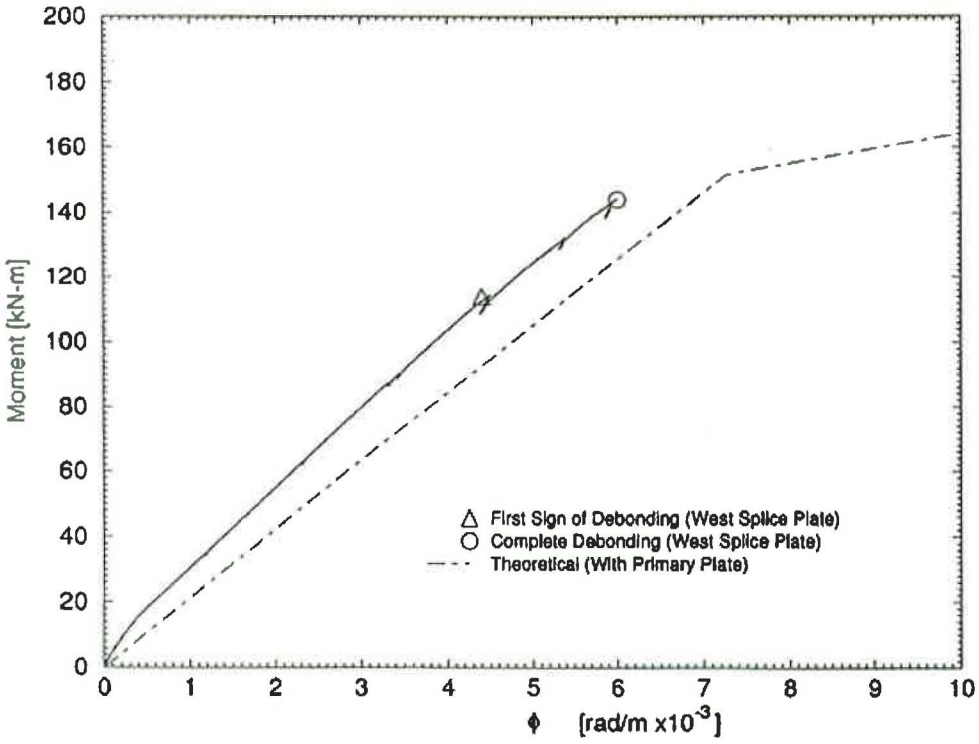

FIGURE 6.69. Moment-Curvature Relationships at Midspan, Beam 6 (ULT 2)

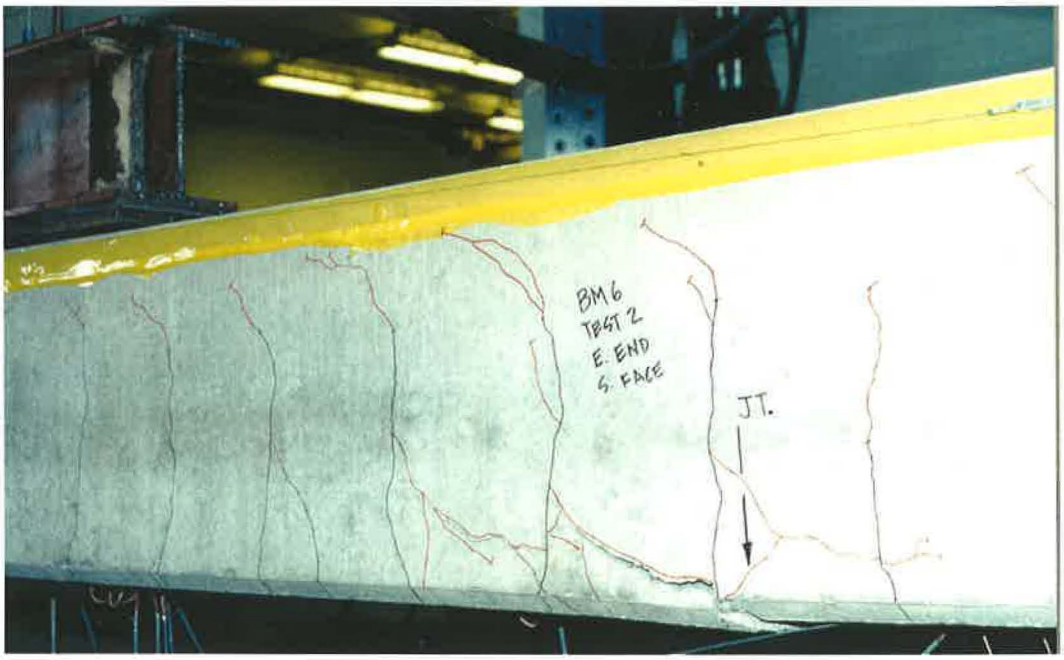

FIGURE 6.70. Typical Shear Failure Pattern at Third Point Splice Plate Locations After Complete Debonding

Beam 7 (ULT)

With a plate selection and beam condition similar to that of Beam 5 (ULT), initial splice plate debonding also occurred at both splice plate locations. At deflections of 33 mm and 35 mm, corresponding to total loads of 105 kN and 108 kN, the first indications of splice plate debonding were observed at the interior ends of the east and west splice plates, respectively. Complete debonding at the interior end of the west plate followed at a deflection of 40 mm and a load of 113 kN. In Figures 6.71 and 6.72, CFRP strain histories recorded at gage locations on the end of the splice plates and off the splices, on the primary plates, are shown.

At the interior end of the east splice, the normal strains at the end of the splice and off the splice, on the primary plate, at initial debond were 666 με and 2202 με, respectively. The difference observed at the end of the splice at the first sign of debonding was 1536 με. In Figure 6.73, CFRP strain-moment relationships, up to first debond, for gage locations at the interior end of the east splice are shown. The theoretical primary plate relationship is also shown in Figure 6.73. The moment at the end of the splice when debonding occurred was 119 kN-m. Using this value, the theoretical primary plate strain was determined to be 1945 με.

In Figure 6.74, CFRP strain-moment relationships, up to first debond, for the west splice plate are shown. Debonding occurred at normal strains at the end of the splice and off the splice, on the primary plate, of 796 με and 2898 με, respectively. The calculated moment at the end of the splice plate at initial

debond was 122 kN-m. The difference in strain levels at the end of the splice was 2102 με. The calculated primary plate strain at first debond was 1994 με.

In Figure 6.75, the experimental CFRP primary plate strain-moment relationships from gage locations in the constant moment region, up to complete debonding of the west plate, as well as the theoretical relationship are shown.

In Figure 6.76, the load-deflection relationship for Beam 7 (ULT) is shown. From the plot, some indication of beam yielding was observed before complete debonding of the west splice. The first indication of beam yielding was observed at a deflection of 33 mm and a total load of 105 kN. The calculated moment at first yield was 160 kN-m. Using the slope of the dashed line before yielding, a service load stiffness of 2.90 kN/mm was determined. In Figure 6.77, experimental and theoretical moment-curvature relationships are shown.

Adhesive failure of both splice plates occurred at the primary plate/adhesive interface. The residual displacement, measured approximately 24 hours after loading, was determined to be 4.83 mm.

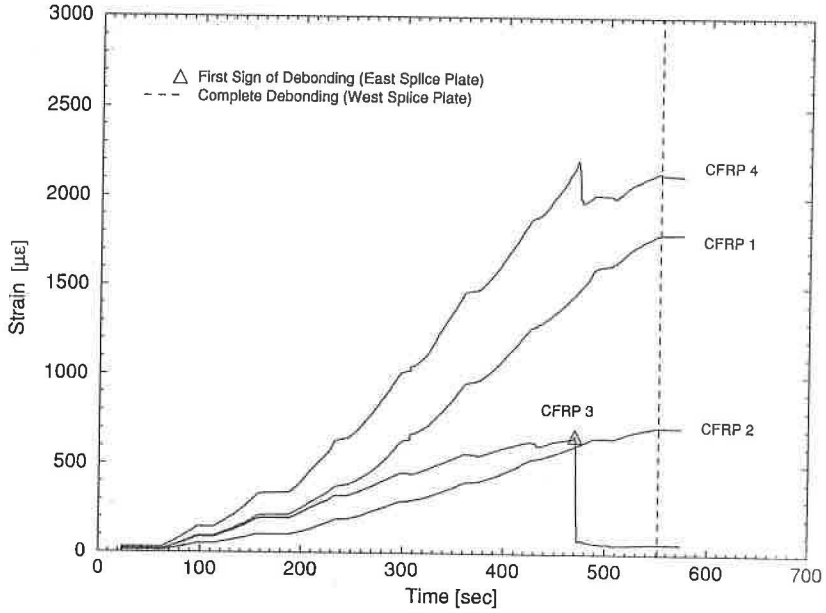

FIGURE 6.71. CFRP Strain Histories from Gage Locations On and Off the East Splice Plate, Beam 7 (ULT)

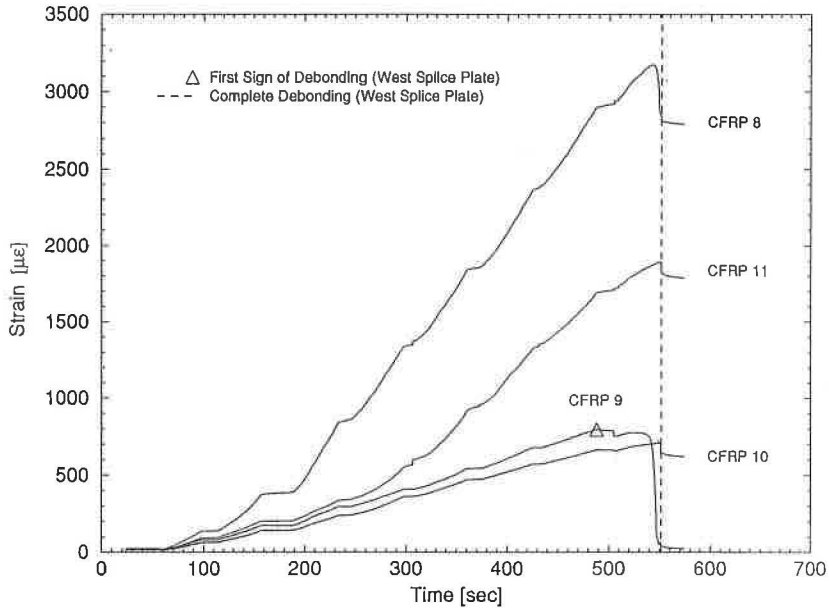

FIGURE 6.72. CFRP Strain Histories from Gage Locations On and Off the West Splice Plate, Beam 7 (ULT)

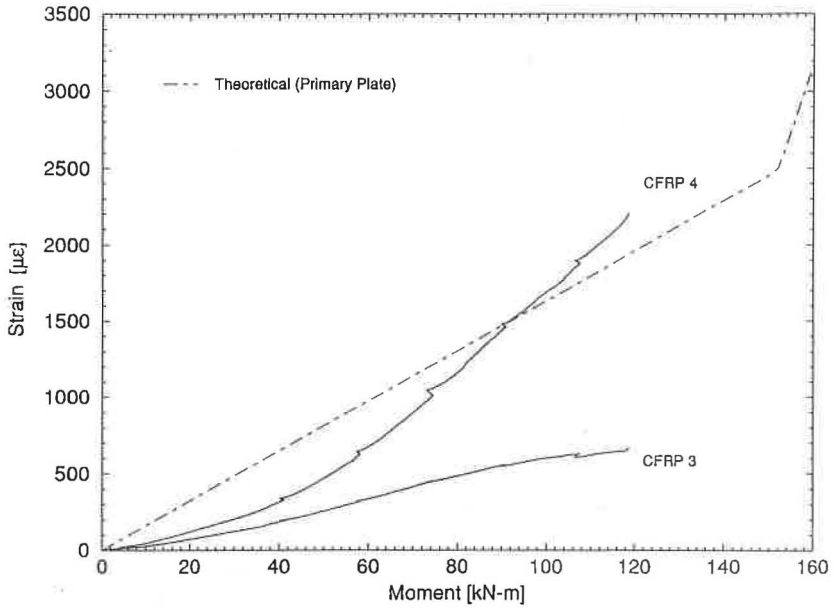

FIGURE 6.73. CFRP Strain-Moment Relationships from Gage Locations On and Off the Interior End of the East Splice Plate, Beam 7 (ULT)

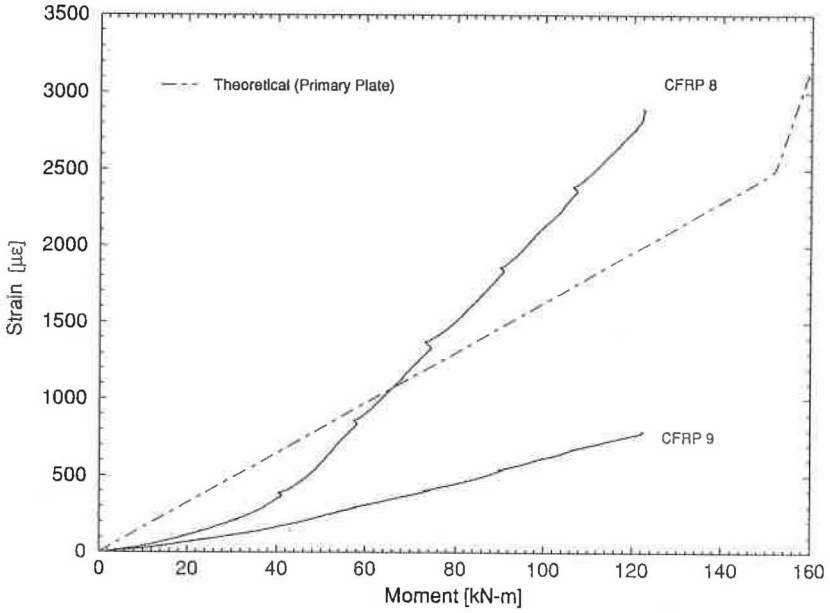

FIGURE 6.74. CFRP Strain-Moment Relationships from Gage Locations On and Off the Interior End of the West Splice Plate, Beam 7 (ULT)

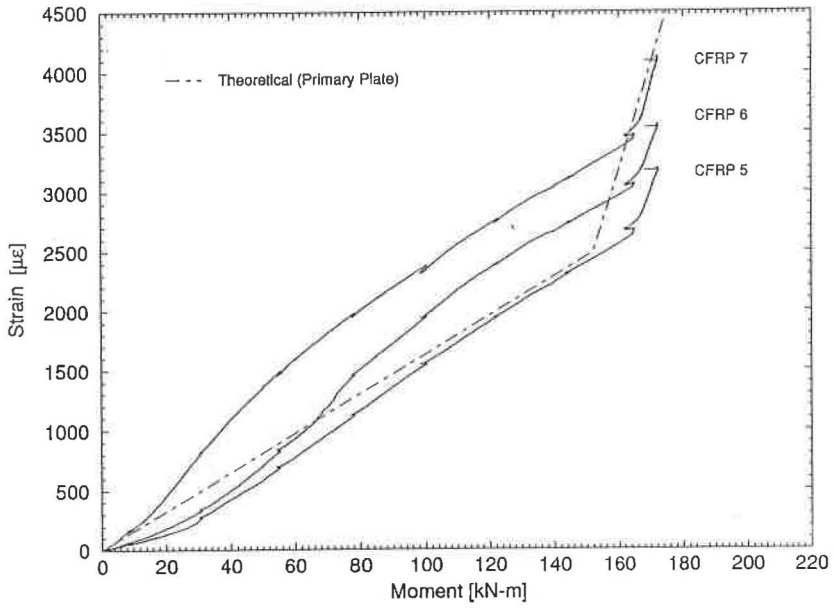

FIGURE 6.75. CFRP Strain-Moment Relationships from Primary Plate Gage Locations in the Constant Moment Region, Beam 7 (ULT)

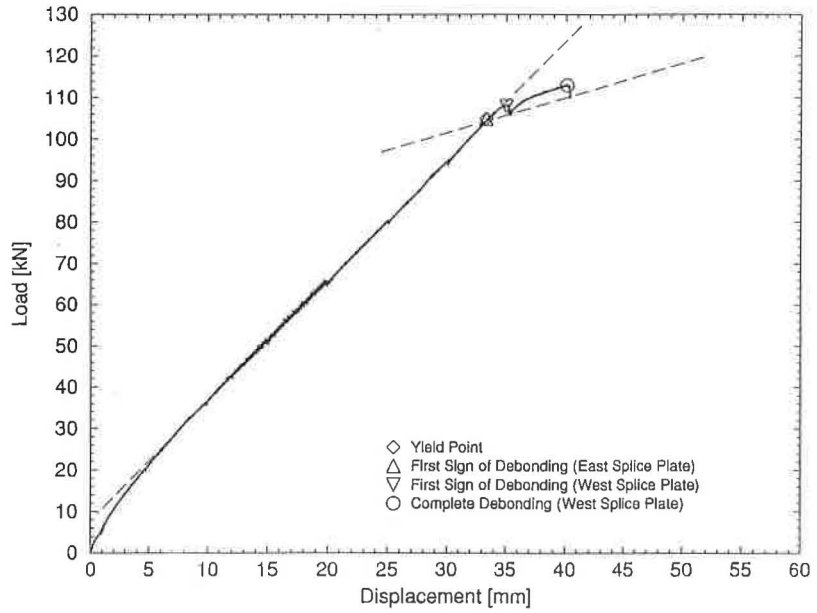

FIGURE 6.76. Load-Deflection Relationship at Midspan, Beam 7 (ULT)

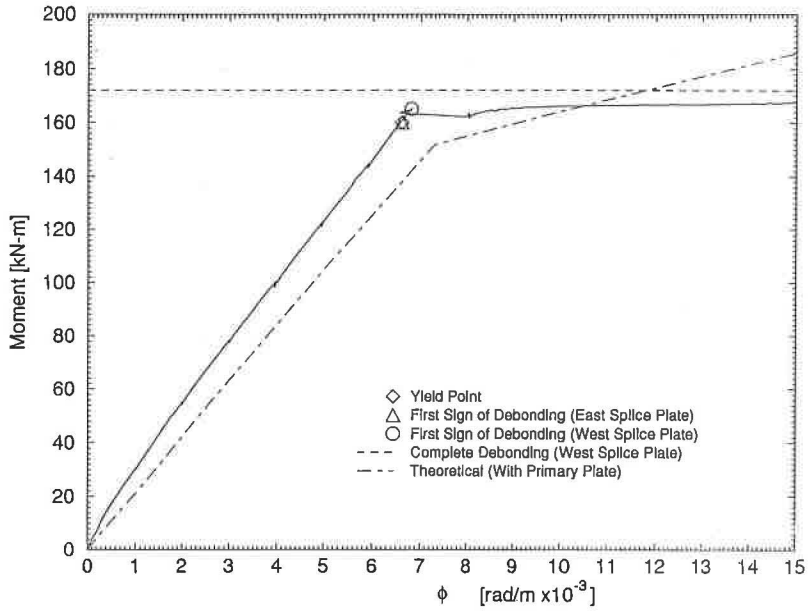

FIGURE 6.77. Moment-Curvature Relationships at Midspan, Beam 7 (ULT)

Beam 8 (ULT)

As was mentioned earlier, the splice plates for Beam 8 were misaligned during the application of the plates due to the positioning of the vacuum valves (see Figure 6.19). Although the plates were not in the desired position, testing of the undamaged beam continued.

At a beam deflection of 35 mm, under a total load of 95 kN, the first indication of splice plate debonding occurred at the interior end of the east plate. Subsequently, debonding of the interior end of the west plate was observed at a deflection of 39 mm and load of 105 kN. In contrast to the preceding tests with similar plate layouts, complete debonding occurred at the exterior side of the east splice plate at a higher deflection and load level. The deflection and load at the point of complete debonding was 67 mm and 131 kN, respectively. This indicates that the performance of the splice plates was not adversely affected by the slight misalignment. The overlapping area of the splice plate on the concrete surface may have been the contributing factor, and would explain why complete debonding occurred at the exterior end of the east splice plate. Complete debonding occurred where there was less overlapping area (see Figure 6.19). In Figure 6.78 and 6.79, CFRP strain histories from gage locations at the end of the splice plates and off the splices, on the primary plates, are shown.

In Figure 6.80, CFRP strain-moment relationships up to first sign of debonding at gage locations at the interior end of the east splice plate and off the splice, on the primary plate, are shown. At the first sign of debonding, normal strains of 1007 με and 2070 με, were observed at the interior end of the splice

plate and off the splice, on the primary plate, respectively. The difference in normal strain levels was 1063 με. At initial debond, the moment at the end of the splice plate was 107 kN-m, corresponding to a theoretical primary plate strain of 1758 με. For the west splice plate, normal strains at the interior end of the splice and off the splice, on the primary plate, were 983 με and 2469 με, respectively (see Figure 6.81). At initial debond, the moment at the interior end of the splice plate was calculated to be 119 kN-m, corresponding to a theoretical primary plate strain of 2469 με.

Average experimental CFRP primary plate strain-moment relationships from gage locations in the constant moment region, as well as the theoretical primary plate relationship, are shown in Figure 6.82. The plot illustrates consistent agreement between the experimental and theoretical results for the uncracked beam.

In Figure 6.83, the load-deflection relationship is shown. The plot clearly indicates a pronounced yield plateau before complete debonding of the splice. The load and deflection at first yield were determined to be 106 kN and 41 mm, respectively. The calculated moment at yield was 162 kN-m. A service load stiffness of 2.28 kN/mm was determined from the slope of the dashed line prior to beam yielding. In Figure 6.84, the experimental and theoretical moment-curvature relationships at midspan for Beam 8 (ULT) are shown.

The crack pattern observed before complete debonding was similar to that exhibited in the Crack Tests. After complete debonding of the east splice plate, the beam was loaded to a deflection at midspan of approximately 78 mm. The

test was discontinued when no additional load could be applied due to formation of a plastic hinge at the east butt joint. No indication of concrete compression failure or primary plate debonding was observed. Residual displacement data was not collected due to the additional load.

After visual inspection of the east splice plate, it was determined that adhesive failure at the primary plate/adhesive interface did occur at the interior and exterior ends of the plate. For the west splice plate, adhesive failure at the primary plate/adhesive interface was also observed. However, debonding was not observed in the area that the splice plate overlapped the concrete surface.

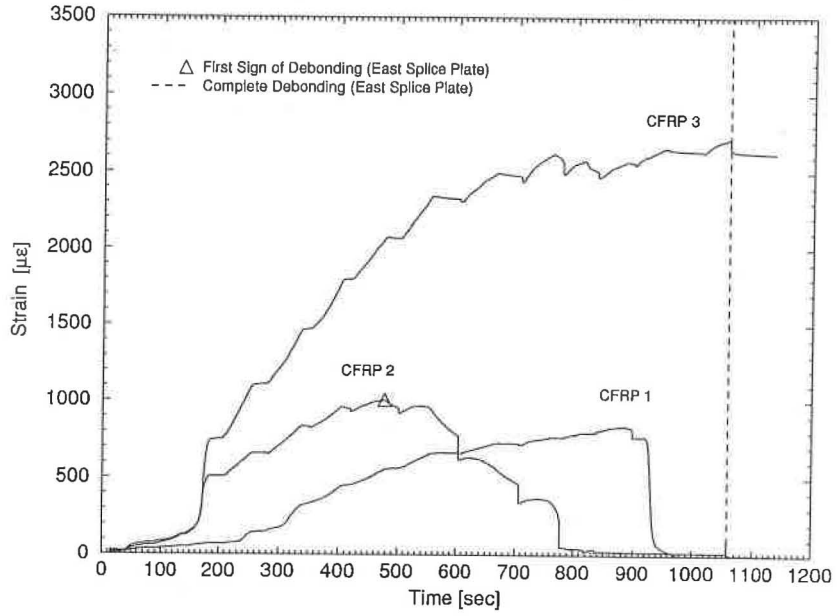

FIGURE 6.78. CFRP Strain Histories from Gage Locations On and Off the East Splice Plate, Beam 8 (ULT)

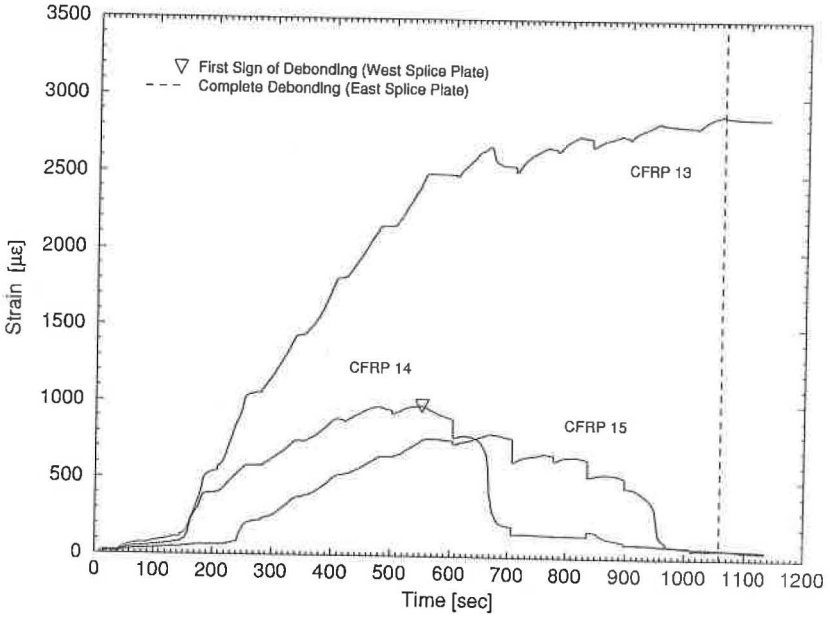

FIGURE 6.79. CFRP Strain Histories from Gage Locations On and Off the West Splice Plate, Beam 8 (ULT)

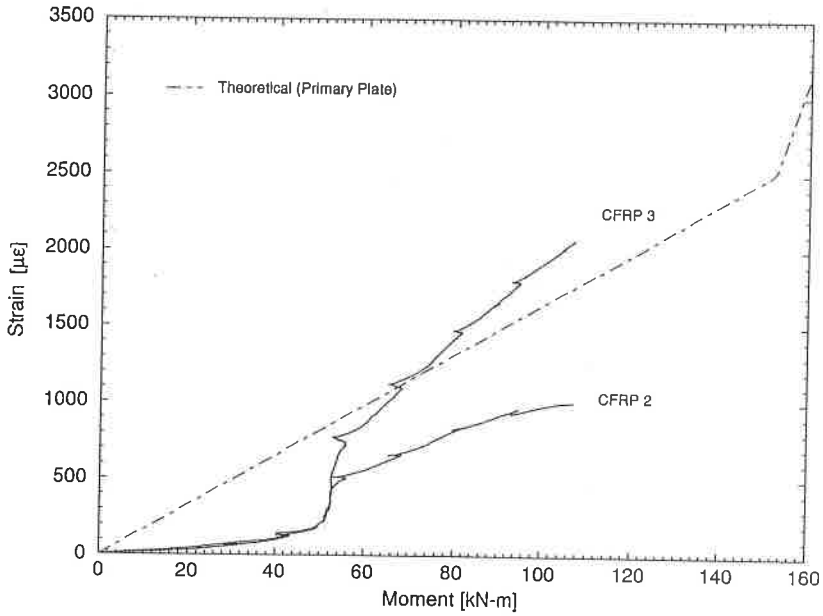

FIGURE 6.80. CFRP Strain-Moment Relationships from Gage Locations On and Off the Interior End of the East Splice Plate, Beam 8 (ULT)

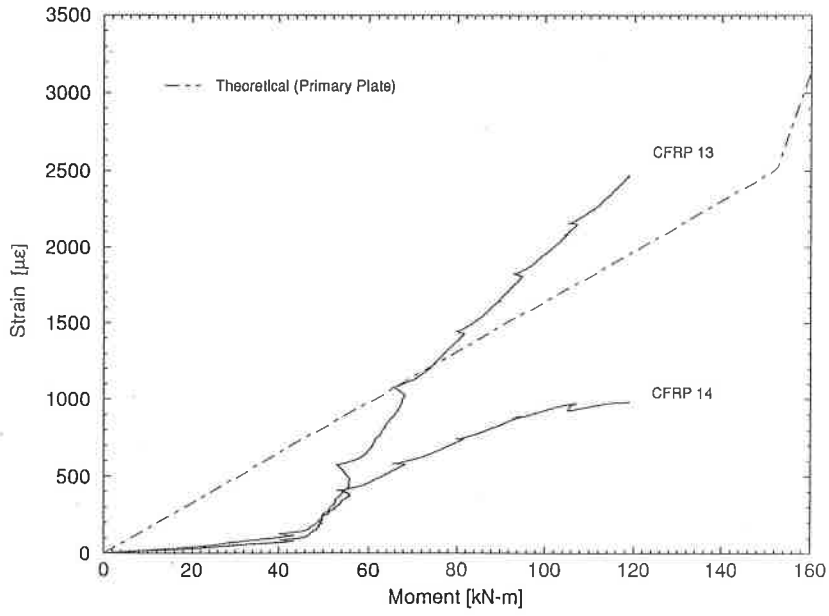

FIGURE 6.81. CFRP Strain-Moment Relationships from Gage Locations On and Off the Interior End of the West Splice Plate, Beam 8 (ULT)

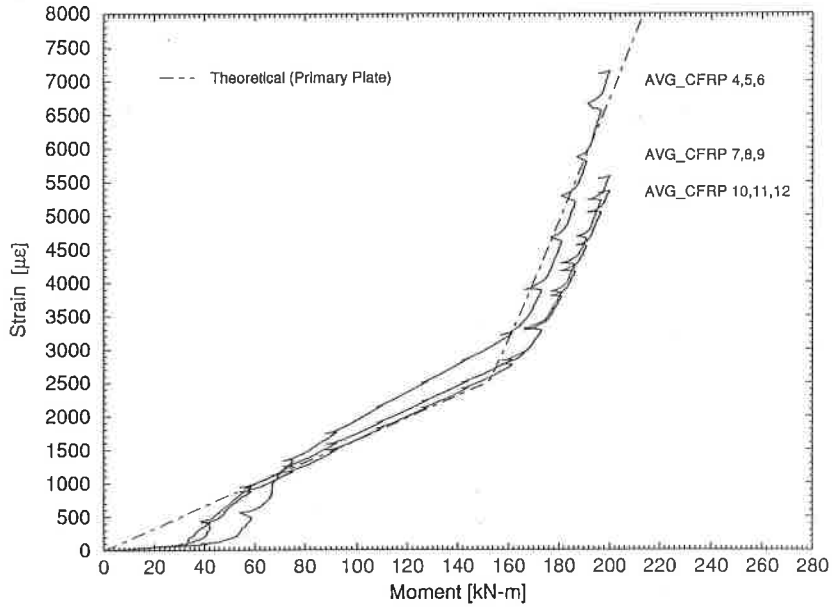

FIGURE 6.82. CFRP Strain-Moment Relationships from Primary Plate Strain Gage Locations in the Constant Moment Region, Beam 8 (ULT)

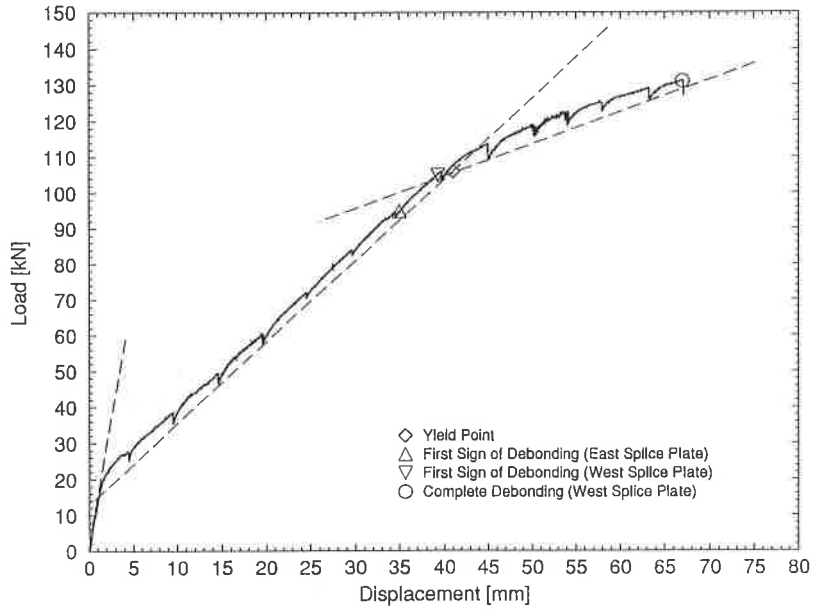

FIGURE 6.83. Load-Deflection Relationship at Midspan, Beam 8 (ULT)

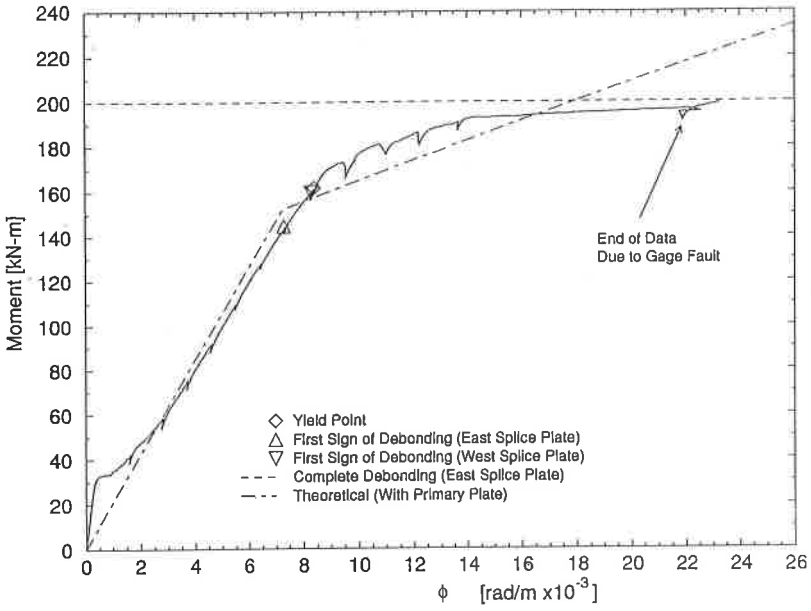

FIGURE 6.84. Moment-Curvature Relationships at Midspan, Beam 8 (ULT)

CHAPTER SEVEN

TENSION TEST SPECIMENS

Introduction

In Chapter Six, results from Fatigue and Ultimate Load Tests provided valuable insight to splice behavior and debonding characteristics. One important characteristic observed was the difference in normal strain levels measured at the end of the splice plates and off the splices, on the primary plates. This is indicative of high shear stress concentration at the primary plate/adhesive interface which initiates debonding of the splice plates. With this hypothesis, the shear stress concentration is a localized affect of the relative strain levels in the primary and splice plate near the end of the splice plate, and not the result of having a butt joint in the primary plate. With this premise, Tension Test specimens where devised to determine if splice plate debonding characteristics could accurately be predicted with simple test procedures, similar to Lap Shear Tests, using representative strengthening materials applied in large scale testing.

In this chapter, a detailed description of the specimen design, instrumentation, test procedure, and results of five Tension Tests are presented. Detailed comparisons between Ultimate Load Tests and Tension Test specimens are made in Chapter Eight, Summary of Results.

Specimen Design

Five Carbon Fiber Reinforced Plastic (CFRP) specimens were tested. The same CFRP and adhesive used in the beam strengthening tests were utilized in the fabrication of Tension Test specimens. Each specimen was comprised of one 457.20 mm long primary plate and two 152.40 mm long dummy plates, each having widths of 25.40 mm. At mid length, on either side of the primary plate, the two dummy plates were bonded (see Figure 7.1). The lengths of the dummy plates were chosen to be approximately six times the specimen width so that the debonding behavior at each end would be independent from the other end.

Before the dummy plates were bonded to the primary plate, all plate surfaces were cleaned with a degreasing agent, Methyl Ethel Ketone (MEK). Once the plates were ready for bonding, the two part adhesive was mixed by weight and applied perpendicular to the length of the dummy plates with a 3.2 mm grooved trowel. The plates were then sandwiched to the primary plate by hand before the vacuum was applied. Using a vacuum technique similar to that employed for the beam specimens, the adhesive was allowed to cure for 8 hours. The vacuum was then removed and the adhesive allowed to cure for a minimum of 72 hours before tests were conducted. In addition, on both sides of the primary plate, a 25.40 x 50.80 mm grip pad was adhered to the ends of the plate before testing.

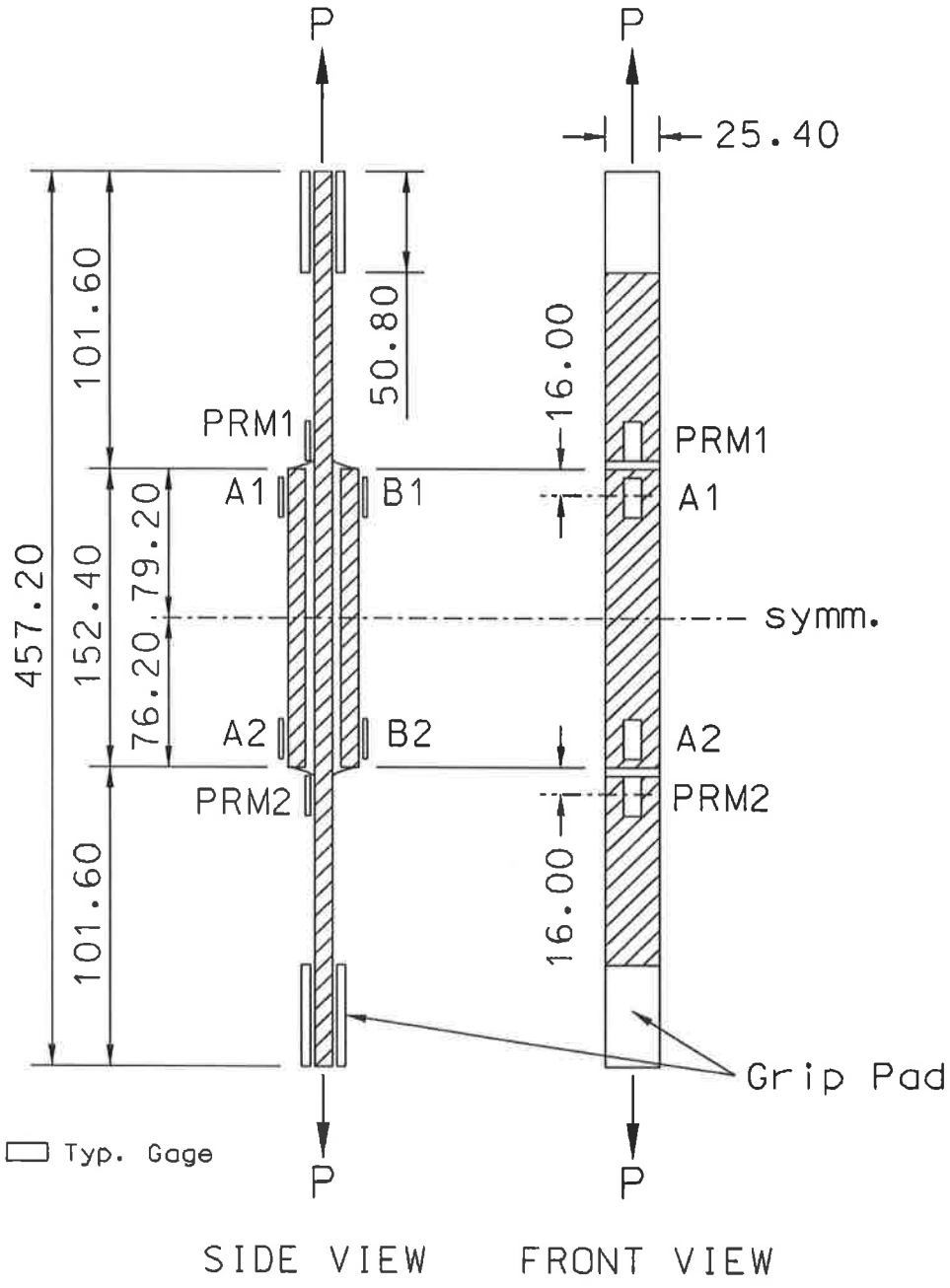

FIGURE 7.1. Tension Test Specimen Geometry, Strain Gage Locations, and Applied Load

Instrumentation and Test Procedure

The instrumentation used in all tests consisted of electrical resistance strain gages, for measuring CFRP primary/splice plate surface strains. To be consistent with those used in beam strengthening tests, all gages had a nominal resistance of 350 ohms with gage lengths of 12.70 mm. A total of six gages were used for each test. Located 16 mm off the ends of the splices, two gages measured primary plate strains and four measured dummy plate strains (see Figure 7.1). The locations were chosen to coincide with those used in measuring primary/splice plate strains in ultimate load tests of Beams 4 through 8.

The test procedure used for all five Tension Test specimens consisted of loading each monotonically, using a 178 kN capacity universal testing machine, until initial debonding occurred at the four ends of the dummy plates. Each specimen was loaded at a rate of approximately 0.03 mm per second. During each test, strain data were recorded from each gage at a sampling rate 25 samples/second/channel.

Results

In all tests, adhesive failure at the primary plate/adhesive interface occurred at each end of the dummy plates. In Figure 7.2, a photo of a typical test specimen before and after loading is shown. Note how the adhesive remained attached to the dummy plate after failure. The results of primary and dummy plate strains in the Tension Test specimens, at first debond, for each end

of the plates as well as the calculated difference are listed in Table 7.1. In Table 7.2, the calculated average primary plate, dummy plate, and difference at the point of first debonding is presented. The averages of all ends, for which debonding occurred, are shown in Table 7.3.

FIGURE 7.2. Typical Tension Test Specimen Before and After Testing

TABLE 7.1. Strains in Tension Test Specimens at Debonding [με]

Point of Debonding[a]	Primary Plate	Splice Plate	Strain Difference
	(a) Specimen 1		
A1	2336	754	1582
A2	2127	591	1536
B2	2234	701	1533
B1	2597	791	1806
	(b) Specimen 2		
A1	2670	758	1912
A2	2573	782	1791
B1	2821	672	2149
B2	2805	566	2239
	(c) Specimen 3		
A1	2184	621	1563
A2	2324	666	1658
B2	2330	687	1643
B1	2352	711	1641
	(d) Specimen 4		
A1	1715	562	1153
B1	1757	502	1255
A2	1973	712	1261
B2	1996	618	1378
	(e) Specimen 5		
A1	2281	586	1695
B1	2420	685	1735
A2	2638	660	1978
B2	2642	703	1939

[a]Order indicates debonding sequence. Gage locations shown in Figure 7.1.

TABLE 7.2. Average Strains in Tension Test Specimens at First Debond [με]

Average Strain in Primary Plate at First Debond	2237
Average Strain in Splice Plate at First Debond	656
Average Difference at First Debond	1581

TABLE 7.3. Average Strains in Tension Test Specimens at Debond [με]

Average Strain in Primary Plate at Debond	2339
Average Strain in Splice Plate at Debond	666
Average Difference at Debond	1672

CHAPTER EIGHT

SUMMARY OF RESULTS

Introduction

In Chapters 6 and 7, detailed results of beam tests and tension test specimens were presented. From the beam tests, it was determined that splice plate debonding, occurring at the ends of the plates, was the dominate mode of failure. Debonding is believed to result from high shear stress concentrations at the primary plate/adhesive interface which are caused by the difference in normal strains at the end of the splice plates and off the splices, on the primary plates. By using dummy plates, it was determined that debonding at the ends of splice plates is independent of the load transfer occurring at the butt joint. Tension Test Specimens also confirmed this failure mode with similar failure characteristics.

In all beam tests, initial splice plate debonding occurred before beam failure. With the exception of Beam 4 (ULT 2), where primary plate tension failure occurred, complete splice plate debonding controlled the failure mode of the beam specimens after the initial signs of debonding. As a result of complete splice plate debonding, only a small percentage of the ultimate strain capacity of the Carbon Fiber Reinforcement was utilized during testing.

TABLE 8.1. Summary of Fatigue/Ultimate Load Tests

Beam	Test	Beam Primary Failure Mode	Initial Debonding Splice/Dummy Plate			Beam Yielding		Beam Failure	
			Plate	Load [kN]	Moment[c] [kN-m]	Load [kN]	Moment[d] [kN-m]	Load [kN]	Moment[d] [kN-m]
1[a]	FT	Complete Splice Plate Debonding	Midspan Splice	N.A.	N.A.	NO	NO	119	181
	ULT	Complete Splice Plate Debonding	Midspan Splice	108	165	100	152		
2[a]	FT	No Failure, Initial Splice Debonding	Midspan Splice	65	99	NO	NO	116	177
	ULT	Complete Splice Plate Debonding	Midspan Splice	74	112	109	166		
3[a]	ULT	Complete Splice Plate Debonding	Midspan Splice	80	122	NO	NO	82	125
4[b]	ULT 1	No Failure, Dummy Plate Debonding	Midspan Dummy	54	82	NO	NO	120	183
	ULT 2	Primary Plate Tension Failure	West Splice East Splice	100 102	113 115	97	148		
5[b]	ULT	Complete Splice Plate Debonding	East Splice West Splice	108 108	122 122	103	157	127	194
6[b]	ULT 1	No Failure, Dummy Plate Debonding	Midspan Dummy Midspan Dummy East Splice	57 57 69	87 87 78	NO	NO	95	145
	ULT 2	Complete Splice Plate Debonding	West Splice	75	85	NO	NO		
7[b]	ULT	Complete Splice Plate Debonding	East Splice West Splice	105 108	119 122	105	160	113	172
8[b]	ULT	Complete Splice Plate Debonding	East Splice West Splice	95 105	107 119	106	162	131	200

[a]Splice plate located at midspan; [b]Splice plates located at approximately third points; [c]Moment at the end of the splice/dummy plate at initial debonding; [d]Moment at midspan; N.A. - Not Available: Due to gage location and testing, point of initial debonding not available; NO - Beam yielding did not occur before failure.

TABLE 8.2. Summary of Plate Strains at Initial Debonding for Fatigue and Ultimate Load Tests [με]

Beam	Test	Point of Initial Plate Debonding	Experimental			Theoretical
			Primary Plate	Splice Plate	Strain Difference	Primary Plate
1[a]	ULT	Midspan Splice	N.A.	2313	N.A.	3606
2[b]	FT	Midspan Splice	1226	870	356	1617
	ULT	Midspan Splice	N.A.	1021	N.A.	1831
3[c]	ULT	Midspan Splice	2301	1329	972	1654
4[d]	ULT 1	Midspan Dummy	2668	835	1833	1340
	ULT 2	West Splice	1693	581	1112	1850
		East Splice	2189	822	1367	1883
5[d]	ULT	East Splice	1744	656	1088	1821
		West Splice	2173	791	1382	1821
6[d]	ULT 1	Midspan Dummy	1942	865	1077	1418
		Midspan Dummy	1826	622	1204	1418
		East Splice	1690	543	1147	1271
	ULT 2	West Splice	1281	468	813	1385
7[d]	ULT	East Splice	2202	666	1536	1945
		West Splice	2898	796	2102	1994
8[d]	ULT	East Splice	2070	1007	1063	1758
		West Splice	2469	983	1486	1957

[a]Gages located 50.80 mm from the end of splice plate.
[b](FT) - Gages located 76.20 mm from the end of the splice plate.
(ULT) - Gage located 50.80 mm from the end of the splice plate.
[c]Gages located 38.10 mm from the end of the splice plate.
[d]Gages located 16.00 mm from the end of the splice/dummy plates.
N.A. - Not Available: Due to gage location, strain at initial debonding not available.

The results of the fatigue/ultimate load tests are summarized in Tables 8.1 and 8.2. In this chapter, comparisons are made between experimental and analytical results to determine the validity of the theoretical program's ability to predict the flexural behavior of the concrete beams reinforced with CFRP primary and splice plates. Flexural performance of damaged and undamaged beam specimens after the application of external reinforcing plates is evaluated. In addition, comparisons are made between experimental normal strains obtained during the ultimate load tests, on and off the ends of splice/dummy plates at initial debond, with those of the tension test specimens. Factors that caused debonding are analyzed.

Comparison of Analytical and Experimental Results

Using the theoretical results presented in Table 4.1 for beams having a continuous externally applied CFRP primary plate as well as the results of the beam tests presented in Table 8.1, comparisons were made between the theoretical and experimental yield moments at midspan to determine the program's ability to predict beam behavior. In Table 8.3, results of the theoretical analysis and experimental tests are listed. From Table 8.3, it can be seen that the model is quite accurate in predicting the yield moment for the beam specimens with externally applied CFRP primary and splice plates. The difference in computed values ranged between -2.0 and +8.4 percent.

Comparisons between experimental CFRP primary plate strain-moment relationships at midspan, at gage locations in the constant moment region, and theoretical primary plate relationships were also considered. In Figure 8.1,

TABLE 8.3. Experimental Versus Theoretical Yield Moments for Beams With Applied CFRP Primary/Splice Plates

Beam	Experimental Yield Moment [kN-m]	Theoretical Yield Moment [kN-m]	Percent Difference
1	152	152	+0.0
2	166	152	+8.4
3	N.A.	151	N.A.
4	148	151	-2.0
5	157	152	+3.2
6	N.A.	152	N.A.
7	160	151	+5.6
8	162	151	+6.8

N.A. - Not Available; Beam yielding did not occur before failure.

CFRP primary plate strain-moment relationships up to complete splice plate debonding, for beams not having a dummy plate at midspan during ultimate load tests (i.e. Beams 5 and 8 (ULT)), as well as the theoretical relationship are shown. The strains plotted in Figure 8.1 are the average from three strain gages at midspan. Figure 8.1 clearly indicates the program's ability to accurately predict primary plate strain levels before and after beam yielding for damaged and undamaged concrete beams.

From the results presented, it is concluded that the analytical model, using strain compatibility relationships, can accurately predict reinforced beam behavior with externally applied CFRP primary and splice plates as well as the strain levels in the primary plate before and after beam yielding. It was not determined however, if the analytical program could predict ultimate strengths. This was due to a lack of flexural failure modes in the constant moment region (i.e. tension failure of the CFRP or concrete compression failure).

Changes in Strength and Stiffness

All of the specimens, for which the yield point was reached before beam failure, exhibited an increase in yield moment or service load range with the application of CFRP primary and splice plates when compared to the calculated average moment at first yield during crack tests, summarized in Table 5.1. As can be seen in Table 8.4, the service load increase ranged from 18 to +32 percent for the beams initially cracked prior to application of the CFRP and 29 percent for the uncracked beam. Since the increase in yield moment for the uncracked beam is at the upper end of the range of values for the cracked

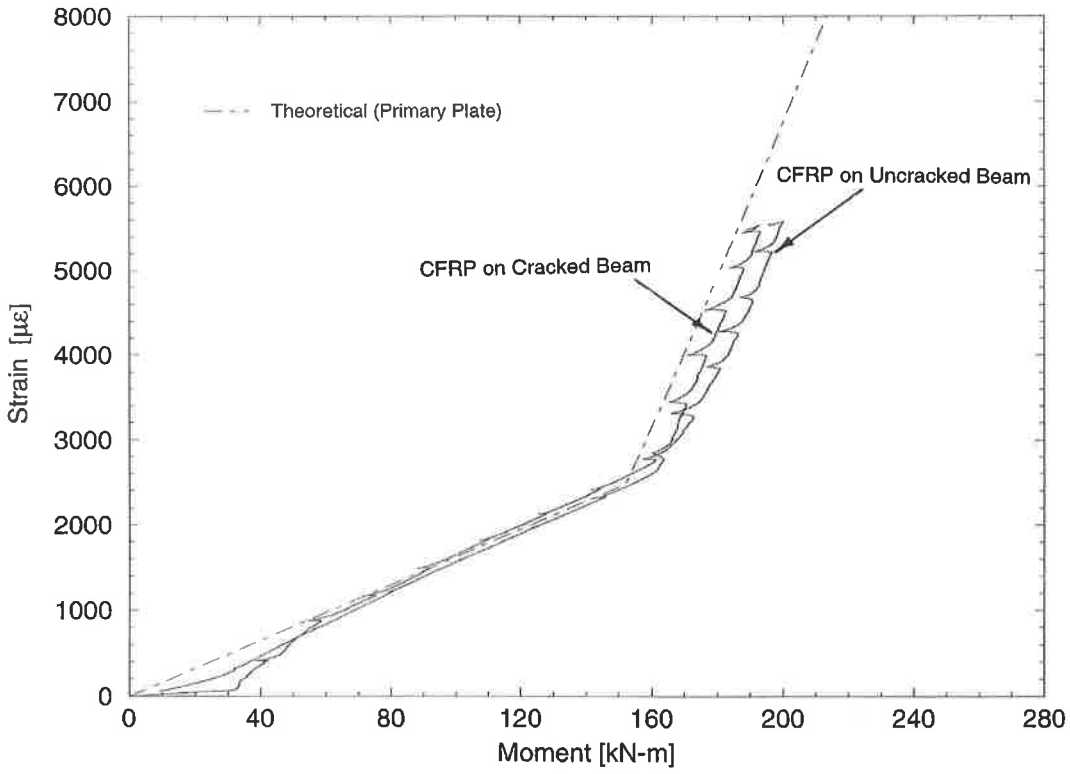

FIGURE 8.1. CFRP Surface Strains at Midspan

beams, the increase in yield moment is attributed entirely to the CFRP and not strain hardening of the steel reinforcement.

The increase in service load stiffness, with the application of the CFRP plates, was difficult to determine for the beams initially damaged during Crack Tests. This was due to variations in stiffness observed during the load tests of Beam 1. However, Beam 1 was subjected to two initial crack tests, a cyclic loading during the second crack test, fatigue loading with applied CFRP plates during which time complete splice plate debonding occurred, and finally a ultimate load test after splice plate repairs were made. In Figure 8.2, load-deflection relationships for all load tests, conducted on Beam 1, are shown. In addition, the service load stiffness for each test is represented with a dashed line. The service load stiffness for each load phase can be defined by the following: (1) static loading of the virgin beam; (2) static loading of the cracked beam; (3) cyclic loading of the damaged beam; (4) cyclic loading of the externally reinforced beam; and (5) static loading of the externally reinforced beam. From Figure 8.2, the difference in the service load stiffness seen between load phase 1 and 2 is quite obvious. The figure also illustrates the similarities in stiffness observed during load phase 2 through 5. The results indicate that the stiffness exhibited by the cracked beam is somewhat greater than that of the virgin beam and that the true stiffness of damaged specimens before the application of the CFRP should be determined from the cyclic load phase after the initial static loading. This is important when considering the actual increase in service

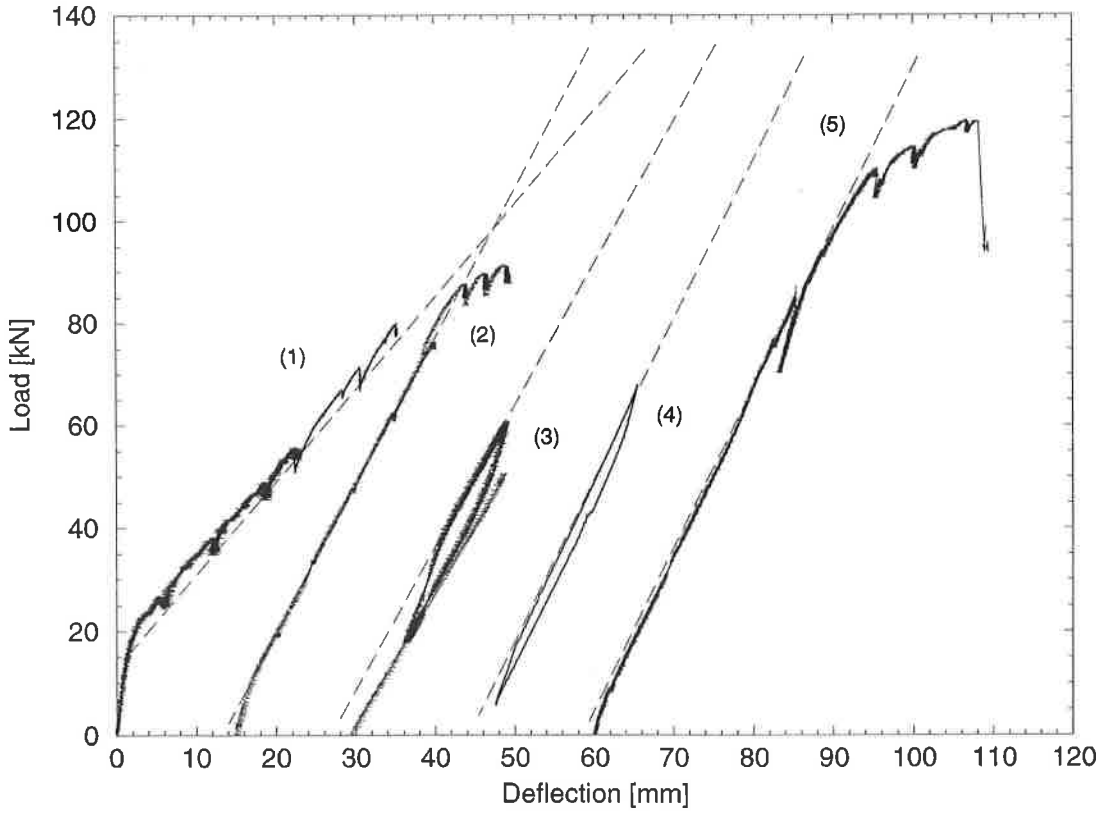

FIGURE 8.2. Load-Deflection Relationships During Load Tests of Beam 1

TABLE 8.4. Service Load Strength Increase

Beam	Beam Condition[a]	Moment at First Yield (Ultimate Load Tests)	Average Moment at First Yield (Crack Tests)	Percent Difference
1	Cracked	152	126	+21
2	Cracked	166	126	+32
3	Cracked	N.A.	126	N.A.
4	Cracked	148	126	+18
5	Cracked	157	126	+25
6	Cracked[b]	N.A.	126	N.A.
7	Cracked	160	126	+27
8	Uncracked	162	126	+29

[a]Cracked - Initial damage produced during Crack Test.
[b]Cracked - Damaged produced during Ultimate Load Test 1 (ULT 1).
[c]Average experimental moment at first yield during crack tests, see Table 5.1.
N.A. - Beam yielding did not occur before failure.

load stiffness, with the application of CFRP plates, for damaged girders in the field.

In previous studies, the method selected for determining the increase in service load stiffness, with the application of external reinforcement, was based on comparing behaviors observed during static load tests of undamaged control specimens to that of similar specimens with external reinforcement. For this study, comparisons are shown in Table 8.5 between the service load stiffness of the damaged beams before the application of the CFRP plates (i.e. cyclic loading during Crack Tests) to that of the stiffness results from the Ultimate Load Tests. In the case of Beams 6 and 8, where Crack Tests were not preformed before the Ultimate Load Tests, the average of all Crack Tests for the initial and cyclic loading were used as the basis for comparison.

In Table 8.5, the results of the experimental service load stiffness seen during the Fatigue and Ultimate Load Tests are presented. In addition, the percent difference between the stiffness from the Fatigue and Ultimate Load Tests to those from the Crack Tests for each specimen is shown. As illustrated in Table 8.5, the increase in stiffness varied between 2 to 21 percent for all specimens. Although there was a wide variation in specimen stiffness resulting from the application of CFRP primary and splice plates, the results presented in Table 8.4 and 8.5 indicate a substantial increase in flexural performance with the application of the plates. A simple calculation of the cracked section transformed moment of inertia before and after application of the CFRP indicates that an increase in stiffness of 16 percent would be expected.

TABLE 8.5. Stiffness and Percent Increase in Service Load Range

Beam	Test	Beam Condition[a]	Service Load Stiffness Fatigue/Ultimate [kN/mm]	Service Load Stiffness Crack Test [kN/mm]	Percent Increase
1	FT	Cracked	2.70	2.65	+2
	ULT	Cracked	3.13	2.65	+18
2	FT	Cracked	3.50	2.90	+21
	ULT	Cracked	3.27	2.90	+13
3	ULT	Cracked	3.00	2.78	+8
4	ULT 1	Cracked	2.97	2.67	+11
	ULT 2	Cracked	3.03	2.67	+14
5	ULT	Cracked	2.80	2.74	+2
6	ULT 1	Uncracked	2.08	1.90[c]	+10
	ULT 2	Cracked[b]	3.20	2.73[d]	+17
7	ULT	Cracked	2.90	2.64	+10
8	ULT	Uncracked	2.28	1.90[c]	+20

[a]Cracked - Initial damage produced during Crack Test.
[b]Cracked - Damaged produced during Ultimate Load Test 1 (ULT 1).
[c]Average service load stiffness during initial load phase of Crack Tests, see Table 5.2.
[d]Average service load stiffness during cyclic load phase of Crack Tests, see Table 5.2.

Comparison of Beam and Tension Test Specimens

As mentioned earlier, splice plate debonding is believed to be the result of high shear stress concentrations occurring at the primary plate/adhesive interface at the end of splice plates. The stress concentration is attributed to the change in geometry and the difference in normal strain levels occurring in the splice plate and primary plate, at the end of the splice plate, and not to the presence of the butt joint. The debonding behavior appears to be independent from the butt joint because there is no difference between the strain levels at initial debonding for the splice plates and dummy plates as shown in Table 8.2. Tension Test specimens were devised to see whether or not splice plate debonding characteristics could be accurately predicted with simple test procedures, similar to Lap Shear tests, using samples of the strengthening materials used in the large scale beam tests.

For all test specimens, beam and Tension Tests, the failure of the splice/dummy plates occurred at the primary plate/adhesive interface. In Table 8.6, strain levels at the ends of the splice/dummy plates and off the splice/dummy plates, on the primary plate, at the point of initial debonding during Ultimate Load Tests are summarized as well as the difference between the two. Results are only shown for beams having gages located 16.00 mm off the ends of the plates (i.e. Beams 4 through 8) since that was the distance used for the strain gages on the tension test specimens (Figure 7.1). The strain results from the tension test specimens at initial debonding, presented in Table 7.1, are also

summarized in Table 8.6. Average strains and strain differences for each test are shown in Table 8.7 and illustrated in Figure 8.3.

The results shown in Table 8.7 and Figure 8.3 do indicate similarities in normal strain levels at the point of initial debonding for the beam and tension test specimens, and the difference in strain levels which cause debonding. In Table 8.7, the average difference in normal strains, 16.00 mm off the ends of the primary and splice/dummy plates, were 1324 με and 1581 με for the beam and Tension Test specimens, respectively. The average percent difference during Ultimate Load Tests was +64, and +71 for Tension Tests. Initial debonding, caused by high shear stress concentrations at the primary plate/adhesive interface, was the direct result of these strain differences. In the case of the beam specimens, initial debonding was the mechanism which lead to complete debonding of the splice plate..

Discrepancies in normal strain levels for the beam and tension test specimens were most likely the result of the loading conditions on each specimen. In the case of the tension test specimens, the CFRP plates were subjected to axial tension only. For the beam specimens however, a combination of axial tension as well as bending may have contributed to the discrepancies. Cracks in the beams could also be a factor. Although there was some variation in normal strain levels at the point of initial debonding for beam and tension test specimens, the Tension Test results could provide a predictive model for normal strain levels in the primary and splice plates at the point of initial debonding as well as the characteristics of splice plate debonding.

Additional testing with a larger number of tension test specimens would provide more definitive results. Also, it is likely that the magnitude of the strains which caused initial debonding for other combinations of CFRP laminates and adhesives will be different than those measured in this study. However, based on the data presented herein, the average theoretical strain at initial debonding for the beam tests (1682 με from figure 8.3) was 75% of the average strain at initial debonding in the tension tests (2237 με from Figure 8.3).

TABLE 8.6. CFRP Normal Strains in Beam and Tension Test Specimens at Initial Debonding for Gages Located 16.00 mm Off the Ends of the Splice/Dummy Plates [με]

Primary Plate	Splice/Dummy Plate	Strain Difference	Percent Difference
(a) Ultimate Load Tests (Beams 4 through 8)			
668	835	1833	+69
1693	581	1112	+66
2189	822	1367	+62
1744	656	1088	+62
2173	791	1382	+64
1942	865	1077	+56
1826	622	1204	+66
1690	543	1147	+68
1281	468	813	+64
2202	666	1536	+70
2898	796	2102	+73
2070	1007	1063	+51
2469	983	1486	+60
(b) Tension Test Specimens			
2336	754	1582	+68
2670	758	1912	+72
2184	621	1563	+72
1715	562	1153	+67
2281	586	1695	+74

TABLE 8.7. Average Strains at Initial Debonding for Gages Located 16.00 mm Off the Ends of the Splice/Dummy Plates [με]

Test	Ultimate Load Tests	Tension Test Specimens
Average Strain in Primary Plate	2065	2237
Average Strain in Splice/Dummy Plate	741	656
Average Difference in Strains	1324	1581
Average Percent Difference	+64	+71

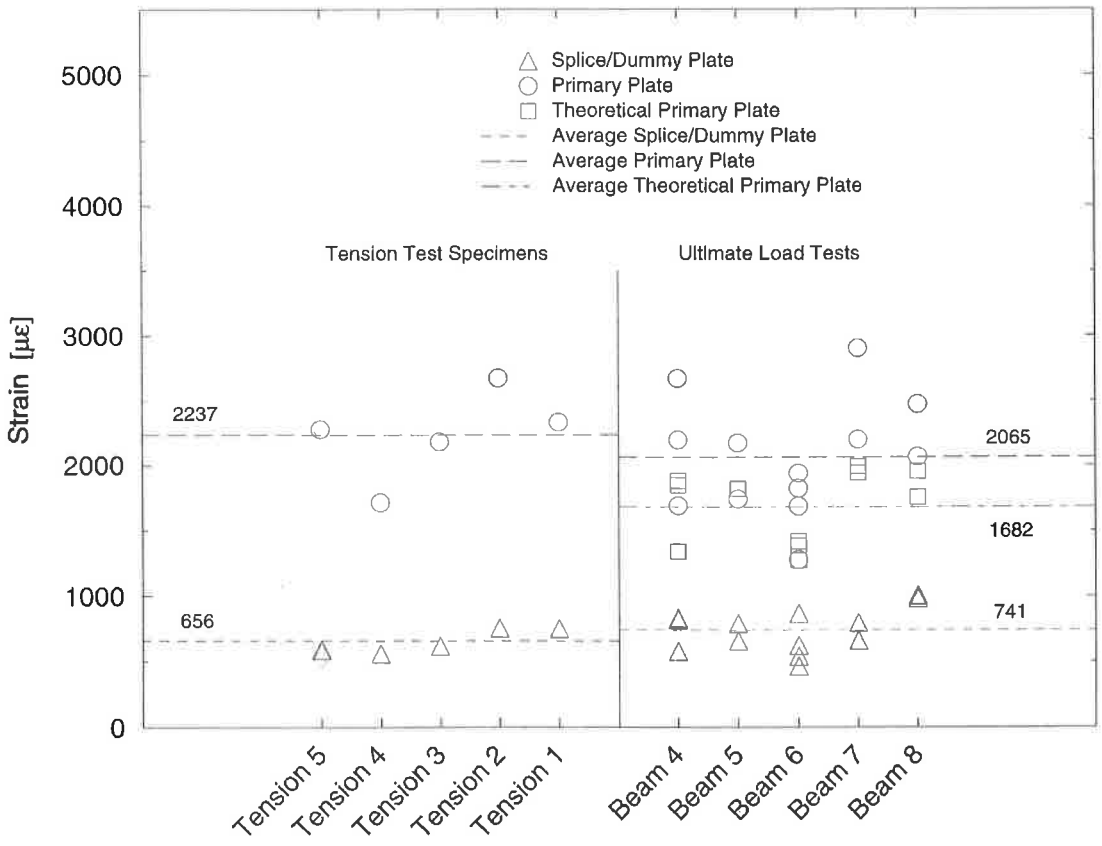

FIGURE 8.3. Normal Strain Levels at Initial Debonding for Gages Located 16.00 mm On and Off the Ends of Splice/Dummy Plates

CHAPTER NINE

CONCLUSION AND RECOMMENDATIONS

Conclusion

The results of the experiments conducted provided valuable insight on limit states for design of Carbon Fiber Reinforced Plastic (CFRP) primary and splice plates for strengthening damaged and undamaged reinforced concrete flexural members. The major problem identified was the presence of high normal strain levels occurring in the primary plate, at the ends of splice plates, which result in high shear stresses in the adhesive bond between the primary and splice plate. During all load tests, some degree of splice plate debonding occurred. All initial signs of splice plate debonding occurred at the end of the splice and propagated toward the butt joint. Adhesive failure at the primary plate/adhesive interface controlled debonding. For all but one beam test, complete splice plate debonding controlled the failure mode of the beam specimen. As a result of splice plate debonding, the ultimate capacity of the CFRP plates was not fully utilized. By the use of dummy plates, it was determined that splice plate debonding was not dependent on the presence of a butt joint.

Tension Tests, devised to replicate debonding characteristics in large scale beam testing, proved effective in predicting strain levels in the primary and splice plates of beam specimens. The results of large scale beam tests and small scale tension tests indicated average differences in normal strain levels for gages located 16.00 mm off the ends of the splice/dummy plates of 1324 με and 1581 με, respectively. Initial debonding, caused by high shear stress at the primary plate/adhesive interface, was a direct result of this difference.

The analytical model, developed using strain compatibility relationships, proved to be a reliable tool for predicting both beam behavior with externally applied CFRP primary and splice plates and normal strain levels in the primary plate at locations away from splice plates. However, due to premature splice plate debonding, it was not determined if the analytical program could predict ultimate strengths of reinforced concrete beams with externally applied CFRP primary and splice plates.

Although splice plate debonding did control the failure mode of most beam specimens, some degree of flexural enhancement resulted from the application of CFRP plates to initially damaged and undamaged beam specimens. The increase in yield strength or service load range varied between +18 to +32 percent for beams initially cracked prior to application of CFRP and +29 percent for the uncracked beam. Changes in service load stiffness varied between +2 to +21 percent.

Recommendations

Until further research is conducted on the behavior of splice plates, caution should be taken before CFRP splice plates are used for the flexural enhancement of new or preexisting concrete structures. If splice plates are used, special attention should be paid to positioning splice plates in regions of low stress levels. Further exploration of the use of less stiff (more flexible) epoxy adhesives to absorb shear stresses at the primary plate/adhesive interface resulting from the strain differences, occurring at the ends of the splice plates, may support the use of CFRP splice plates in structural rehabilitation. This type of testing may be accomplished with simple test procedures like the Tension Tests described in Chapter Seven.

Additional tests should be performed with the analytical model to validate predicted ultimate strengths of reinforced concrete beams with external CFRP reinforcement.

REFERENCES

An, W., Saadatmanesh, H., Ehsani, M.R. (1991). "RC Beams Strengthened with FRP Plates. 2: Analysis and Parametric Study." *Journal of Structural Egineering.*, ASCE, 117(11), 3434-3455.

American Concrete Institute (ACI). (1989). *Building Code Requirement for Reinforced Concrete*. Detroit, Michigan.

Chajes, M.J., Thomson, T.A. Jr., Januszka, T.F., and Finch, W.W. Jr. (1994). "Flexural Strengthening of Concrete Beams Using Externally Bonded Composite Materials." *Construction and Building Materials.*, 8(3),191-201.

Meier, U., and Kaiser, H. (1991). "Strengthening of Structures with CFRP Laminates.", *Advanced Composites Materials in Civil Engineering Structures Proceedings.*, ASCE, Las Vegas 1991, 224-232.

Meier, U., Deuring, M., Meier, H., and Schwegler, G. (1992). "Strengthening of Structures with CFRP Laminates: Research and Applications in Switzerland." *Advanced Composite Materials in Bridges and Structures.*, CSCE, Montreal 1992, 243-250.

Park, R., and Paulay, T. (1975). *Reinforced Concrete Structures.* John Wiley and Sons, Inc., New York, N.Y.

Ritchie, P.A., Thomas, D.A., Lu, L.W., and Connelly, G.M. (1991). "External Reinforcement of Concrete Beams Using Fiber Reinforced Plastics." *ACI Structural Journal.*, 88(4), 490-500.

Saadatmanesh, H., Ehsani, M.R. (1990). "Fiber Composite Plates Can Strengthen Beams.", Concrete International: Design & Construction., 12(3), 65-71.

Tedesco, J.W., Stallings, J.M., El-Mihilmy, M., and McCauley, M. (1996). "Rehabilitation of a Concrete Bridge Using FRP Laminates." Materials for the New Millennium., *Proceedings of the Fourth Materials Engineering Conference.*, Washington, DC, November 10-14, 1996, ASCE, New York, NY, 631-637.

APPENDIX A

ANALYTICAL ANALYSIS PROGRAM

```
**********************************************************************
**********************************************************************
C       Fortran 77 program, written by Nathan M. Porter,
C       to analyze doubly reinforced concrete beam behavior
C       with applied CFRP plates.  All calculations are based on
C       theoretical moment-curvature relationships derived
C       by R. Park and T. Paulay.  Input Units [U.S.], Output
C       Units [S.I.]
**********************************************************************
**********************************************************************
        program MOMENT_CURVATURE

        integer i,num
        real As1,As2,Acfrp,d1,d2,fc,fcc,b,eult,h,
     +          Ec,Es,Ecfrp,eo,fy,kd1(1000),kd2(1000),
     +          ecm(1000),alpha(1000),gama(1000),es2(1000),
     +          kd(1000),x(1000),y(1000),z(1000),phi(1000),
     +          M(1000),es1(1000),Acfrp,fu,fucfrp,dcfrp,
     +          eecfrp(1000)
**********************************************************************
**********************************************************************
C       Description of variables used in program.
C       As1             area of steel compression reinforcement
C       As2             area of steel tension reinforcement
C       Acfrp           area of CFRP tension reinforcement
C       d1              depth of As1
C       d2              depth of As2
C       dcfrp           depth of Acfrp
C       Es              modulus of elasticity of steel
C       Ec              modulus of elasticity of concrete
C       Ecfrp           modulus of elasticity of CFRP
C       fc              concrete cylinder compressive strength
C       fcc             reduced compressive strength (k3*fc)
C       b               width of beam
C       h               heigth of beam
C       eult            maximum compressive strain of concrete
C       eo              concrete stress-strain parameter
C       fy              yield strength of steel
C       fu              ultimate strength of steel
C       fucfrp          ultimate strength of CFRP
C       ecm             incremental concrete strain in extreme
C                       compression fiber of concrete
C       es1             incremental strain in steel compression reinforcement
C       es2             incremental strain in steel tension reinforcement
C       eecfrp          incremental strain in CFRP tesion reinforcement
```

```
C       phi             curvature
C       M               moment
C       kd1,kd2         quadratic equation values
C       x,y,z           quadratic equation variables (i.e. a,d,c)
C       alpha           mean stress factor
C       gama            centroid factor
**********************************************************************
**********************************************************************

        open (unit=10,file='input.dat',status='old')
        open (unit=20,file='phi-m.dat',status='unknown')
        open (unit=30,file='m-ecfrp.dat',status='unknown')

C       Data read from input file (input.dat)

        read(10,*) As1,As2,d1,d2,Es,Fy,Fu
        read(10,*) Acfrp,dcfrp,Ecfrp,fucfrp
        read(10,*) b,h,fc,eult,Ec

        fcc = fc*0.93
        eo = 2*fcc/Ec
        num = eult/0.00001

        M(1) = 0.0
        phi(1) = 0.0
        ecm(1) = 0.0

        do 10 i=1,num+1
              if (ecm(i).le.eo) then
              alpha(i) = (ecm(i)/eo)-((ecm(i)**2)/(3*eo**2))
              gama(i) = 1-((2/(3*eo)-ecm(i)/(4*eo**2))/(1/eo-ecm(i)/
     +                    (3*eo**2)))

              else
              alpha(i) = 1-eo/(3*ecm(i))+(0.15/(0.0038-eo))*(eo-
     +              ecm(i)/2-eo**2/(2*ecm(i)))
              gama(i) = 1-((ecm(i)**2/2-eo**2/12+(0.15/(0.0038-eo))*
     +                    (eo*ecm(i)**2/2-ecm(i)**3/3-eo**3/6))/
     +                (ecm(i)**2-eo*ecm(i)+2*eo*ecm(i)/3+(0.15/
     +                (0.0038-eo))*(eo*ecm(i)**2-ecm(i)**3/2-
     +                eo**2*ecm(i)/2)))

              endif

              ecm(i+1) = ecm(i)+0.00001
```

```
10   continue

     kd(1) = 0.0

     do 20 i=2,num+1

          x(i) = alpha(i)*fcc*b
          y(i) = ecm(i)*Es*As1+ecm(i)*Es*As2+ecm(i)*Ecfrp*Acfrp
          z(i) = -1*(d1*ecm(i)*Es*As1+d2*ecm(i)*Es*As2+
     +          dcfrp*ecm(i)*Ecfrp*Acfrp)

          kd1(i) = (-y(i)+((y(i)**2)-(4*x(i)*z(i)))**0.5)/(2*x(i))
          kd2(i) = (-y(i)-((y(i)**2)-(4*x(i)*z(i)))**0.5)/(2*x(i))

          if (kd1(i).gt.kd2(i)) then
               kd(i) = kd1(i)
          else
               kd(i) = kd2(i)
          endif

          M(i) = alpha(i)*fcc*b*kd(i)*(h/2-gama(i)*kd(i))+
     +          ecm(i)*((kd(i)-d1)/kd(i))*Es*As1*(h/2-d1)+
     +          ecm(i)*((kd(i)-d2)/kd(i))*Es*As2*(h/2-d2)+
     +          ecm(i)*((kd(i)-dcfrp)/kd(i))*Ecfrp*Acfrp*
     +          (h/2-dcfrp)

          phi(i) = ecm(i)/kd(i)

          es2(i) = ecm(i)*(kd(i)-d2)/kd(i)

          if (Es*abs(es2(i)).gt.fy) then

               x(i) = alpha(i)*fcc*b
               y(i) = ecm(i)*Es*As1+
     +               (abs(ecm(i)*((kd(i)-d2)/kd(i)))/
     +               (ecm(i)*((kd(i)-d2)/kd(i))))*fy*As2+
     +               ecm(i)*Ecfrp*Acfrp
               z(i) = -1*(d1*ecm(i)*Es*As1+dcfrp*ecm(i)*Ecfrp*
     +               Acfrp)

               kd1(i) = (-y(i)+((y(i)**2)-(4*x(i)*z(i)))**0.5)/
     +                 (2*x(i))
               kd2(i) = (-y(i)-((y(i)**2)-(4*x(i)*z(i)))**0.5)/
     +                 (2*x(i))
```

```
                if (kd1(i).gt.kd2(i)) then
                        kd(i) = kd1(i)
                else
                        kd(i) = kd2(i)
                endif

                M(i) = alpha(i)*fcc*b*kd(i)*(h/2-gama(i)*kd(i))+
+                       ecm(i)*((kd(i)-d1)/kd(i))*
+                       Es*As1*(h/2-d1)+
+                       (abs(ecm(i)*((kd(i)-d2)/kd(i)))/
+                       (ecm(i)*((kd(i)-d2)/kd(i))))*fy*As2*
+                       (h/2-d2)+
+                       ecm(i)*((kd(i)-dcfrp)/kd(i))*Ecfrp*Acfrp*
+                       (h/2-dcfrp)

                phi(i) = ecm(i)/kd(i)

                if (d1.eq.0.0) then
                        es1(i) = 0.0
                else
                        es1(i) = ecm(i)*(kd(i)-d1)/kd(i)
                endif

        endif

        if (Es*abs(es1(i)).gt.fy) then
                x(i) = alpha(i)*fcc*b
                y(i) = (abs(ecm(i)*((kd(i)-d1)/kd(i)))/
+                       (ecm(i)*((kd(i)-d1)/kd(i))))*fy*As1+
+                       (abs(ecm(i)*((kd(i)-d2)/kd(i)))/
+                       (ecm(i)*((kd(i)-d2)/kd(i))))*fy*As2+
+                       ecm(i)*Ecfrp*Acfrp
                z(i) = -1*(dcfrp*ecm(i)*Ecfrp*Acfrp)

                kd1(i) = (-y(i)+((y(i)**2)-(4*x(i)*z(i)))**0.5)/
+                       (2*x(i))
                kd2(i) = (-y(i)-((y(i)**2)-(4*x(i)*z(i)))**0.5)/
+                       (2*x(i))

                if (kd1(i).gt.kd2(i)) then
                        kd(i) = kd1(i)
                else
                        kd(i) = kd2(i)
                endif
```

```
                M(i) = alpha(i)*fcc*b*kd(i)*(h/2-gama(i)*kd(i))+
     +               (abs(ecm(i)*((kd(i)-d1)/kd(i)))/
     +               (ecm(i)*((kd(i)-d1)/kd(i))))*
     +               fy*As1*(h/2-d1)+
     +               (abs(ecm(i)*((kd(i)-d2)/kd(i)))/
     +               (ecm(i)*((kd(i)-d2)/kd(i))))*
     +               fy*As2*(h/2-d2)+
     +               ecm(i)*((kd(i)-dcfrp)/kd(i))*Ecfrp*Acfrp*
     +               (h/2-dcfrp)

                phi(i) = ecm(i)/kd(i)

            endif

            if (dcfrp.eq.0.0) then
                eecfrp(i) = 0.0
            else
                eecfrp(i) = ecm(i)*((kd(i)-dcfrp)/kd(i))
            endif

            if (Ecfrp*abs(eecfrp(i)).gt.fucfrp) then
                write(20,*) 'CFRP FIBER FAILURE'
                num = i-1
                goto 30
            endif

  20    continue
  30    continue

* UNIT CONVERSION*******************************
        do 40 i=1,num
            M(i) = (M(i)/12)*1.3558
            phi(i) = phi(i)*1000*(1/.0254)
            write(20,1020) phi(i),M(i)
            eecfrp(i) = -eecfrp(i)*1000000
            write(30,1020) eecfrp(i),M(i)
  40    continue

 1000   format(1x,F7.5,3x,F10.8,3x,F10.8)
 1020   format(1x,F12.4,3x,F10.4)

        end
*********************************************************************
```

APPENDIX B

CRACK TEST PLOTS

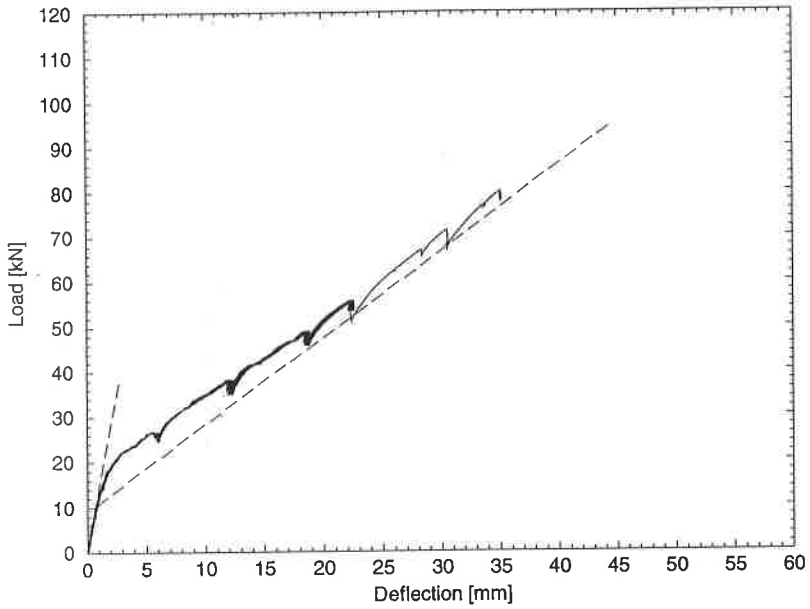

FIGURE B.1. Load-Deflection Relationship at Midspan, Beam 1 (Test 1)

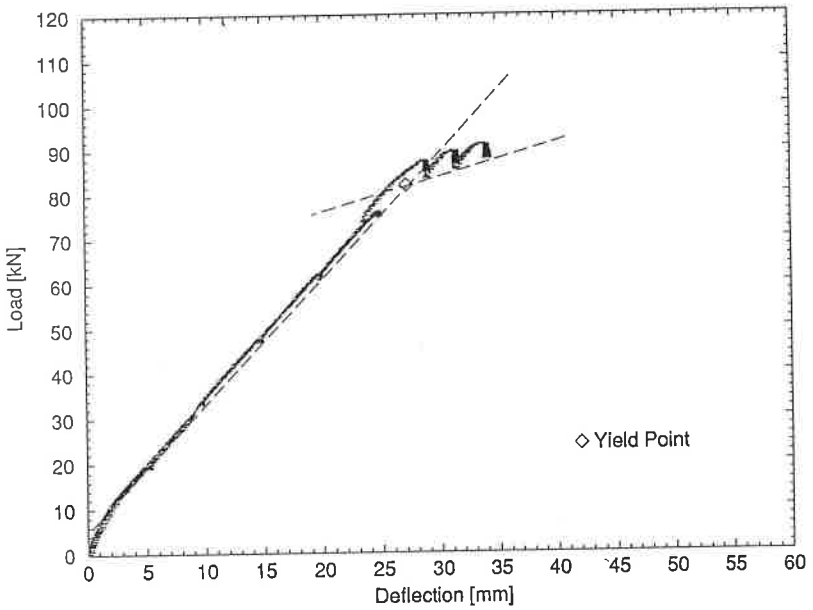

FIGURE B.2. Load-Deflection Relationship at Midspan, Beam 1 (Test 2)

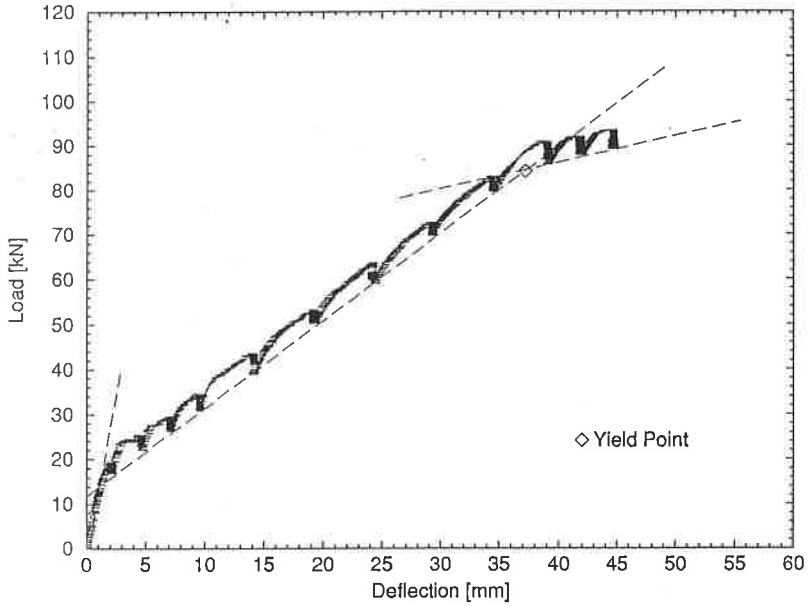

FIGURE B.3. Load-Deflection Relationship at Midspan, Beam 2

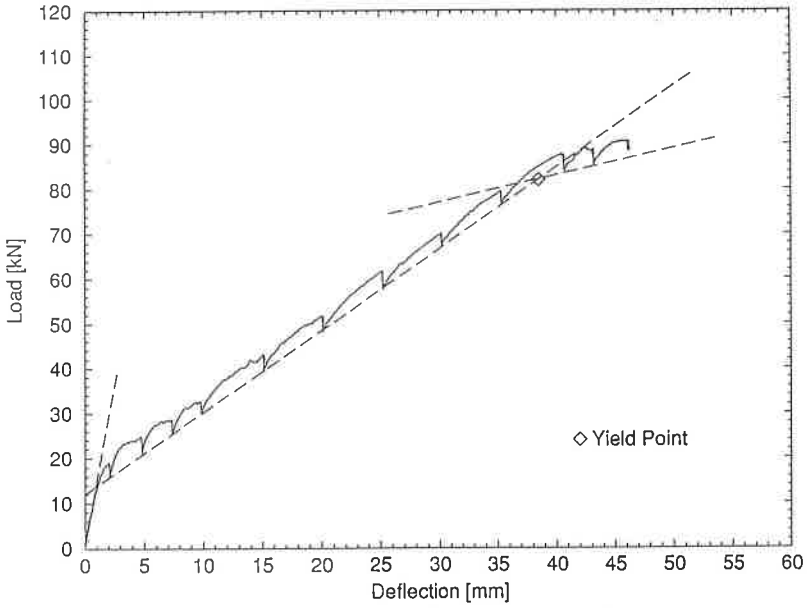

FIGURE B.4. Load-Deflection Relationship at Midspan, Beam 3

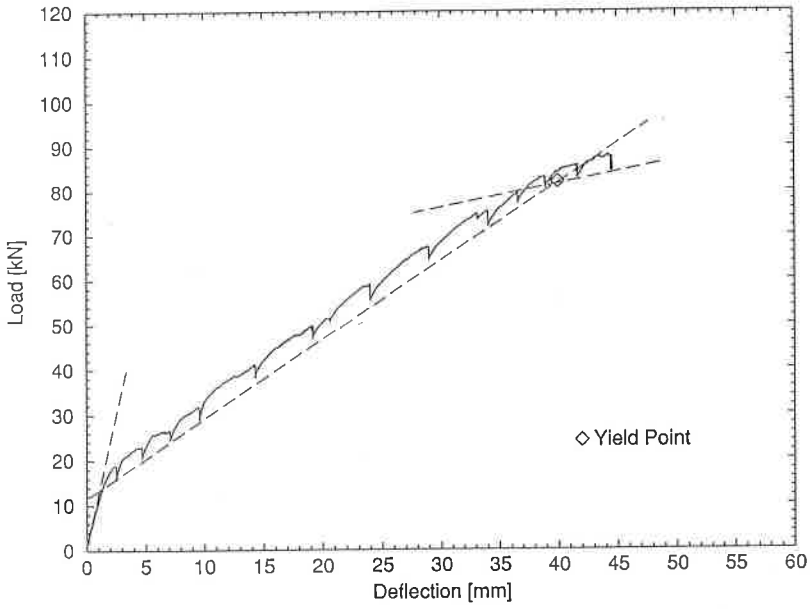

FIGURE B.5. Load-Deflection Relationship at Midspan, Beam 4

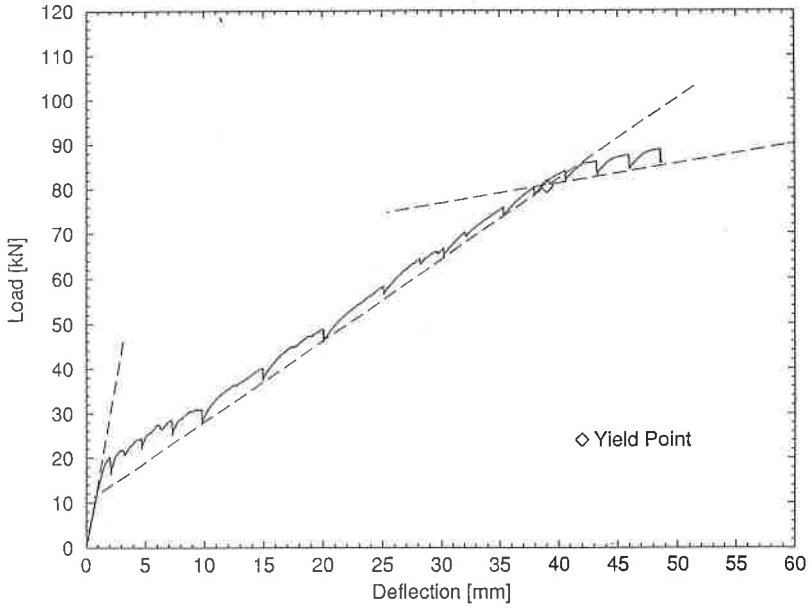

FIGURE B.6. Load-Deflection Relationship at Midspan, Beam 5

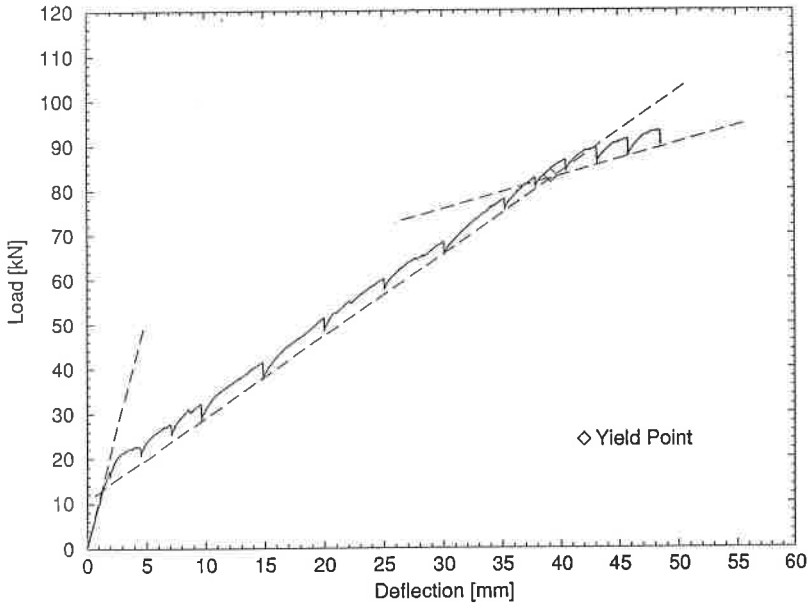

FIGURE B.7. Load-Deflection Relationship at Midspan, Beam 7

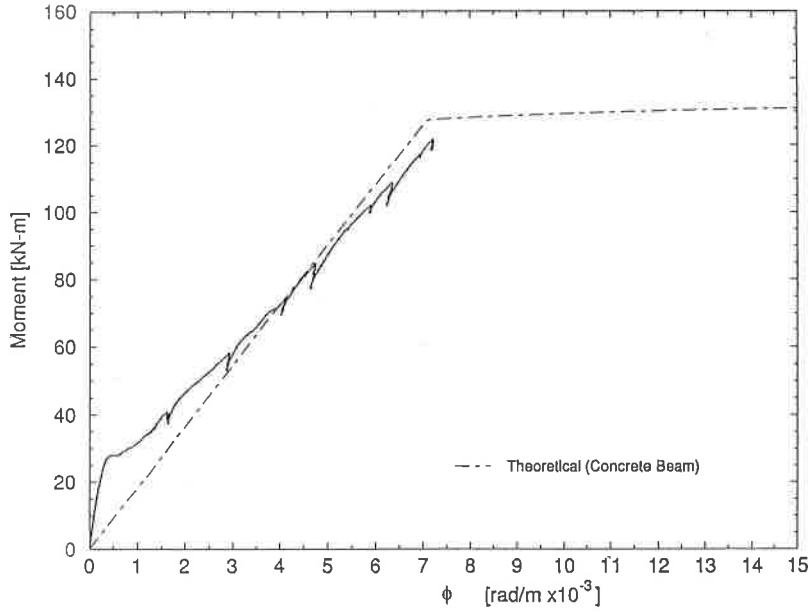

FIGURE B.8. Moment-Curvature Relationships at Midspan, Beam 1 (Test 1)

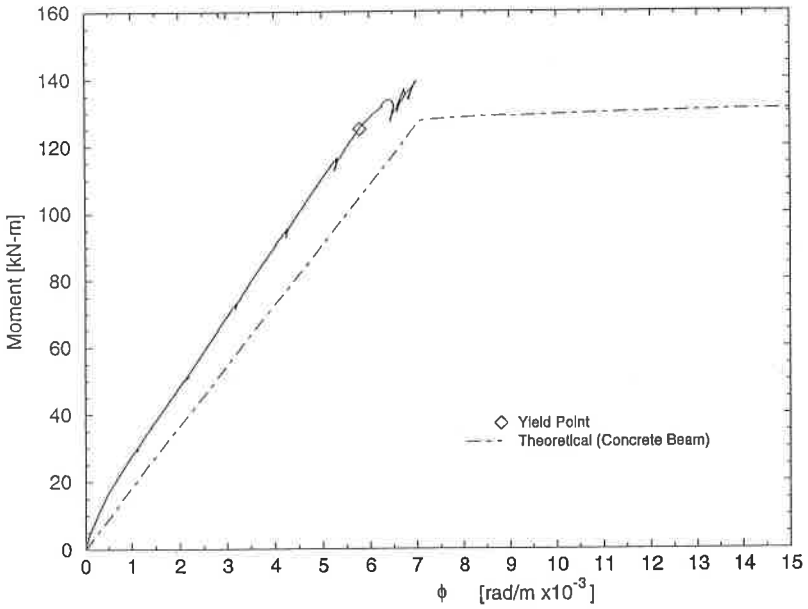

FIGURE B.9. Moment-Curvature Relationships at Midspan, Beam 1 (Test 2)

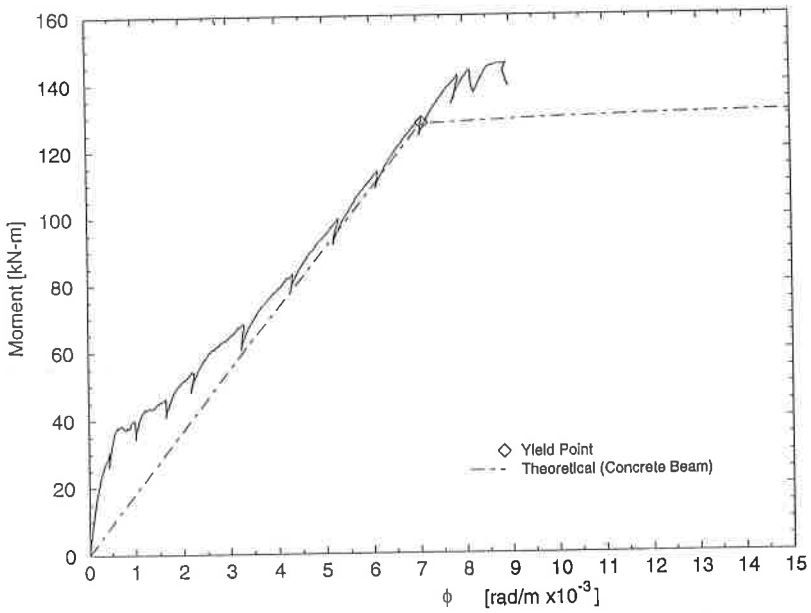

FIGURE B.10. Moment-Curvature Relationships at Midspan, Beam 2

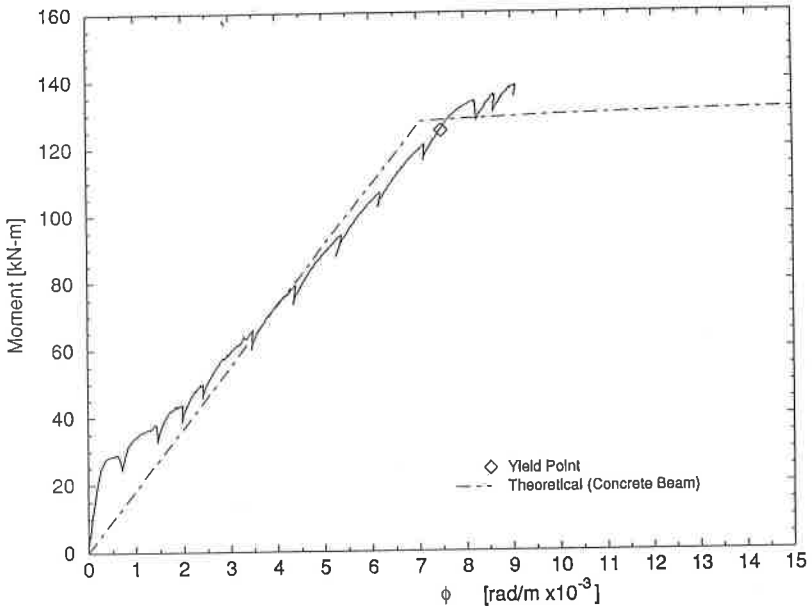

FIGURE B.11. Moment-Curvature Relationships at Midspan, Beam 3

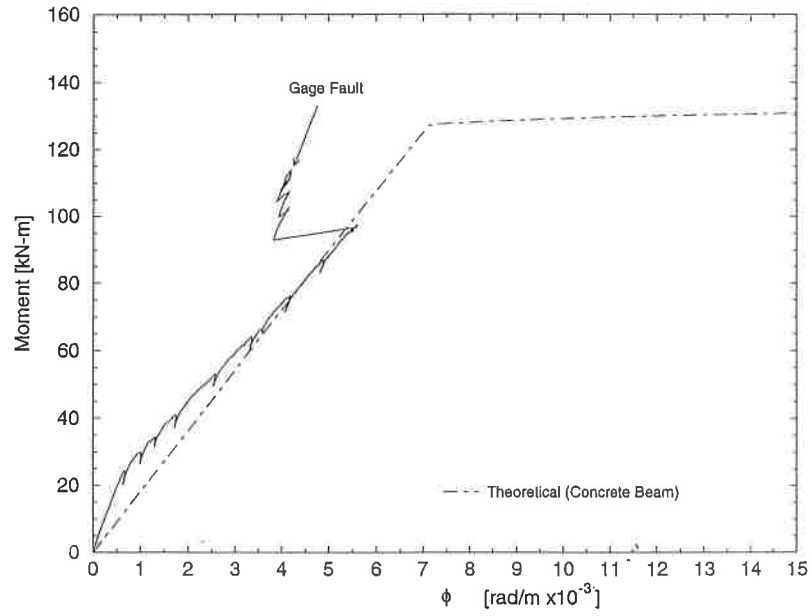

FIGURE B.12. Moment-Curvature Relationships at Midspan, Beam 4

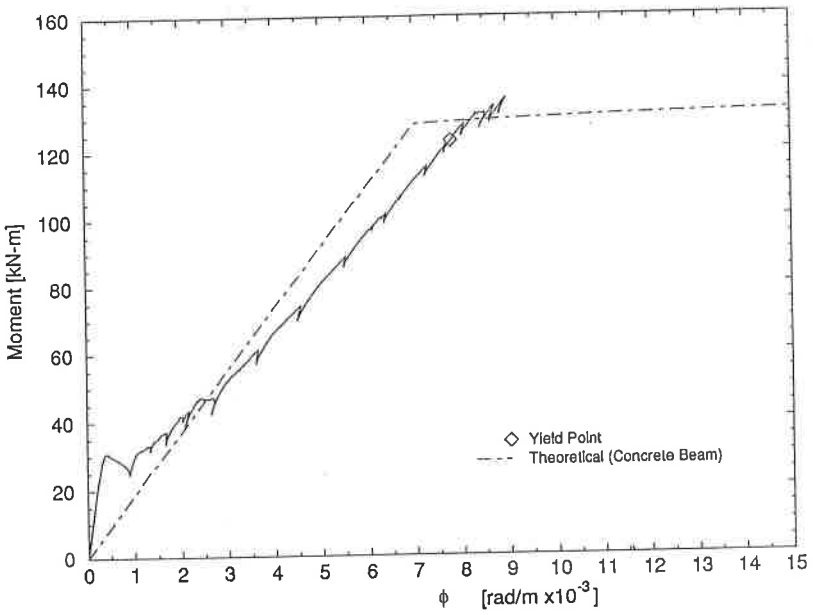

FIGURE B.13. Moment-Curvature Relationships at Midspan, Beam 5

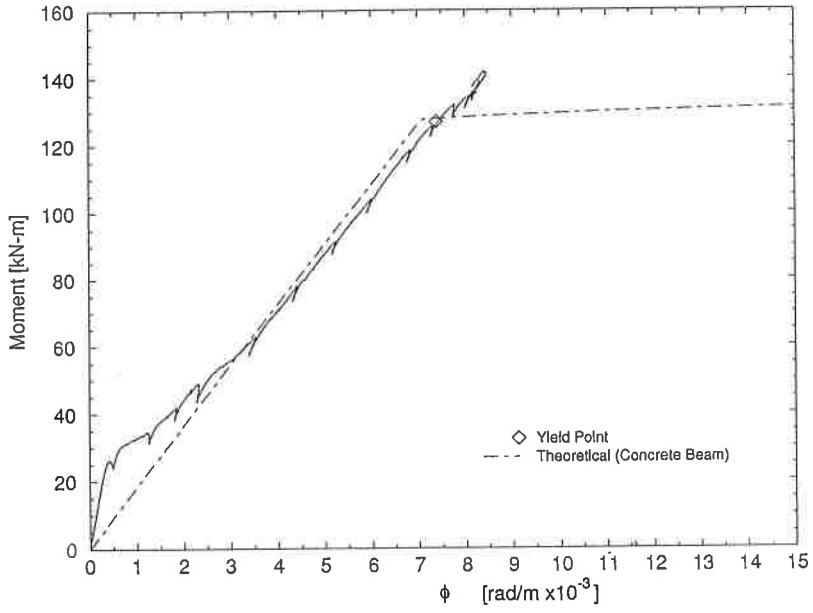

FIGURE B.14. Moment-Curvature Relationships at Midspan, Beam 7

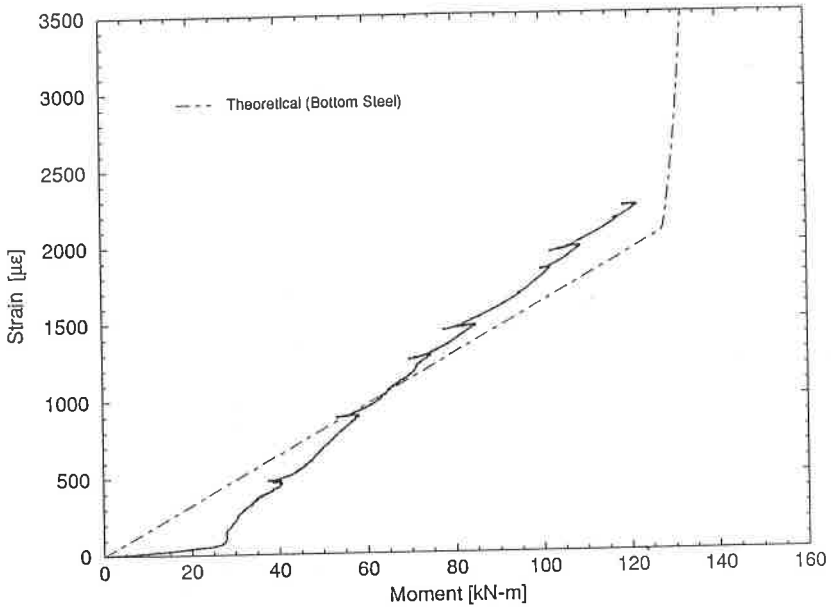

FIGURE B.15. Bottom Steel Strain-Moment Relationships at Midspan, Beam 1 (Test 1)

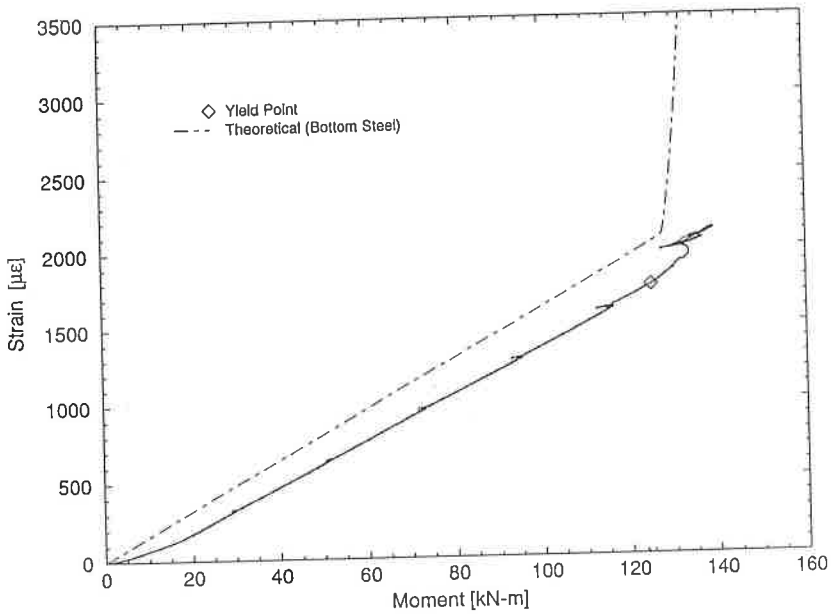

FIGURE B.16. Bottom Steel Strain-Moment Relationships at Midspan, Beam 1 (Test 2)

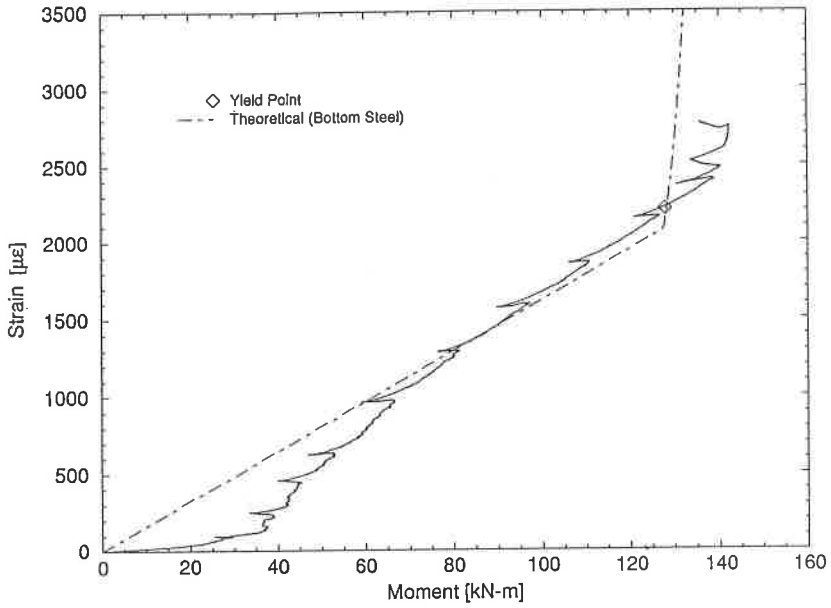

FIGURE B.17. Bottom Steel Strain-Moment Relationships at Midspan, Beam 2

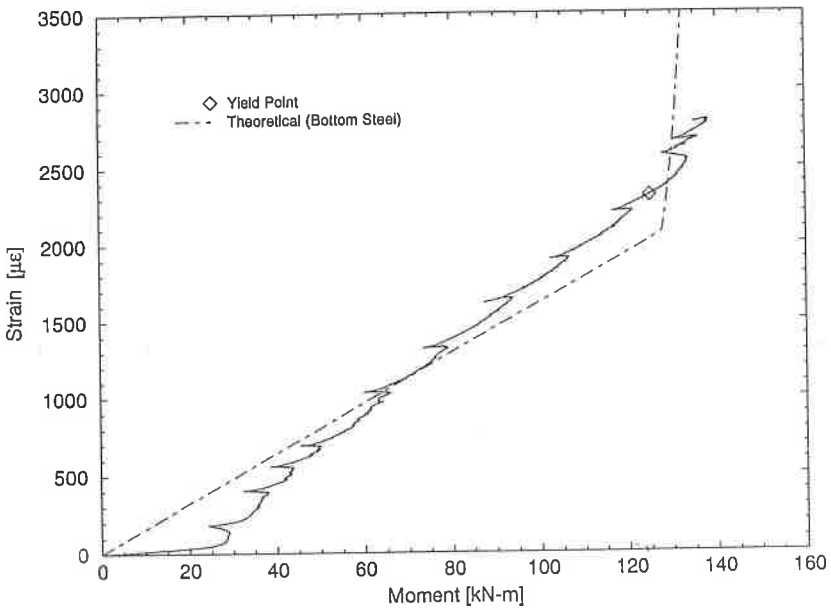

FIGURE B.18. Bottom Steel Strain-Moment Relationships at Midspan, Beam 3

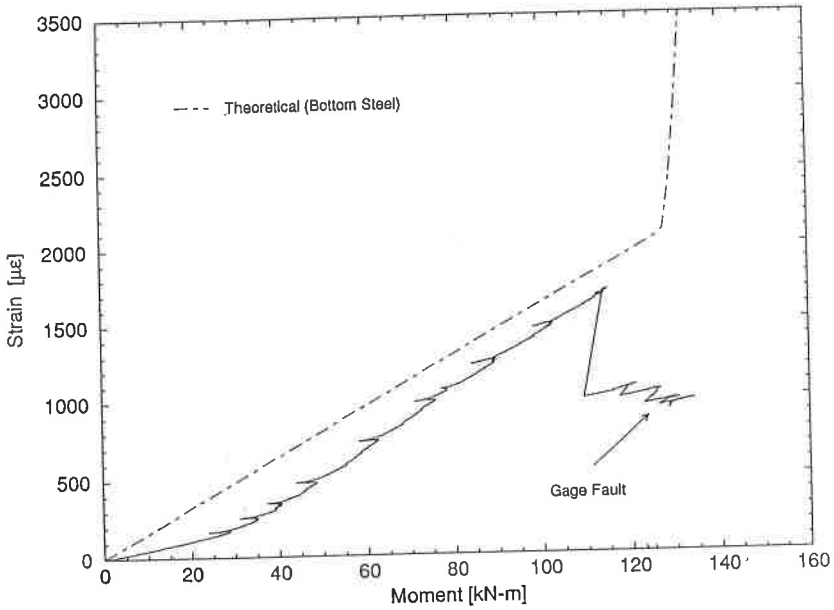

FIGURE B.19. Bottom Steel Strain-Moment Relationships at Midspan, Beam 4

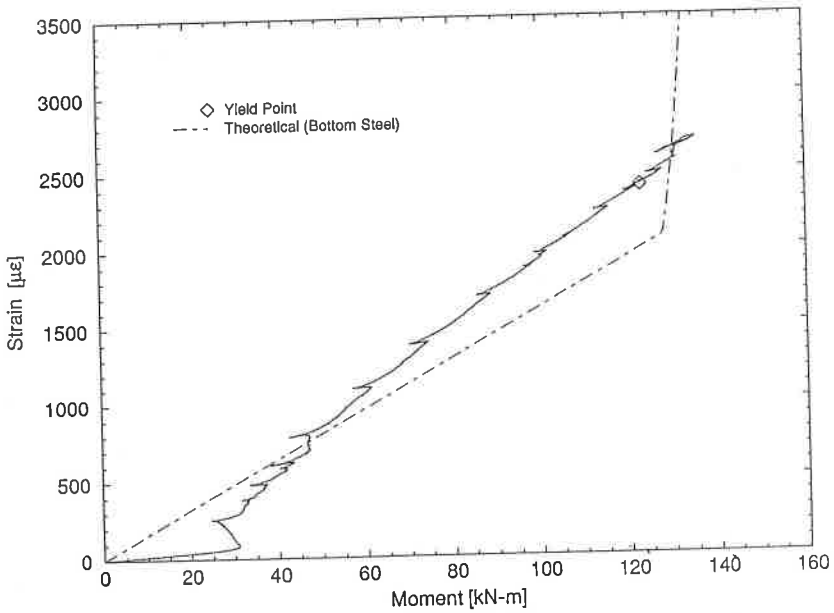

FIGURE B.20. Bottom Steel Strain-Moment Relationships at Midspan, Beam 5

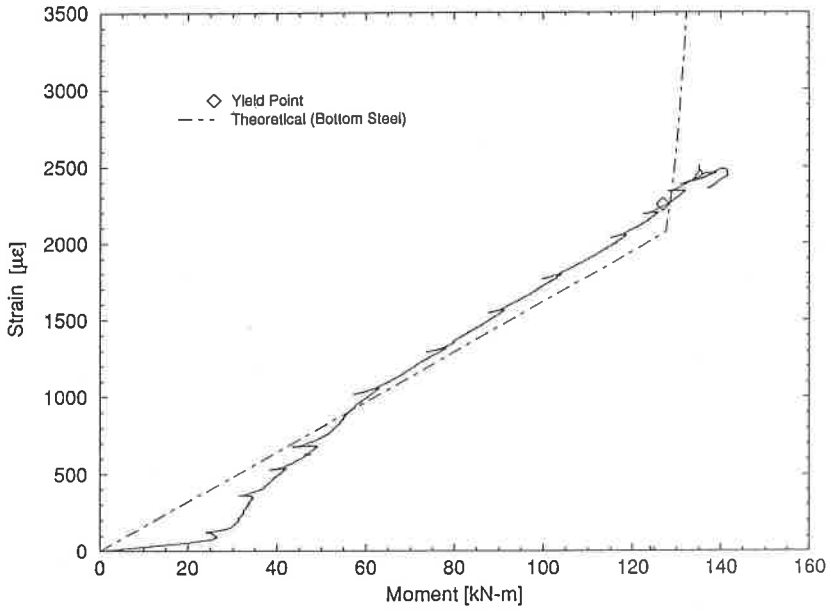

FIGURE B.21. Bottom Steel Strain-Moment Relationships at Midspan, Beam 7